DEPARTMENT OF PHYSICS, UNIVERSITY OF JYVÄSKYLÄ
RESEARCH REPORT No. 3/1996

ALPHA DECAY SPECTROSCOPY OF NEUTRON-DEFICIENT ASTATINE, RADON AND FRANCIUM NUCLEI USING A GAS-FILLED SEPARATOR

BY
TIMO ENQVIST

Academic Dissertation
for the Degree of
Doctor of Philosophy

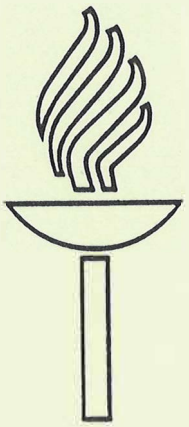

Jyväskylä, Finland
May 1996

URN:ISBN:978-951-39-9476-1
ISBN 978-951-39-9476-1 (PDF)
ISSN 0075-465X

Jyväskylän yliopisto, 2023

ISBN 951-34-0785-3
ISSN 0075-465X

DEPARTMENT OF PHYSICS, UNIVERSITY OF JYVÄSKYLÄ
RESEARCH REPORT No. 3/1996

ALPHA DECAY SPECTROSCOPY OF NEUTRON-DEFICIENT ASTATINE, RADON AND FRANCIUM NUCLEI USING A GAS-FILLED SEPARATOR

BY
TIMO ENQVIST

Academic Dissertation
for the Degree of
Doctor of Philosophy

To be presented, by permission of the
Faculty of Mathematics and Natural Sciences
of the University of Jyväskylä,
for public examination in Auditorium FYS-1 of the
University of Jyväskylä on May 31, 1996,
at 12 o'clock noon

Jyväskylä, Finland
May 1996

Preface

I would like to express my warm gratitude to all members in the RITU-group and other people partisipating in our experiments. Especially I wish to praise my supervisor, assoc. prof. Matti Leino for an encouraging and supporting quidance during my studies, and M.Sc. Juha Uusitalo for numerous discussions and the technical maintenance of our separator, and assoc. prof. Kari Eskola for fruitful comments concerning the topic of this thesis.

I would also like to thank our foreign collaborators for their valuable work for experiments.

It has been a priviledge to work in the fine atmosphere created by the physicist, and in the new and modern buildings of the Department of Physics and the Accelarator Laboratory.

The financial support from the University of Jyväskylä is gratefully acknowledged. I want to state my thanks also for Suomen Tiedeseura (The Finnish Society of Sciences and Letters) and Suomalainen Tiedeakatemia (Finnish Academy of Science and Letters) for the financial support for participating in several foreign nuclear physics conference.

Finally, I wish to thank for my dad, Jukka, Anja, and my brother, Antti, for their support.

Jyväskylä, May 1996

Timo Enqvist

Abstract

Alpha particle decay properties (alpha particle energy and half-life) of neutron-deficient astatine, radon and francium isotopes are studied in this thesis. These nuclei in the close vicinity of the proton drip-line were produced using three different heavy-ion-induced fusion-evaporation reactions. The reactions were ^{141}Pr(^{56}Fe, xn)$^{197-x}$At, ^{169}Tm(^{35}Cl, xn)$^{204-x}$Rn, ^{170}Yb(^{35}Cl, xn)$^{205-x}$Fr and the beam particles were delivered by the K = 130 MeV heavy ion cyclotron of the Accelerator Laboratory of the Department of Physics, University of Jyväskylä. The gas-filled recoil separator RITU was used to separate reaction products from the primary beam. The method of time and position correlated alpha particle decay chains were used for analysing the experimental data. Nine previously unpublished alpha particle transition from five different isotopes (^{193,194,195}At, ^{197}Rn and ^{200}Fr) were observed in the present work. Measured alpha particle energies and half-lives are compared with the systematics of heavier isotopes and with theoretical predictions. The systematics of isomerism and shell model intruder states are also shown.

Table of contents

1 Introduction

Alpha particle decay properties (i.e. alpha particle energy and half-life) and nuclear structure of very neutron-deficient astatine ($^{193-195}$At), radon (^{197,198}Rn) and francium ($^{200-203}$Fr) isotopes have been studied in the present work. The region of interest in the present work is shown in figure 1.1 together with the whole chart of the nuclides.

The isotopes studied here were produced using heavy-ion-induced fusion reactions followed by evaporation of neutrons. The reactions were ^{141}Pr(^{56}Fe, 2-4n)$^{193-195}$At, ^{169}Tm(^{35}Cl, 6-7n)^{197,198}Rn and ^{170}Yb(^{35}Cl, 2-5n)$^{200-203}$Fr. (In the latter reaction, the 2n and 3n exit channels were probably due to the relatively large amount of impurities in the target material.) This is the most efficient method for the production of neutron-deficient isotopes of heavy elements. A heavy element, in this work, is defined as an element heavier than lead. The production cross sections of very neutron-deficient isotopes from spallation reactions, for example, in this region are too small and these reactions can not be used. Heavy ion beams of ^{35}Cl and ^{56}Fe used in the present work were produced by an ECR ion source and accelerated by the K = 130 MeV heavy ion cyclotron [Hei95] at the Accelerator Laboratory of the Department of Physics of the University of Jyväskylä (JYFL). The new MIVOC method (Metal Ions from VOlatile Compounds) [Koi94] was used for preparing the ^{35}Cl and ^{56}Fe beams. Measurements were carried out in April and December 1994 and in April 1995.

The production cross sections of the most neutron-deficient nuclei in the region relevant to this work are much smaller than 1 mb and the half-lives much shorter than 1 s. Consequently, an efficient and fast experimental technique is needed to separate reaction products from the primary beam and unwanted reaction products and to transport them to the detector system. In the present work, the gas-filled recoil separator RITU (Recoil Ion Transport Unit) [Lei95a] combined with a position sensitive focal plane detector was used. RITU is a new and powerful device and one has yet not been able to fully utilize its properties in measurements completed in this work. See chapter 3 for more information.

Determination of the production cross sections of nuclei formed by evaporation of neutrons (or protons or alpha particles) from the complete fusion reaction gives information on the survival probability of moderately hot compound systems against fission. Excitation energies of ^{197}At, ^{204}Rn and ^{205}Fr compound nuclei varied between 24 and 54 MeV, 80 and 94 MeV, and 54 and 65 MeV, respectively, in the present work.

The experimental observation of the shell model ($\frac{1}{2}^+$) intruder states in odd-mass bismuth isotopes and in ^{197}At [Coe85, Coe86] gives the motivation for nuclear structure studies in this region. Based on systematics it has been suggested [Coe86] that the ground state configuration in ^{195}At is ($\frac{1}{2}^+$). The observation of favoured or non-hindered (i.e. hindrance factor near to unity) alpha decay provides a strong spectroscopic tool for studying these intruder states. A favoured alpha decay indicates that the transition connects initial and final states with the same spin and parity. Reduced alpha decay widths calculated as proposed by Rasmussen [Ras59] are useful in estimation of alpha decay hindrance. The reduced alpha particle widths for nuclei studied in the present work are discussed in chapter 5.

Another typical physical property in these heavy neutron-deficient nuclei is the existence of (alpha particle decaying) isomeric states. Isomerism has been observed, for example, in all known odd-mass even-Z isotopes in this region and it is due to the ($\frac{13}{2}^-$) neutron orbital.

Astatine and francium isotopes studied in the present work lie very close to the proton drip-line calculated according to the semiempirical mass formula of Liran and Zeldes [Lir76]. Even though there exist more recent mass formulae, the one of Liran and Zeldes was used in the present work because it is known to reproduce experimental masses quite well. The crossing of the proton drip-line would make ground state proton decay a possible decay mode. Calculated proton decay half-lives are, however, too long for proton decay to compete with alpha decay at the proton drip-line. Part of the calculated proton drip-line is shown in figure 1.1 separately for heavy even-Z and odd-Z elements.

The identification of (unknown) activities in the present work was based on time and position correlated chains of the type evaporation residue – mother alpha particle – daughter alpha particle. In this method the average counting rate of

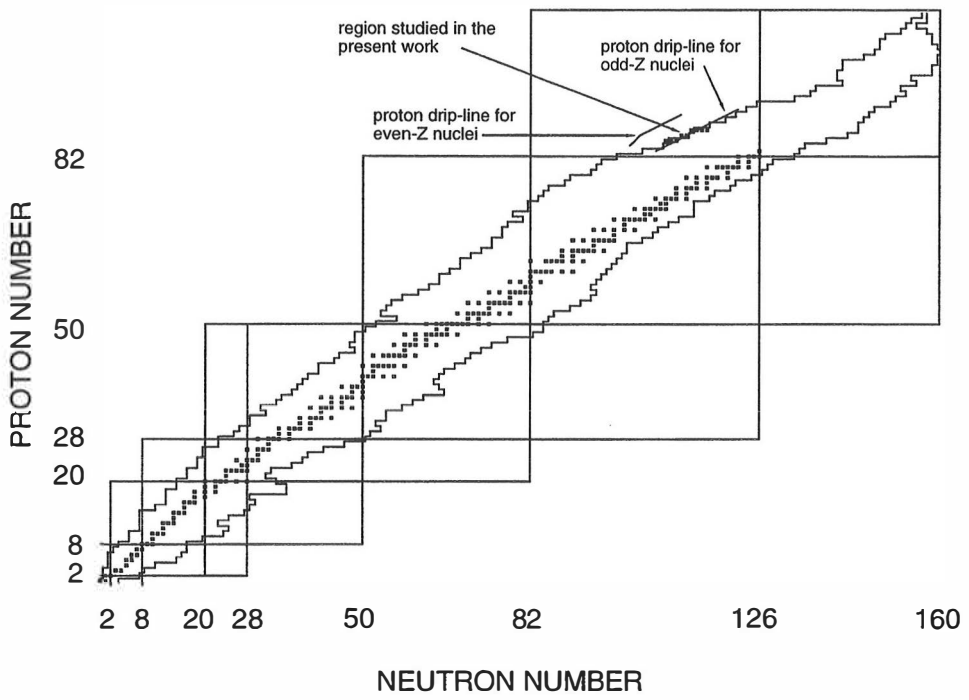

Figure 1.1 Chart of the nuclides. Heavy nuclei studied in the present work are shown together with the proton drip-line which is calculated from mass tables of Liran and Zeldes [Lir76]. Stable isotopes have been marked with a black square. The figure is drawn according to the Chart of the Nuclides - Strasbourg 1992. The region of interest is shown in more detail in figure 4.1.

evaporation residues has to be low enough to avoid accidental correlations. The number of accidental correlations or the probability to produce an accidental correlation were used for estimation of the significance of the identification.

There is no previous information on the isotope ^{193}At. Properties of isotopes ^{194,195}At have been reported in theses of S. Yashita and M. Leino [Yas83, Lei83], but they are not published. ^{197}Rn was found and identified independently also at RIKEN [Mor95]. The isotope ^{198}Rn has been identified by Calaprice et al. [Cal84] and we confirm their result. ^{200}Fr was also identified independently at RIKEN [Mor95], but their half-life value differs greatly from ours. Isotopes ^{201,202}Fr have been identified by Ewan et al. [Ewa80] but our results provide the link to the

daughter At isotopes. In the present work alpha decay properties of five previously unpublished isotopes will be reported.

In chapter 2 background related to physics dealt with in this work is presented briefly. Experimental methods are explained in chapter 3 and experimental results in chapter 4. Conclusion and discussion is presented in chapter 5.

The present work includes new results not published elsewere. Part of the results presented in this work has been reported also in the following publications:

[Lei95a] M. Leino, J. Äystö, T. Enqvist, P. Heikkinen, A. Jokinen, M. Nurmia, A. Ostrowski, W.H. Trzaska, J. Uusitalo, K. Eskola, P. Armbruster and V. Ninov: Gas-filled Recoil Separator for Studies of Heavy Elements. Nuclear Instruments and Methods in Physics Research **B99** (1995) 653 - 656.
https://doi.org/10.1016/0168-583X(94)00573-7

[Lei95b] M. Leino, J. Äystö, T. Enqvist, A. Jokinen, M. Nurmia, A. Ostrowski, W.H. Trzaska, J. Uusitalo, K. Eskola, P. Armbruster and V. Ninov: Research on Heavy Elements using the JYFL Gas-filled Recoil Separator RITU. Acta Physica Polonica **B26** (1995) 309 - 322.

[Lei95c] M. Leino, T. Enqvist, W.H. Trzaska, J. Uusitalo, K. Eskola, P. Armbruster and V. Ninov: Alpha decay properties of very neutron-deficient isotopes with $85 \leq Z \leq 90$. Proc. Int. Conf. on Exotic Nuclei and Atomic Masses ENAM95, Arles, France, 1995, Edition Frontiéres, Gif sur Yvette (in press).

[Enq96a] T. Enqvist, P. Armbruster, K. Eskola, M. Leino, V. Ninov, W.H. Trzaska and J. Uusitalo: Alpha Decay of the New Isotope ^{197}Rn. Zeitschrift fiir Physik **A354** (1996) 9.
https://doi.org/10.1007/s002180050005

[Enq96b] T. Enqvist, K. Eskola, A. Jokinen, M. Leino, W.H. Trzaska, J. Uusitalo, V. Ninov and P. Armbruster: Alpha Decay Properties of $^{200-202}$Fr. Zeitschrift fiir Physik **A354** (1996) 1.
https://doi.org/10.1007/s002180050001

2 Physical background

Physical properties of isotopes of the elements between lead and uranium beyond the closed 126 neutron shell and their alpha particle decay properties are discussed in this chapter. Typical properties of these nuclei are isomerism and the shell model intruder states. The reduced alpha particle width and the predicted nuclear deformation are also discussed.

Alpha particle decay is a good tool to be used as a probe for investigating nuclear structure because it can be measured at a high efficiency (up to 100%) and a good energy resolution (down to about 15 keV). Typical properties given by alpha particle decay studies are, among other things, ground state decay energies and mass excess values. Alpha particle decay provides information also on assigments of spin and parity of ground and excited states and on excitation energies of excited levels.

Some of the figures referred to in this chapter will be presented in chapter 5 together with discussion and comments concerning results obtained in this work.

2.1 Nuclear deformation

Recent theoretical study [Möl95] of the ground state properties of heavy neutron-deficient nuclei with neutron number less than 126 has predicted the possible onset of nuclear deformation around ^{200}Rn. In the neutron-deficient astatine – francium region there is a quite steep increase in the absolute value of the calculated ground state quadrupole deformation. Values around 0.2 at about mass 200 are calculated for the ground state quadrupole deformation parameter in this region with increasing trend with decreasing number of neutrons.

A clear indication of nuclear deformation would be, for example, an experimental observation of fine structure in the alpha particle decay of an even-even nucleus to the first excited 2^+ state of the daughter nucleus. Information on nuclear deformation can also be obtained by studying its effect on alpha particle energies.

This is, however, more difficult to establish. Nuclear deformation in ^{200}Rn will be discussed in more detail in chapter 5.

2.2 Nuclear isomerism

Experimental studies show the systematic occurrence of isomerism in all odd-mass isotopes of the even-Z elements with neutron number less than 126. The alpha particle energy systematics as a function of neutron number for even-Z elements polonium, radon and radium are shown in figure 5.4 (see chapter 5 for more details). In odd-Z elements observed cases of isomerism do not occur as regularly. However, the isotopes of astatine with neutron numbers of 112, 113 and 115 have isomeric states decaying primarily by alpha particle emission. An isomeric state in ^{202}At (N = 117) has a very small alpha particle branching ratio. Occurrence and systematics of alpha particle decaying isomeric states in neutron-deficient astatine, radon and francium isotopes are discussed in more detail in chapter 5.

The change in total angular momentum for isomeric transitions should correspond to a multipolarity of E3, M3, or higher. Another feature for isomeric transitions is a small energy difference between initial and final states. These conditions are satisfied only for A $\geq$ 39 and isomerism does not exist in the light elements. Isomeric states are not spread uniformly among all heavier nuclei, but instead they are concentrated in "islands" of nuclei with proton or neutron number close to the magic numbers 50, 82 and 126.

These properties of isomeric transitions, small transition energy and large change in total angular momentum, can be explained satisfactorily using the concepts of the shell model. Figure 2.1 shows the shell model energy levels of nuclei with spin–orbit coupling taken into account. In even-even nuclei the pairing interaction is too strong to allow the formation of isomers. The "islands of isomerism" can be explained by studying figure 2.1, where proton and neutron levels are separated. For low mass numbers up to 40 nucleons (about 20 protons and 20 neutrons) the energy levels involved have angular momentum j $\leq \frac{5}{2}$, and there are no possibilities for large angular momentum differences between energetically close-lying levels. For heavier nuclides, just below the magic numbers 50, 82 or 126 there are close-

lying energy levels with j = $\frac{1}{2}$, $\frac{9}{2}$ (50) and j = $\frac{1}{2}$, $\frac{11}{2}$ (82) and j = $\frac{1}{2}$ or $\frac{3}{2}$, $\frac{13}{2}$ (126), resulting in a large change in total angular momentum and giving a chance for the appearance of isomerism.

Isotopes studied in the present work are situated above the closed proton shell 82 and below the closed neutron shell 126. In the odd-mass radon isotope ^{197}Rn thc isomeric state can be understood in terms of the $i_{13/2}$ neutron level and in the odd-mass astatine isotope ^{193}At in terms of the $s_{1/2}$ (intruder) proton level. In the odd-odd isotopes (astatine ^{194}At in the present case) coupling between the odd proton and odd neutron should be considered.

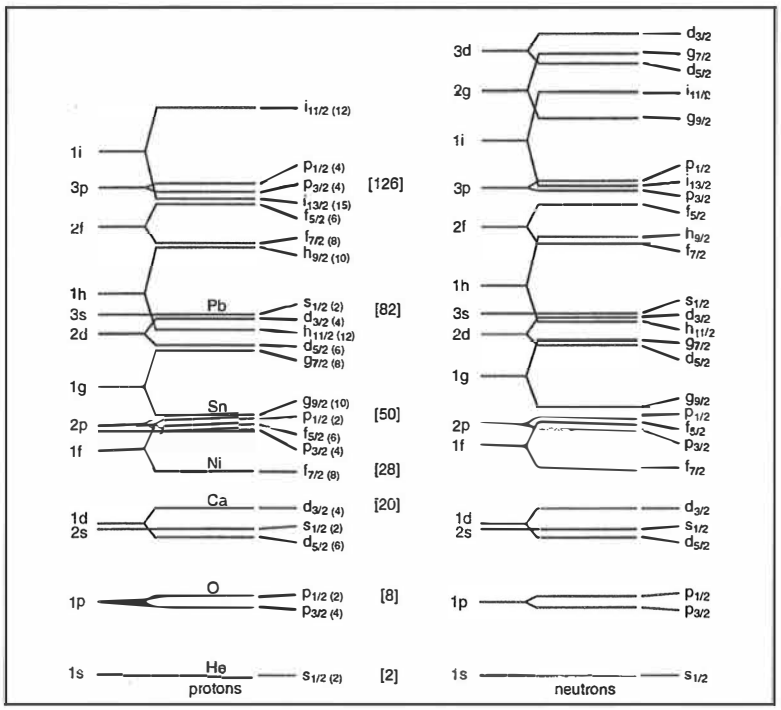

Figure 2.1 The shell model energy levels of a nucleus. Levels for protons and neutrons are shown separately. Spin-orbit interaction has been taken into account. Adopted from [May79].

2.3 Reduced alpha particle width and hindrance factor

The reduced alpha particle widths of the s-wave ground state to ground state transitions between even-even nuclei are generally taken for a standard of unhindered alpha particle decay and used as a reference for the alpha particle decay in the neighbouring odd-mass and odd-odd isotopes and for the alpha particle decay to excited levels. The hindrance factor may be defined as the ratio of the measured (partial) half-life to (for example) the semiempirical half-life of the same or the most nearest even-even nucleus. The hindrance factor of the alpha particle transition between ground states of even-even nuclei is near unity (1.0). Semiempirical expressions for the half-life can be found, for example, in refs. [Taa61, Sea90]. In the present work, hindrance factors are calculated as the ratio of the experimental half-life to the half-life obtained using the method of Rasmussen [Ras59].

According to the procedure proposed by Rasmussen, the reduced alpha particle width δ^2 is proportional to the ratio of the alpha particle decay rate λ and the barrier penetration factor P, the constant of proportionality being Planck's constant h. In the present work, the reduced alpha particle widths are scaled with respect to that of ^{212}Po and the screening correction has been taken into account when applying the method of Rasmussen.

The barrier penetration factor describes the probability for an alpha particle to tunnel through the potential barrier consisting of Coulomb and centrifugal barriers. The alpha particle decay rate can be obtained from the experimental half-life $T_{1/2}$ and the alpha particle decay branching ratio b_α. The uncertainty of the reduced alpha particle width is mainly due to the uncertainty in the half-life and especially of the branching ratio, while the accuracy of the alpha particle energy is normally sufficient.

The reduced alpha particle width describes the probability of forming an alpha particle inside the nucleus and it contains most of the nuclear structure information. The systematics of the reduced alpha particle widths is used to extract nuclear information such as the effect of shell closures and changes in deformation.

Reduced alpha particle widths for s-wave transitions behave in a regular fashion as a function of both neutron and mass number. They are largest for a few nucleons beyond a closed shell, with a sharp minimum at the closed shell and they then decrease as the next shell closure is approached. This systematic behaviour can be seen in figure 5.6 for even-N neutron-deficient isotopes of elements polonium, astatine and radon, including new isotopes studied in the present work. In chapter 4 the expected half-lives calculated by using the method of Rasmussen are presented instead of reduced alpha particle widths. In chapter 5 the systematics of reduced alpha particle widths of neutron-deficient isotopes of elements polonium, astatine and radon are discussed.

2.4 Intruder states

In the spherical shell model, the proton $\pi h_{9/2}$ particle state lies above the closed 82 proton shell, while the proton $\pi s_{1/2}$ particle state lies below. Any $\pi h_{9/2}$ configurations in elements below lead and $\pi s_{1/2}$ configurations in elements above lead are referred to as proton intruder states. A great deal of experimental results have shown that the excitation energies of the $\pi h_{9/2}$ intruder configurations of odd-mass Tl and Au isotopes have a parabolic dependence as a function of the neutron number with a minimum when the neutron number is half-way between (N = 104 in the present case) the major shell closures 82 and 126 [Hey83].

The odd-mass bismuth isotopes have a $\pi h_{9/2}$ ground state and a low lying $\pi s_{1/2}$ isomeric intruder state. There is also experimental evidence for parabolic behaviour of $\pi s_{1/2}$ intruder state energies in neutron-deficient bismuth isotopes [Lei81, Coe85, Bat95]. The $\pi s_{1/2}$ intruder state in ^{197}At with an excitation energy of (52 ± 10) keV was identified by Coenen et al. [Coe86]. They concluded that the low excitation energy of the intruder state in ^{197}At suggests that for ^{195}At the intruder state becomes the ground state. This will be discussed in chapter 5.

It has been pointed out by Coenen et al. [Coe85] that alpha particle decay studies are the only way to determine the intruder-state excitation energies of neutron-deficient isotopes of elements in the lead region. The reason is that transitions between intruder and ground states are of the type $\frac{1}{2}^+ \longleftrightarrow \frac{9}{2}^-$ (M4) in these

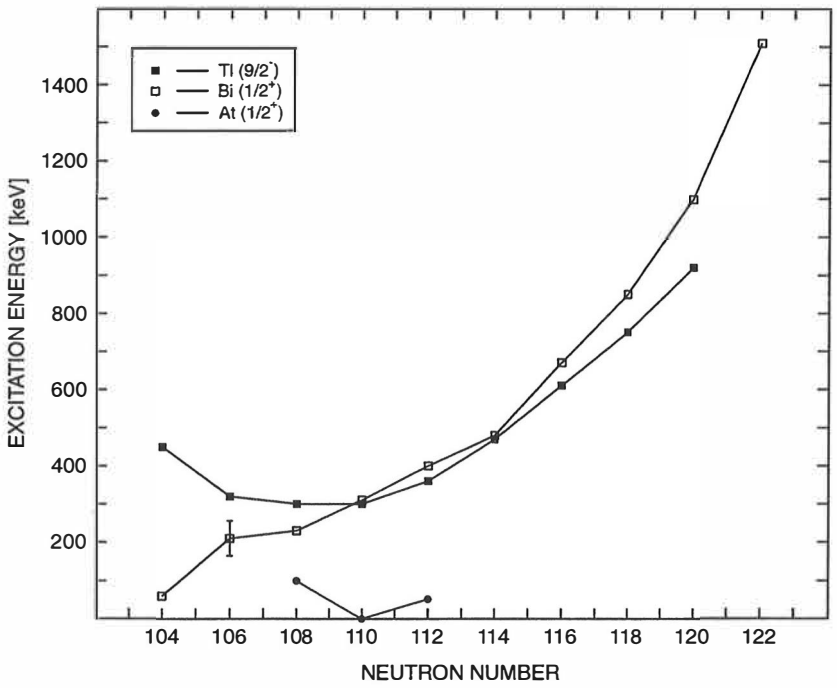

Figure 2.2 The systematics of the intruder state excitation energies of the odd-mass (even-N) thallium, bismuth and astatine isotopes as a function of the neutron number. The data are taken from refs. [And93, Bat95, Coe85] for thallium and bismuth and from [Coe86] and the present work for astatine isotopes. The excitation energy of the intruder state in ^{189}Bi has been taken to be 210 keV from [And93, Bat95].

nuclei and these particular M4 transitions are observed [Bra80] to be the most strongly hindered M4 transitions known in any odd-mass nuclei.

Figure 2.2 shows a plot of intruder state level energies for neutron-deficient odd-mass Tl, Bi and At isotopes as a function of neutron number. The excitation energies of $\pi h_{9/2}$ levels in thallium follow a parabola-shaped curve. In bismuth, the minimum of the $\pi s_{1/2}$ level excitation energy is probably not reached yet, but due to the similar behaviour with thallium isotopes the parabolic behaviour can be expected. There have been discrepancies of experimental alpha particle energies of ^{189}Bi^{m} between [Sch84a] and [And93, Bat95]. Coenen et al. [Coe85] reported the value of 92 keV measured by Schneider for the excitation energy of the intruder state in ^{189}Bi. In figure 2.2, the excitation energy of the intruder state in ^{189}Bi

has been calculated from alpha particle energies obtained by Batchelder et al. and Andreyev et al. [Bat95, And93]. A value of 210 keV has been used. The excitation energy of 60 keV for the $(\frac{1}{2}^+)$ intruder state in ^{187}Bi was also reported by Coenen et al. [Coe85] (and measured by Schneider [Sch84a]) and according to figure 2.2 it does not fit to the systematics. On the other hand, the minimum in excitation energy is expected to occur in the middle of the closed neutron shell at N = 104. The data for astatine isotopes come from [Coe86] and this work (see chapter 5).

3 Experimental techniques

Experimental techniques from the production to the identification of evaporation residues are briefly discussed in this chapter. Methods used in the present work are not new but they are not so common in experimental nuclear physics.

3.1 Heavy ion reactions

The most effective way to produce neutron-deficient nuclei in the region from lead to uranium is to use heavy-ion-induced fusion reactions followed by neutron evaporation (see e.g. [Bas80]). Fusion between a heavy projectile and a heavy target nucleus leads to the formation of a compound nucleus with excessive excitation energy. During the de-excitation process, neutron evaporation competes with charged particle evaporation and fission.

The production probability of evaporation residues can roughly be divided into two factors describing the reaction mechanism before and after the formation of a compound nucleus: the production cross section of a compound nucleus and the probability of neutron evaporation against fission and charged particle evaporation.

The more neutrons it is needed to evaporate from the compound nucleus the higher is the excitation energy needed and the smaller is the cross section of the final product due to competition from fission and evaporation of charged particles. The high excitation energy of the compound nucleus allows several exit channels. The higher angular momentum of the compound nucleus associated with heavier projectiles will decrease the height of the fission barrier making fission more probable in comparison with particle evaporation.

Production cross sections of evaporation residues studied in the present work vary from a few nanobarns to hundreds of nanobarns. Nuclei produced via evaporation of up to seven neutrons were observed in the present work.

The lower limit of the projectile kinetic energy for producing nuclei via particle (neutron) evaporation is determined by the repulsive Coulomb barrier (in the center-of-mass system):

$$B_C = \frac{e^2}{4\pi\epsilon_0}\frac{Z_p Z_t}{r}, \tag{3.1}$$

where Z_p and Z_t are atomic numbers of the projectile and target nuclei, respectively, and r is the interaction radius; $r = R_0(A_p^{1/3}+A_t^{1/3})$, $R_0 = 1.44$ fm. The excitation energy E^* of the compound nucleus can be calculated by using the equation

$$E^* = \frac{A_t}{A_p + A_t}E + Q, \tag{3.2}$$

where A_p and A_t are mass numbers of the projectile and target nuclei and E is the kinetic energy of the incident projectile in the laboratory system. Q is the rest mass difference before and after the formation of the compound nucleus. In the present work reaction Q-values were estimated from mass defect values calculated by Liran and Zeldes [Lir76].

In general, evaporation of one neutron in the neutron-deficient region will reduce the excitation energy of the compound nucleus by an amount of approximately 12 MeV, where 10 MeV goes to the binding energy and 2 MeV to the kinetic energy of the neutron.

3.2 Experimental apparatus

3.2.1 Methods for studying short lived activities

The alpha decay half-lives of neutron-deficient astatine, radon and francium isotopes studied in the present work are in the millisecond region and their production cross sections are estimated to be below one microbarn. This requires a technique

allowing a fast and an efficient separation of reaction products from unwanted background of projectiles and target-like products.

3.2.2 Principle of operation of a gas-filled separator

A gas-filled recoil separator provides an effective tool for studying fusion reaction products from heavy-ion-induced reactions. The separation method is based on the use of a dipole magnet with the field region filled with a dilute gas such as hydrogen or helium to collect all ionic charge states of fusion reaction products. Figure 3.1 shows a schematic view of the separation method. Fusion reaction products are separated in-flight from the primary beam according to their average magnetic rigidity. The method was first used by Cohen and Fulmer [Coh58] for separation and studies of fission products. A few years later this technique was further developed by Armbruster et al. [Arm61]. Karnaukhov et al. [Kar69] at Dubna and Ghiorso et al. [Ghi88] at LBL, Berkeley used a gas-filled separator for the study of nuclei produced in heavy ion reactions.

Gas-filled separators in operation are, besides RITU, among others GARIS [Miy87] (GAs-filled Recoil Isotope Separator) at RIKEN and the one in Dubna [Laz93]. Gas-filled separators not used any more are among others SASSY [Ghi88] (Small Angle Separating SYstem) at LBL, Berkeley and HECK [Nin95] (HElium Charge exchange Kaleidoscope) at GSI, Darmstadt.

The expression for the average magnetic rigidity $B\rho$ of an ion moving in a gas can be written in the form [Ghi88]

$$B\rho = 0.0227 \frac{A}{Z^{1/3}} \quad [\mathrm{Tm}], \tag{3.3}$$

where Z and A are the atomic and mass number of the ion, respectively. The above formula has been obtained using the Thomas-Fermi model of the atom and it is approximative. The two important first order properties of the gas-filled separator can be seen from equation (3.3): the average magnetic rigidity is independent of the velocity and of the initial charge distribution of the particles. It can also be used to

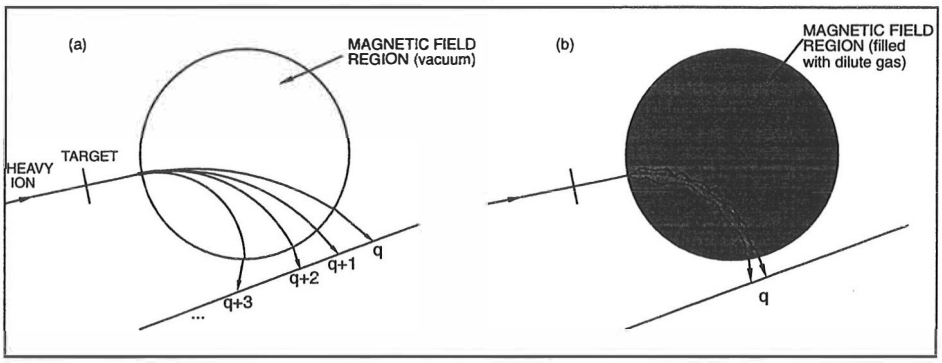

Figure 3.1 Heavy-ion-induced fusion reaction products recoiling out from a thin target have a broad charge and momentum distribution.
(a) In a magnetic field in vacuum they follow discrete trajectories defined by the charge states.
(b) When they enter a magnetic field filled with a dilute gas they follow an average trajectory determined by their momenta and average charge state.
Figure adopted from ref. [Pau89].

calculate the ratio of rigidities for estimating the degree of the separation between fusion evaporation residues and target-like products and scattered projectiles.

The average charge state $\bar{q}$ of an ion moving in a dilute gas with velocity range $1 \langle v/v_0 \langle Z^{2/3}$ can be written from the Thomas-Fermi model of the atom to be

$$\bar{q}(v,Z) = \frac{v}{v_0} \cdot Z^{1/3}, \tag{3.4}$$

where Z is the atomic number of the moving ion and v_0 is the Bohr velocity, $v_0 = 2.19 \cdot 10^6$ m/s. (In fact, this formula has been used to obtain equation (3.3)). The experimental average charge state can be parametrized by the equation [Bet72]

$$\bar{q}(v,Z) = Z[1 - C_1 \cdot \exp\{-C_2 \frac{v}{v_0} \cdot Z^{2/3}\}]. \tag{3.5}$$

The two parameters C_1 and C_2 can be determined by a fit to experimental data. Ghiorso et al. [Ghi88] obtained values $C_1 = 1.04$ and $C_2 = 0.91$. For $C_1 = C_2 = 1$ a first order expansion of the exponential gives the expression of equation (3.4). Another parametrization of experimental average charge states as a function of

velocity and atomic number of the moving ion has been presented by Oganessian et al. [Oga91]

$$\bar{q}(v, Z) = 0.00871 \cdot (\frac{v}{v_0})^{1.54} \cdot Z^{1.10} + 2.05. \quad (3.6)$$

The average charge states calculated by using the above equations for evaporation residues studied in the present work are compared with each other in table 3.1.

Table 3.1 Comparison between average charge states calculated using equations (3.4-3.6) for evaporation residues produced in the present work.

Beam	E_{lab} [MeV/nucl.]	Evaporation residue	v/v_0	$\bar{q}_1$	$\bar{q}_2$	$\bar{q}_3$
^{35}Cl	5.6	$^{197,198}Rn$	2.58	11.4	6.70	7.07
	5.7		2.60	11.5	6.80	7.15
	5.9		2.63	11.6	6.90	7.23
	6.0		2.66	11.7	7.00	7.32
	6.1		2.69	11.9	7.10	7.40
^{35}Cl	4.9	$^{200,201}Fr$	2.41	10.7	6.09	6.64
	5.1		2.45	10.9	6.24	6.76
	5.3		2.51	11.1	6.45	6.93
^{56}Fe	4.1	$^{194,195}At$	3.66	16.1	10.6	10.6
	4.4		3.80	16.7	11.1	11.1
	4.7		3.91	17.2	11.4	11.5
	4.9		3.97	17.5	11.7	11.7

$\bar{q}_1$: Formula (3.4).
$\bar{q}_2$: Formula (3.5).
$\bar{q}_3$: Formula (3.6).

A gas-filled recoil separator typically consists of a dipole magnet followed by a quadrupole doublet. The main function of a gas-filled separator is to separate fusion reaction products from the primary beam and to transport the separated reaction products to the focal plane detector system. Due to the filling gas, the transmission of evaporation residues up to 50% may be achieved. In a typical heavy-ion-induced fusion reaction the transmission is around 20% – 30%. Such a high transmission allows the identification of an activity with production cross section below 1 nb. The lower limit of life time is given by the flight time of an ion through the separator and is typically a few microseconds. A high transmission

of evaporation residues has been obtained at the expense of mass resolving power. The gas-filled separator used in the present work cannot in practise make any separation between evaporation residues. This means that the identification of an evaporation residue is performed off-line and is based on the use of a versatile detector system. The procedure used in the present work for identification of an evaporation residue is described in section 3.4.

Figure 3.2 gives an example on the pressure dependence of the Bρ-resolution. Full circles are experimentally determined resolutions and the different contributions have been calculated. The range of the optimum pressure is quite broad, as can be seen from the figure. The lowest possible pressure in this range should be selected as the working condition to minimize the losses of ions from multiple scattering.

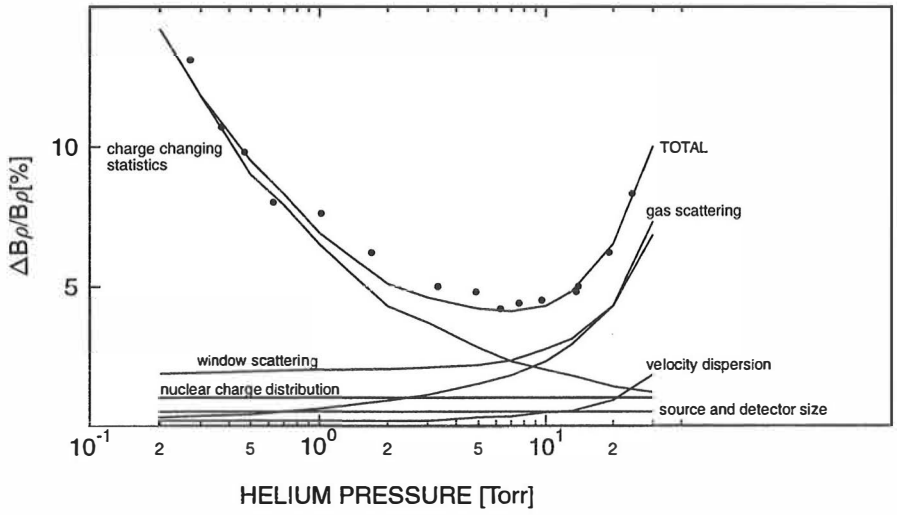

Figure 3.2 The typical behaviour of the Bρ-resolution as a function of the pressure of the filling gas in gas-filled separators. Full circles are experimentally determined values and the different contributions to the resolution have been calculated. The curve marked by 'TOTAL' is the sum of all the contributions.
Figure adopted from ref. [Arm71].

The description of the typical detector system that is used in connection with recoil separators and with our separator RITU in particular is presented in section 3.3. The gas-filled recoil separator RITU will be described next.

3.2.3 The JYFL gas-filled recoil separator RITU

The technical properties of the gas-filled recoil separator operating at the Accelerator Laboratory of the Department of Physics of the University of Jyväskylä (JYFL) will be introduced in this section. Experimental details that are relevant for the experiments discussed in the present work are also considered. The detector system is described in section 3.3.

The separator vacuum chamber (see the shaded area in figure 3.3) is normally filled with dilute helium gas with the pressure of about 1 mbar from the target area to the detector chamber. A 0.45 mg/cm^2 nickel foil was used to separate the helium filling from the high vacuum of the cyclotron beam line. The gas pressure inside the dipole chamber was monitored and a continuous pumping of helium from the vacuum chamber to remove gaseous impurities from the separator field region was used. The helium gas was fed into the target chamber, regulated by a mass flow controller.

Heavy ion beams of ^{35}Cl and ^{56}Fe used in the present work were produced by an ECR ion source using the MIVOC method [Koi94] and were delivered to the target by the K = 130 MeV heavy ion cyclotron [Hei95]. The intensities of ^{35}Cl and ^{56}Fe beams were about $3{\cdot}10^{11}$ particles/s (300 nA) and $1{\cdot}10^{11}$ particles/s (200 nA), respectively, measured from a Faraday cup in front of the beam window. A pulsed beam was employed in some of the experiments with beam on to beam off ratios of 10 ms/30 ms and 10 ms/10 ms for ^{35}Cl and ^{56}Fe beams, respectively. Degrader foils (havar: 1.8 mg/cm^2, nickel: 0.45, 0.9, 1.4, 1.8 and 2.7 mg/cm^2) were used to adjust the beam energy.

Targets used in the present work were ^{141}Pr, ^{169}Tm, and ^{170}Yb and their thicknesses were ~0.2, 0.67 and 0.35 mg/cm^2, respectively. The ^{141}Pr target was prepared by depositing the material on a 40 μg/cm^2 carbon backing using the off-line isotope separator at the Accelerator Laboratory of the University of Helsinki. The ^{169}Tm target was prepared at GSI (Gesellschaft für Schwerionenforschung, Darmstadt, Germany) by evaporating on 40 μg/cm^2 carbon backing. The ^{170}Yb target was delivered by Micromatter and it was also prepared by evaporating on 40 μg/cm^2 carbon backing. The enrichment of the ^{170}Yb target was 72%. Stationary targets mounted on a manually operated rotating wheel were used in all experiments. The

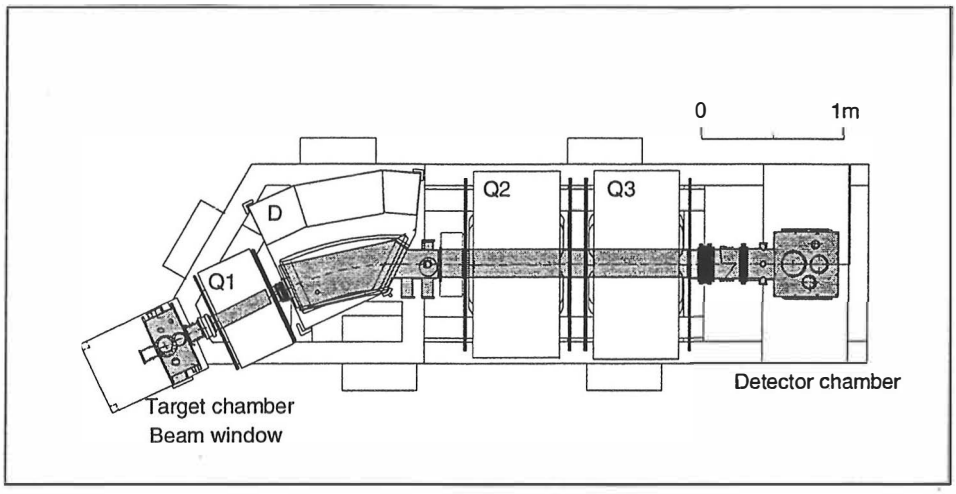

Figure 3.3 Schematic layout of the gas-filled separator RITU. The shaded area describes the vacuum chamber filled with dilute helium gas. The target and detector chambers are shown. The beam window separates the high vacuum of the cyclotron from the gas-filling of RITU. The dashed line describes the optical axis.

filling gas of the separator acted also as a cooling gas for targets.

The magnetic field strength of the dipole magnet was measured continuously by a HALL-probe. A value of around 1 T was generally used. In the experiments, the strength of the field was initially calculated using equation (3.5) and then fine-tuned to get the distribution to the middle of the focal plane detector. The widths of the vertical and horizontal distributions were adjusted by tuning the gradients of the quadrupoles. A safety system for avoiding the sweeping of the primary beam across the focal plane detector was based on an analog signal from the HALL-probe. In case of a decrease of the field strength of about 10%, the Faraday cup was introduced automatically into the beam.

The ion optical configuration of the gas-filled recoil separator RITU (Recoil Ion Transport Unit) is QDQQ where Q stands for quadrupole and D for dipole magnet. It differs from the standard configuration in the way that a small, strong vertically focusing quadrupole magnet has been placed in front of the dipole magnet. The reason is to achieve better matching to the dipole magnet acceptance, which is expected to lead to approximately 30% higher angular acceptance than for the standard DQQ configuration. The schematic view of the separator is shown in

figure 3.3. The shaded area describes the separator vacuum chamber filled with dilute helium gas. See the figure caption for more details. All four magnets and their stand and power supplies were delivered by DANFYSIK A/S according to specifications determined by JYFL.

The dipole magnet has a central radius of curvature of 1.850 m and a deflection angle of 25°. The pole face of the exit of the dipole has been rotated by 25° in clockwise direction relative to optical axis to achieve some horizontal focusing. The maximum rigidity of a particle is 2.2 Tm. Angular acceptances of ±80 mrad and ±30 mrad for vertical and horizontal direction, respectively, have been calculated.

First production runs with the new separator were performed in late 1993 and all of its properties have not been studied completely so far. The determination of the performance of the separator has partly suffered from inadequate beam line diagnostics. However, some performance studies have been performed [Lei95a]. The absolute efficiency of the separator was determined using the reaction ^{175}Lu(^{40}Ar,4–5n)^{210,211}Ac with a bombarding energy of 4.6 MeV/nucleon. A reference for the production cross section of ^{210,211}Ac was obtained from ref. [Ver84] and a comparison gave a value of 25% for the efficiency of our separator. A 100% transmission of the ^{40}Ar projectiles from the Faraday cup to the target was assumed in our calculations. The efficiency of 25% should thus be considered a lower limit.

The maximum efficiency as a function of helium gas pressure was reached at a pressure of 1.5 mbar using the reaction ^{165}Ho(^{40}Ar,xn)$^{205-x}$At. The result was somewhat higher than expected on the basis of the longer path length of an ion in the helium gas, as compared with ref. [Ghi88]. This observation is consistent with results obtained using the Dubna gas-filled separator [Oga95].

A typical energy spectrum of the low amplification branch observed at the focal plane detector system is shown in figure 3.4 (see the next section for more details of the detector system used in RITU). The spectrum is taken from the reaction ^{35}Cl + ^{170}Yb at bombarding energy of 5.3 MeV/nucleon. From the figure, the suppression factor of the full energy ^{35}Cl beam particles was calculated to be $8{\cdot}10^{-14}$. Similarly, for the full energy ^{56}Fe beam particles the suppression factor was calculated to be $2{\cdot}10^{-12}$ at a bombarding energy of 4.57 MeV/nucleon.

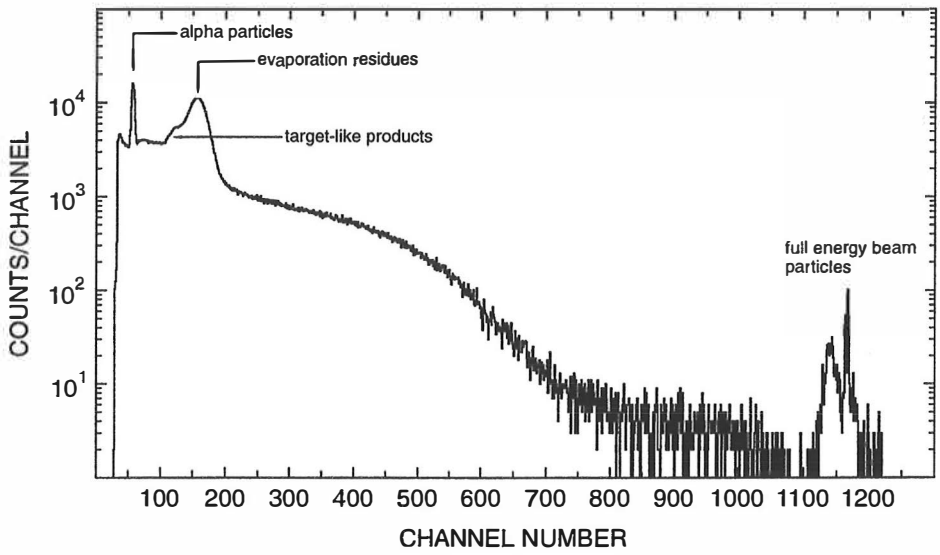

Figure 3.4 The low amplification branch energy spectrum from the reaction $^{35}Cl + ^{170}Yb$ at bombarding energy of 5.3 MeV/nucleon observed at the focal plane detector system. The full energy beam particles do not occur in one peak because different PAD-strips had different amplifications.

Activities having production cross sections of a few nanobarns have been studied so far with the gas-filled recoil separator RITU. Observation of activities with production cross sections below one nanobarn should be possible. The most important parameters of RITU are shown in table 3.2.

Transmission of heavy ions as determined by simulation

A simulation program was developed in the present work for determining the transmission and obtaining the ideal magnetic (quadrupole) settings of our gas-filled separator.

In the simulation program both the multiple scattering and the electronic charge exchange between a heavy ion and the helium-gas atom were taken into consideration. The multiple scattering process was calculated according to the procedures

Table 3.2 The most important RITU parameters.
D = the dipole magnet,
Q_1 = the first quadrupole magnet,
Q_{23} = the second and the third quadrupole magnet.

maximum beam rigidity	2.2 Tm	pole face rotation of D	0^o, -25^o
horizontal acceptance	±30 mrad	aperture diameter of Q_1	105 mm
vertical acceptance	±80 mrad	maximum gradient of Q_1	13.5 T/m
dispersion	10 mm/%	length of Q_1	350 mm
transmission	1 - 50 %	aperture diameter of Q_{23}	200 mm
beam suppression	10^{-12} - 10^{-15}	maximum gradient of Q_{23}	6.0 T/m
bending radius of D	1850 mm	length of Q_{23}	600 mm
maximum field of D	1.2 T	total length	4.8 m
bending angle of D	25^o	total mass	17500 kg
pole gap of D	100 mm	total cost	2.3 MFIM

proposed by Biersack and Haggmark [Bie80] and Eastham [Eas75]. The charge exchange process was taken into account according to the procedure proposed by Paul et al. [Pau89]. For calculating the emission angle of a heavy ion from the target, formulas suggested by Dionisio et al. [Dio89] were used. This emission angle is determined by the multiple scattering of a heavy ion inside the target and the evaporation of neutrons from the compound nucleus. The path of a heavy ion was obtained by integrating the equation of motion. The average charge state was calculated using the equation (3.6). The tables of Northcliffe and Shilling [Nor70] were used to estimate the heavy ion energy loss.

Figure 3.5 shows a few examples of simulated transmission calculations of ^{194}At and ^{211}Ac isotopes, which were produced in reactions ^{141}Pr(^{56}Fe, 3n)^{194}At and ^{175}Lu(^{40}Ar, 4n)^{211}Ac, respectively, with bombarding energies 4.43 and 5.0 MeV/nucleon. The target thicknesses were 200 and 300 μg/cm^2 for ^{141}Pr and ^{175}Lu, respectively, and the pressure of the helium gas was 1.5 and 1.0 mbar. The number of simulated ions was 6000.

Two different sets of curves are shown in each figure. The upper set in each figure (full symbols) is the transmission, i.e. the number of ions at the focal plane. The lower set of curves (open symbols) describes the number of ions implanted on the focal plane detector with the size of 80 mm × 35 mm, corresponding to the size of our PIPS detector. The transmission curves are plotted as a function of the

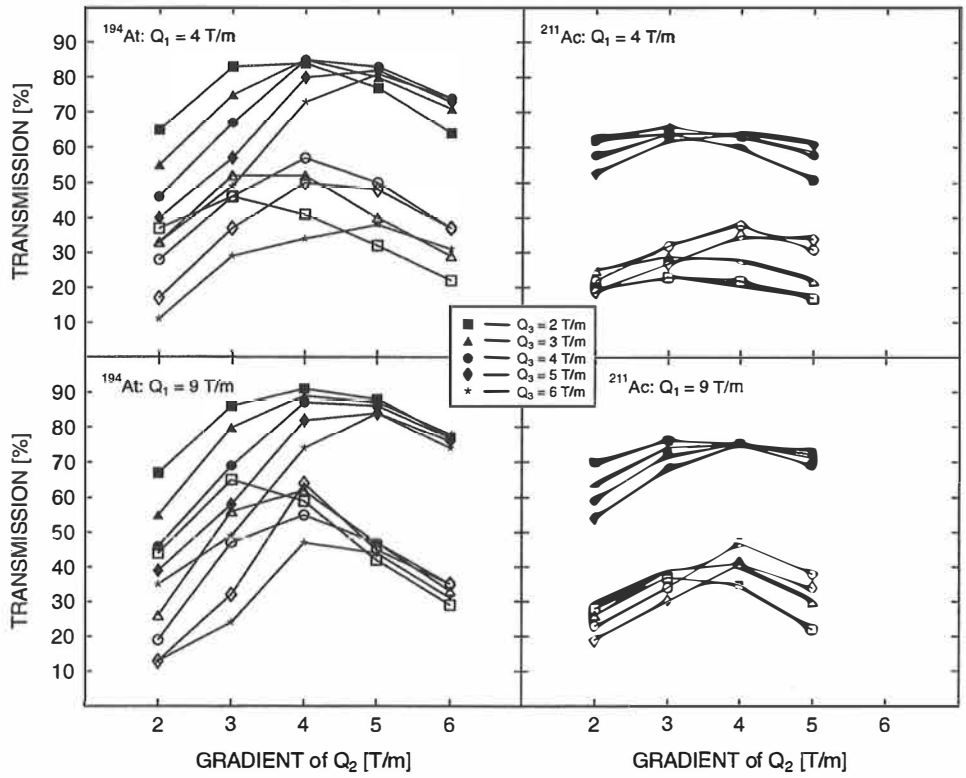

Figure 3.5 Simulated transmission of ^{194}At and ^{211}Ac ions as a function of gradients of the three quadrupoles of the gas-filled separator RITU. See text for more details.

gradient of the second and the third quadrupoles (Q_2 and Q_3) and for two gradient values of the first quadrupole (Q_1).

By comparing different sections of figure 3.5 it can be seen that the transmission of ^{194}At ions is about 20% higher than the transmission of ^{211}Ac ions. This is purely due to the reaction kinematics: the heavier beam particle gives the higher momentum to the compound nucleus and the effect of the multiple scattering inside the target and in the gas-filling is smaller.

The first quadrupole focuses vertically giving a better matching to the aperture of the dipole chamber. In the case of iron beam, angular spread of ^{194}At ions is quite narrow and the effect of the first quadrupole is quite small. A better

transmission of about 10% relative increase is given in the case of ^{211}Ac when the higher gradient of the first quadrupole is used. In the vertical direction essentially all of the transmitted particles can be collected into the focal plane detector. This can be seen from the experimental and simulated focal plane distributions.

The gradient of 9 T/m is not necessarily the optimum value but rather a typical value. The value of about 4 T/m was used in measurements in the present work. The reason for the lower value was a relatively high background of beam particles if higher gradient values were used in the first quadrupole. This problem was later on solved by readjusting our beam dump system, and the full range of the gradient of the first quadrupole can now be used.

3.3 The detector system

The gas-filled recoil separator RITU has been designed to select all evaporation residues from the primary beam coming from the cyclotron and to transport the separated reaction products to the detector system at the end of the device. The primary beam is guided into a beam dump for possible beam current measurement. The mass separation between evaporation residues is not possible due to the multiple scattering with gas atoms. Consequently, a versatile detector system is needed to identify evaporation residues. Commonly used detector systems consist of a position sensitive semiconductor stop detector at the focal plane and of a time-of-flight (TOF) detector. With the TOF detector scattered low energy beam particles can be separated from alpha decay events in off-line data analysis using an anticoincidence condition. The TOF detector can be used also for rough mass determination.

In the present work, RITU has been equipped with a focal plane semiconductor detector. It is a position sensitive PIPS (Passivated Implanted Planar Silicon) detector from Canberra Semiconductor, Belgium, with sixteen individual position sensitive strips in horizontal direction. These strips are called PADs and, due to the shortage of electronic components they were connected into pairs in the present work. The thickness of the PIPS detector is 300 μm and the effective size is 80 mm

in horizontal and 35 mm in vertical direction. Almost all (70% – 90%, depending on the reaction) of the transmitted evaporation residues were normally collected into the detector.

Signals obtained from both ends of each detector were amplified simultaneously with two different gains, one optimized for alpha particles (high amplification) and the other suitable for evaporation residues (low amplification). The full-scale gains were 20 MeV for high and 300 MeV for low amplification branch. Events registered inside the detector were collected into a computer hard disk in time ordered list mode for later off-line analysis. Magnetic tapes (EXABYTEs) were not needed due to the small average total counting rate. Each event consisted of the time of the occurrence and PAD number, energy and position (called TOP and BOTTOM) of high and low amplification, and beam phase (on/off) if pulsed beam was used. The energy of an event was obtained as a sum of the two signals and the two positions by dividing both signals by the sum (of the two signals). The purpose of the pulsed beam was to reduce the low energy background caused by scattered beam particles, because no TOF detector or other anticoincidence signal were used.

Figure 3.6 shows a block diagram of the PIPS detector and electronics components needed in the detector system. The system was planned and constructed by Juha Uusitalo [Uus96] on the basis of a similar system used by the SHIP-group at GSI (S. Hofmann). The time of the occurrence of an event was recorded with a precision of 0.1 ms. This was the precision of the so called fast clock. There was an overflow of the fast clock at every 6553.5 ms and the slow clock was incremented by one unit. The capacity of the slow clock was 256. The time cycle restarts from zero after the overflow of the slow clock.

The energy resolution in the high amplification branch of each PAD was typically 30 – 35 keV (FWHM) at about 7000 keV alpha particle energy. The detector was cooled down to about 10°C for some of the measurements. Lower temperatures cannot be achieved because of the heat of the filling gas of the separator. The size of the energy spectrum was 2 kbytes in the high amplification branch. The position resolution in the vertical direction was determined to be better than 0.5 mm (FWHM). The size of the position spectra was 1 kbyte. Position windows with sizes typically below 10 and 20 channels were used in the correlation search

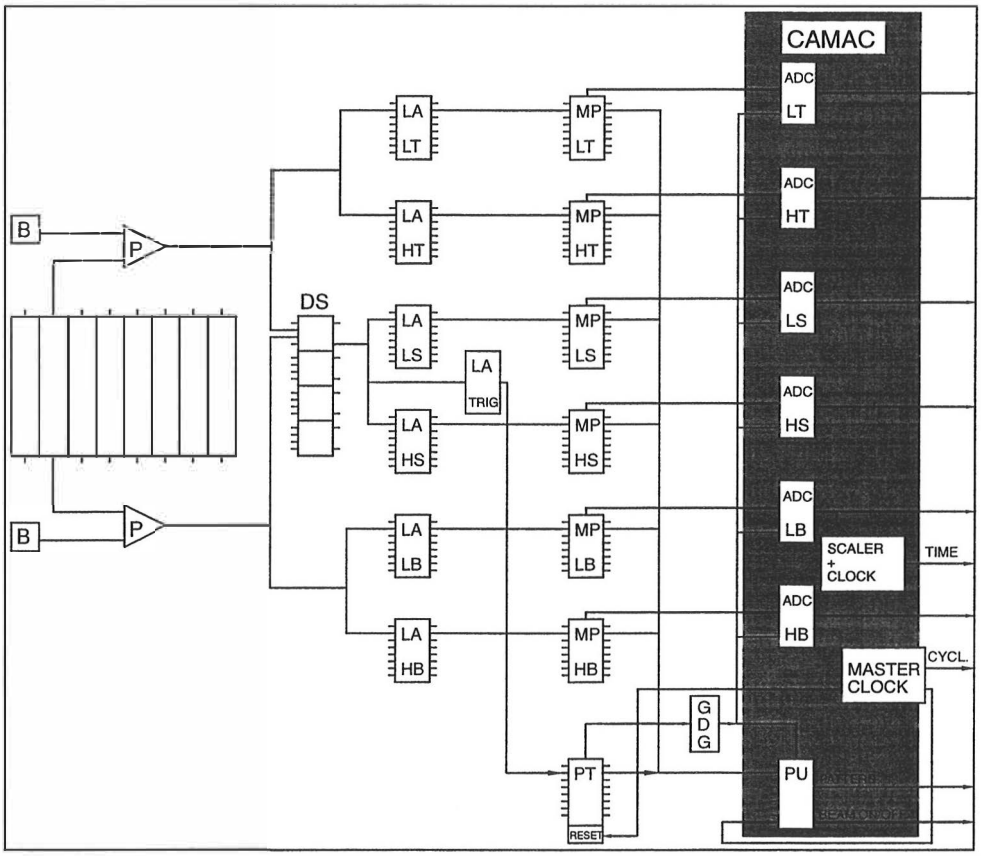

Figure 3.6 A block diagram showing the PIPS detector and measurement electronics. B = BIAS voltage supply, P = preamplifier (GSI-type) (16), DS = dual sum (TENNELEC TC253) (4), LA = octal main amplifier (GSI MA8000) (6), MP = 8 input analog multiplexer (GSI MX8000) (6), PT = 8 channel pattern trigger (GSI PT8000) (1), PU = 16 P pattern unit (1). (In parenthesis, the type and number of units is given).
H(L)T = High (Low) amplification TOP, H(L)B = High (Low) amplification BOTTOM, H(L)S = High (Low) amplification SUM.

of evaporation residues – mother alpha particles and mother alpha – daughter alpha particles pairs, respectively, corresponding a position resolution of about 2.5%. The dead time of the electronics/DAQ system was about 200 μs.

The implantation depth of evaporation residues is less than the range of 5 - 10 MeV alpha particles in silicon which means that alpha particles flying into backward directions (i.e. toward the target) do not deposit all of their energy and escape from the detector. The detection efficiency of full energy alpha particles was about

55%, depending on the reaction.

During the experiment, the collected data were monitored on-line with personal computers using programs developed by W.H. Trzaska, a member of our group. The data reduction software for obtaining alpha particle energies and half-lives from correlated alpha particle decay chains were written using VAX/VMS C-compilcr and cxccuted in a DEC Alphastation.

3.4 Data analysis

An introduction to the method used in the present work to obtain the alpha particle energy and the half-life of an activity is given in this section.

The technique of genetic correlations was applied for the analysis of experimental data. The whole data processing procedure was carried out off-line using data reduction software developed by our RITU group. The output of an experiment was a large number of files of ASCII format on the computer hard disk consisting of time ordered events registered by the focal plane detector. One event consisted of twelve parameters, but all parameters were not necessarily used in every experiment.

This tcchnique is suitable for the determination of activities with short half-lives only. The production rate of evaporation residues on the one hand and the counting rate of alpha-like events on the other hand limit the use of this technique for long half-lives. The upper limit can be estimated from the probability to produce decay chains by random correlations.

In the next sections, the technique of genetic correlations is described in more detail. In section 3.4.2, the method used in the present work to calculate alpha particle decay properties will be presented. In the last section of this chapter, a method for estimating the number of decay chains produced by random correlations will be described.

3.4.1 Correlated decay chains

Activities studied in the present work were identified off-line using the method of correlated alpha particle decay chains (see e.g. [Sch79, Sch84]). Chains of the type evaporation residue followed by a cascade of alpha particles are looked for. The method is based on the fact that the range of recoil nuclei from the alpha particle decay are small compared with the dimensions of individual detector units. The decay chain is then observed in the same small detector area determined by the position resolution. In the present work the use of the method was restricted to chains of the type evaporation residue – mother alpha particle – daughter alpha particle, where mother alpha particle stands for the alpha particle decay event of an evaporation residue and daughter alpha particle for the alpha particle decay event of the daughter nucleus which is assumed to be known. The previously unknown nucleus can thus be identified by its known daughter alpha particle decay.

In the following, chains of the type evaporation residue – mother alpha particle – daughter alpha particle are also called correlated triple chains.

In the correlation search, predefined energy, position and time windows for alpha particle decay of mother and daughter nuclei have to be determined. The energy window of evaporation residues was determined from the low amplification sum spectrum (see, for example, figure 3.4). Alpha particle energy windows are naturally determined by the estimated decay energy of the mother nucleus and the known decay energy of the daughter nucleus. The size of the position window is defined by the position resolution of the detector. The time window (i.e. the maximum time which can be used to look for alpha particle decay) depends on the one hand on the estimated half-life and on the other hand on the average counting rate of evaporation residues in the case of mother alpha particle decay.

Usually, half-lives of mother nuclei are so short that search times which are long enough for reliable half-life determination can be used. The average counting rate in the daughter alpha particle energy region is, in general, much higher than in the mother alpha particle energy region, and the maximum search time for daughter alpha particle decay is primarily determined by that counting rate. In case of a short maximum search time a correction to the measured half-life has to be made (see the next section).

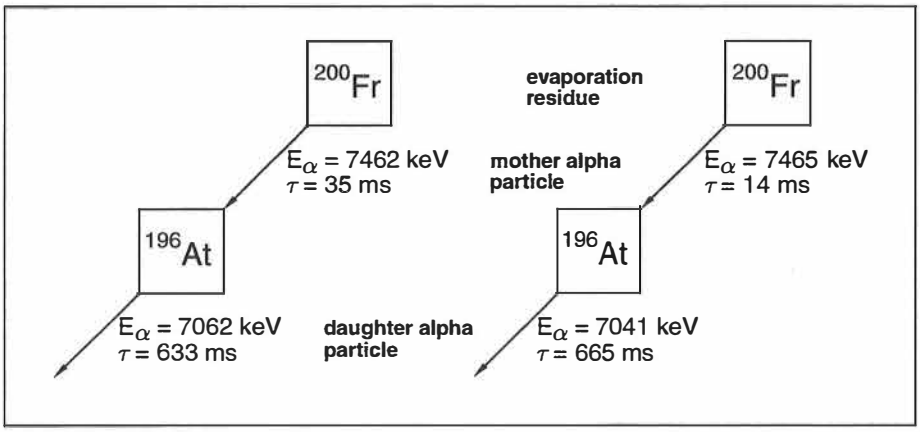

Figure 3.7 Two examples of typical decay chains of the type evaporation residue – mother alpha particle – daughter alpha particle observed at the focal plane detector in the present work. All members of a chain occur in the same small area determined by the position resolution of the detector.
These two decay chains belong to the new isotope ^{200}Fr discussed in chapter 4.

In figure 3.7 two typical correlated triple chains observed in the present work are shown. Initially, the mother nucleus (evaporation residue) was unknown but by showing that its daughter alpha particle decay originates from ^{196}At, the mother decay was identified as belonging to the new isotope ^{200}Fr. Altogether six chains of the type evaporation residue – mother alpha particle – daughter alpha particle were assigned to ^{200}Fr. See chapter 4 for a detailed discussion on experimental results.

3.4.2 Maximum likelihood method

The methods of determination of alpha particle decay properties, i.e. the alpha particle energy and half-life, used in the present work, will be described. The alpha particle half-life $T_{1/2}$ was determined by calculating the arithmetic mean of individual life times. This method is called the maximum likelihood method. In a case of small statistics, this method is more reliable than making a fit of a semilogarithmic decay curve of number of counts versus time. The correction to the life time τ of an activity due to the finite search time T can be calculated iteratively from the equation [Seg65]

$$\tau = \frac{1}{N}\sum_{n=1}^{N}\tau_n + \frac{T}{e^{T/\tau}-1}, \tag{3.7}$$

where N is the number of nuclei and τ_n is the lifetime of the n:th individual nucleus. The lower and upper limits τ_ℓ and τ_u, respectively, of the life time at the 68.3% confidence level can be calculated from equations [Sch84]

$$\begin{aligned} \tau_\ell &= \frac{\tau}{1+1/\sqrt{N}}, \\ \tau_u &= \frac{\tau}{1-1/\sqrt{N}}. \end{aligned} \tag{3.8}$$

These equations are valid for $N \geq 2$. Figure 3.8 shows an example of a life time distribution curve. The horizontal axis (life time) is plotted on logarithmic scale, which is the more suitable way in a case of small statistics. Three different confidence levels are also shown in the figure, they are 68.3%, 95.5% and 99.7% corresponding to the widths of 1σ, 2σ and 3σ, respectively. In the present work, error limits of the half-life are calculated using 68.3% confidence level.

The alpha particle energy E_α was calculated, if possible, as an aritmethic mean of the individual alpha particle energies $E_{\alpha n}$:

$$E_\alpha = \frac{1}{N}\sum_{n=1}^{N} E_{\alpha n}. \tag{3.9}$$

If equation (3.9) could not be used, the alpha particle energies were determined by making a fit of gaussian curves of counts versus energy. This kind of situation occurs when there are several alpha particle energies which are so close to each other that it is not possible to separate the decay energies. The instrumental part on the error of the alpha particle energy was calculated assuming 30 keV or 35 keV energy resolution (FWHM) at around 7000 keV alpha particle energy. In the energy calibration it was assumed that channel numbers were free of errors.

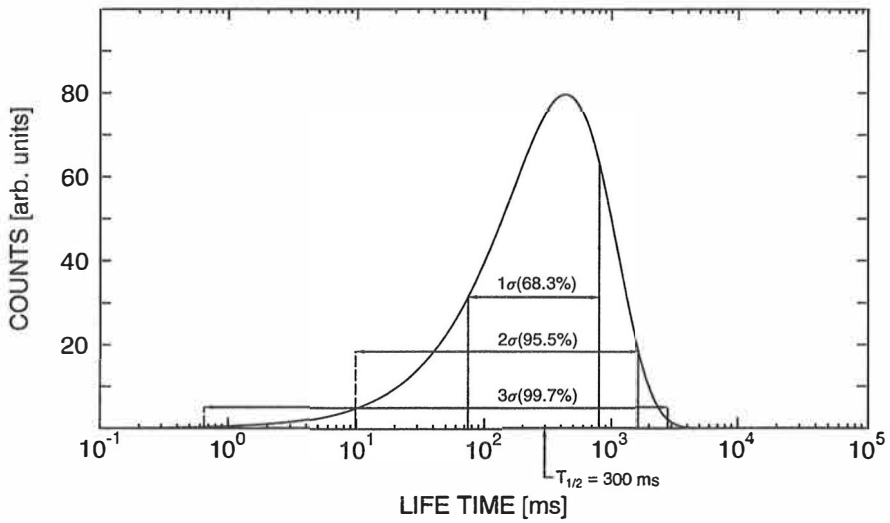

Figure 3.8 Life time distribution calculated for an activity with $T_{1/2}$ = 300 ms showing three different confidence levels. The 68.3% confidence level is used in this work. Note the logarithmic time (horizontal) axis.

3.4.3 The number of accidental correlations

The number of chains of the type evaporation residue – mother alpha particle – daughter alpha particle produced by random correlations can be estimated from the average counting rates of evaporation residues and mother and daughter alpha-like events in a single detector unit [Sch84]. It has been assumed that the average counting rate of the events that produce accidental triple correlations is constant and that the events are independent of each other, i.e. they obey Poisson statistics.

The number of accidental correlations, N_{acc}, can be obtained from the equation [Sch84]

$$N_{acc} = \sum_{i=1}^{n_u} N_{evaps}(i) \cdot \frac{\lambda_m(i) \cdot \lambda_d(i)}{\lambda_t(i)^2} [1 - e^{-\lambda_t(i)\Delta t_m}] [1 - e^{-\lambda_t(i)\Delta t_d}], \qquad (3.10)$$

where n_u is the assumed number of single detector units and $N_{evaps}(i)$ is the number of evaporation residues in detector unit i. $\lambda_m(i)$ and $\lambda_d(i)$ are average counting

rates of mother and daughter alpha-like events in detector unit i, respectively. $\lambda_t(i)$ is the total counting rate (i.e. the sum of the average counting rates of evaporation residues and mother and daughter alpha particles) and Δt_m and Δt_d are maximum search times for mother and daughter alpha particles, respectively.

It should be stressed that the number N_{acc} obtained from equation (3.10) is valid for triple chains with ALL members produced randomly. It cannot be used for triple chains where 'true' correlation is known to occur between two events because Poisson statistics is not applicable any more.

The significance of the observed correlated triple chains, i.e. the probability that the observed number of correlated triple chains, N_{obs}, would have been produced by random correlations is given by

$$P_{err} = \sum_{n=N_{obs}}^{\infty} \frac{N_{acc}^n}{n!} e^{-N_{acc}}, \tag{3.11a}$$

and, if condition $N_{acc} \ll 1$ is fulfilled, the error probability can be approximated by the equation

$$P_{err} = \frac{N_{acc}{}^{N_{obs}}}{N_{obs}!}. \tag{3.11b}$$

The assignment of a new activity based on the use of genetic correlations relies on probabilities of producing random correlations. Correlated decay chains (triple chains in the present work) can be accepted if there is only a small probability to produce the observed number of triple chains by random correlations.

3.5 Calibration procedures

Position calibration. Due to two different amplification branches, one for alpha particles and the other for heavy evaporation residues, a calibration between vertical positions of alpha particles and evaporation residues was needed in each PAD. To avoid accidental evaporation residue – mother alpha correlations, a shortlived

activity that was seen as a peak in the singles alpha spectrum was used for position calibration. When pulsed beam was used only alphas observed during the beam pause were accepted. The upper limit on the half-life of the position calibration activity depends on the average counting rate of evaporation residues. In the present work activities with a half-life of a few hundred milliseconds were used.

From the position calibration coefficients new (TOP and BOTTOM) positions were calculated for alpha particles and they were then compared with the original (TOP and BOTTOM) positions of evaporation residues in the case of possible correlations. The position window used in the correlation search for evaporation residue – mother alpha particle pairs was obtained from the distribution of the position differences between alpha particle positions and original evaporation residue positions in the calibration run. (For an example, see figure 4.10 in section 4.2).

Energy calibration. A correction to the alpha particle energy signal was made before energy calibration. There was a very small dependence between the vertical position and observed energy of the alpha particle. This energy correction was taken from a linear fit to data points consisting of the BOTTOM position and energy of the alpha particle (BOTTOM position was used because of its better resolution compared with TOP position). The same activity was used in the determination of position calibration coefficients and energy correction.

The alpha particle energy calibration was a fit between channel numbers and corresponding alpha particle energies. Channel numbers (centroids) were assumed to be free of errors and only the error in energy was taken into account. Energy references were taken from the compilation of Rytz [Ryt91] if possible. The energy calibration procedure was performed separately for each of the detectors.

4 Experimental results

Measured alpha particle decay properties of neutron-deficient astatine, radon and francium isotopes produced in the present work are presented in this chapter. These activities were produced using reactions

$$^{141}\mathrm{Pr}(^{56}\mathrm{Fe},\ \mathrm{xn})^{197-x}\mathrm{At},$$
$$^{169}\mathrm{Tm}(^{35}\mathrm{Cl},\ \mathrm{xn})^{204-x}\mathrm{Rn},$$
$$^{170}\mathrm{Yb}(^{35}\mathrm{Cl},\ \mathrm{xn})^{205-x}\mathrm{Fr}.$$

The region of the nuclei studied can be seen in figure 4.1. Alpha decay properties, i.e. alpha particle energy and half-life were determined for the nuclei $^{193-195}$At, ^{197,198}Rn and $^{200-203}$Fr and these nuclei are framed with a thick solid line in figure 4.1. All these nuclei were produced in heavy-ion-induced fusion reactions followed by de-excitation by neutrons. Decay properties of isotopes formed by evaporation of protons or alpha particles were not determined in the present work.

Inadequate beam diagnostics did not allow an accurate determination of the production cross sections of evaporation residues in the present work. Consequently, the production cross sections are given only in the form of tables with obtained maximum values presented, no excitation curves are shown. The accuracy of production cross sections was estimated to be a factor between two and three. All necessary corrections such as particle losses due to finite search times, escaping alpha particles and assumed efficiency of the separator were taken into account in the calculations. The behaviour of the production cross sections as a function of bombarding energy was, however, quite as expected supporting the assignments.

Identification of astatine isotopes ^{194,195}At has not been published but has been reported in theses of S. Yashita [Yas83] and M. Leino [Lei83]. Alpha particle decay of isotopes ^{197}Rn and ^{200}Fr was observed independently by Morita et al. [Mor95] at RIKEN. All these studies were made using a gas-filled separator.

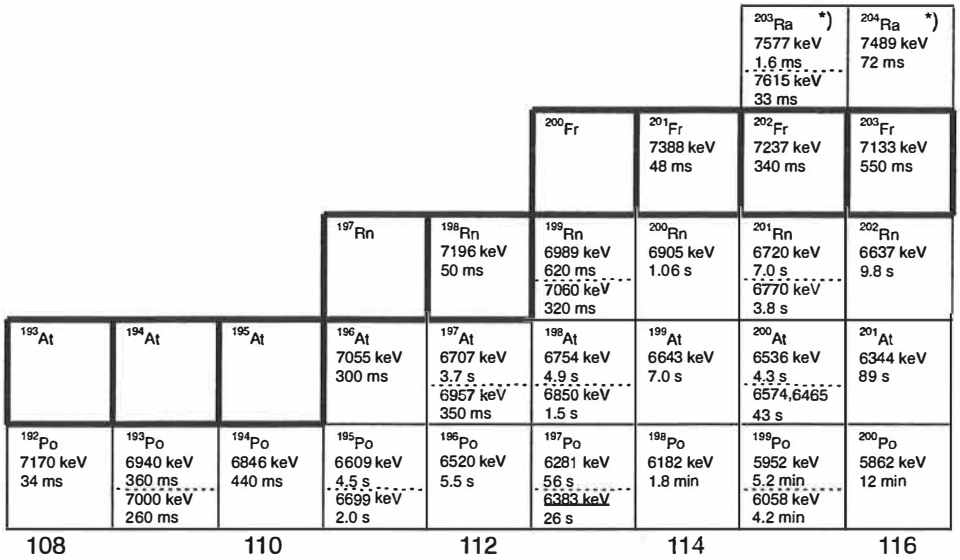

Figure 4.1 The region of the nuclei studied in the present work. Alpha particle decay properties were determined for nuclei that are framed with a thick solid line. If no alpha particle energy and half-life are given then the isotope was previously unpublished (see, however, the text for isotopes ^{197}Rn and ^{200}Fr).
*)Radium isotopes ^{203,204}Ra were also unknown isotopes; they were produced and identified at our gas-filled separator and their alpha decay properties are discussed in refs. [Lei96, Uus96].

In the next sections, experimental details and results from the three different measurements mentioned above are given. Section 4.1 deals with the reaction ^{56}Fe + ^{141}Pr and in sections 4.2 and 4.3 the reactions ^{35}Cl + ^{169}Tm and ^{35}Cl + ^{170}Yb, respectively, are discussed.

4.1 The reaction ^{56}Fe + ^{141}Pr

The reaction ^{141}Pr(^{56}Fe, xn)$^{197-x}$At was used for the production of neutron-deficient astatine isotopes. Ten different bombarding energies of $^{56}Fe^{11+}$, ranging from 4.11 to 4.86 MeV/nucleon, were used and they were adjusted by degrader foils of havar and nickel with thicknesses of 1.8 mg/cm^2 (havar) and 1.4, 0.9 and 0.45 mg/cm^2 (nickel). Corresponding excitation energies of the ^{197}At compound

nucleus were calculated to range from 24 to 54 MeV. The original beam energy from the cyclotron was 5.05 MeV/nucleon (283 MeV). The beam window of 0.45 mg/cm^2 nickel separated the high vacuum of the cyclotron and the filling gas (pressure 1.6 mbar) of the separator. The thicknesses of the two ^{141}Pr targets were 100 μg/cm^2 (evaporated on a 390 μg/cm^2 nickel foil) and 270 μg/cm^2 (evaporated on a 40 μg/cm^2 carbon foil).

The beam current of ^{56}Fe varied from 150 to 350 nA measured from a Faraday cup in front of the target. Beam macro pulsing with a ratio of 10 ms beam on and 10 ms beam off was applied for several bombarding energies. Irradiation times were between four and nine hours, except for the two highest bombarding energies they were 20 and 14 hours, respectively. The energy region of evaporation residues was determined to be between 20 – 45 MeV (nominal) in the low amplification branch.

Table 4.1 Activities used for alpha particle energy and position calibrations. The ^{194}Po alpha peak, produced with a high cross section in nearly all bombardments, was used for making a position calibration between evaporation residues and alpha particles. ^{150}Dy was produced in transfer reactions at lower bombarding energies.

Nuclide	E_α	Ref.	$T_{1/2}$	Ref.
^{150}Dy	4233±3 keV	[Mat86]	7.17±0.05 min	[Mat86]
^{191}Bi	6310±3 keV	[Ryt91]	12±1 s	[Bro89]
^{193}Po^g	6940±20 keV	[Shi90]	360±50 ms	[Shi90]
^{193}Po^m	7000±20 keV	[Shi90]	260±20 ms	[Shi90]
^{194}Po	6844±3 keV	[Ryt91]	440±60 ms	[Sin89]
^{195}Po^g	6613±7 keV	[Ryt91]	4.5±0.5 s	[Chu89]
^{195}Po^m	6701±4 keV	[Ryt91]	2.0±0.2 s	[Chu89]

Activities used for the alpha particle energy and position calibrations are shown in table 4.1. Position calibration between evaporation residues and mother alpha particles was obtained from the short lived activity ^{194}Po. The sizes of the position windows between evaporation residue and mother alpha particle and mother alpha and daughter alpha particles were estimated to be ±6 and ±9 units, respectively, corresponding to the position resolution better than 1.5%. See the end of chapter 5 for a discussion of the production of ^{150}Dy.

A low energy germanium detector (LeGe) was installed behind the position sensitive PIPS detector for detecting gamma rays and X-rays in coincidence with alpha particles. The width of the coincidence gate was 10 μs. The active area of the LeGe detector was 1000 mm^2 and its thickness 10 mm.

Irradiations were processed in three different groups according to the astatine isotope (^{193,194,195}At) that was produced most abundantly at a certain bombarding energy. Group I consists of the three lowest bombarding energies (4.11, 4.23 and 4.29 MeV/nucleon) and the main astatine product was ^{195}At. In group II (at bombarding energies 4.39, 4.43 and 4.57 MeV/nucleon) the main astatine product was ^{194}At. ^{193}At was looked for at the four highest bombarding energies of 4.68, 4.71, 4.79 and 4.86 MeV/nucleon (group III). Correlation plots of groups I, II and III are shown in figures 4.2, 4.4 and 4.7, respectively, together with corresponding singles alpha particle energy spectra.

Group I

Mother and daughter alpha particle energies for correlated triple chains obtained at bombarding energies of 4.11, 4.23 and 4.29 MeV/nucleon (group I) are shown in figure 4.2a. Maximum search times of 4.0 s and 70 s (beam off) and 2.4 s and 40 s (beam on) were used in the correlation search of evaporation residue – mother alpha particle pairs and mother alpha – daughter alpha particle pairs, respectively. Correlated triple chains with both mother and daughter alpha particles occurring during a beam on period have been discarded if macro pulsed beam was used. The reason was a relatively high estimated number of randomly produced triple chains of such type. The alpha particle energy window was 6900 keV – 7700 keV for mother and 6000 keV – 7000 keV for daughter alpha particles.

The daughter alpha particle energy and half-life of (6871 ± 4) keV and (91^{+20}_{-14}) ms, respectively, were determined for correlated triple chains labelled by (3) in figure 4.2a. This decay was assigned to the alpha decay of an isomeric state in ^{191}Bi (E_α = (6874 ± 5) keV and $T_{1/2}$ = (150 ± 15) ms [Lei81, Ryt91]). The number of observed triple chains was 30 at the three lowest bombarding energies. The corresponding mother alpha particle energy of (6953 ± 4) keV and half-life of (390^{+100}_{-60}) ms were measured and assigned to the new isotope ^{195}At. The number of triple chains produced by random correlations in group I was estimated to be

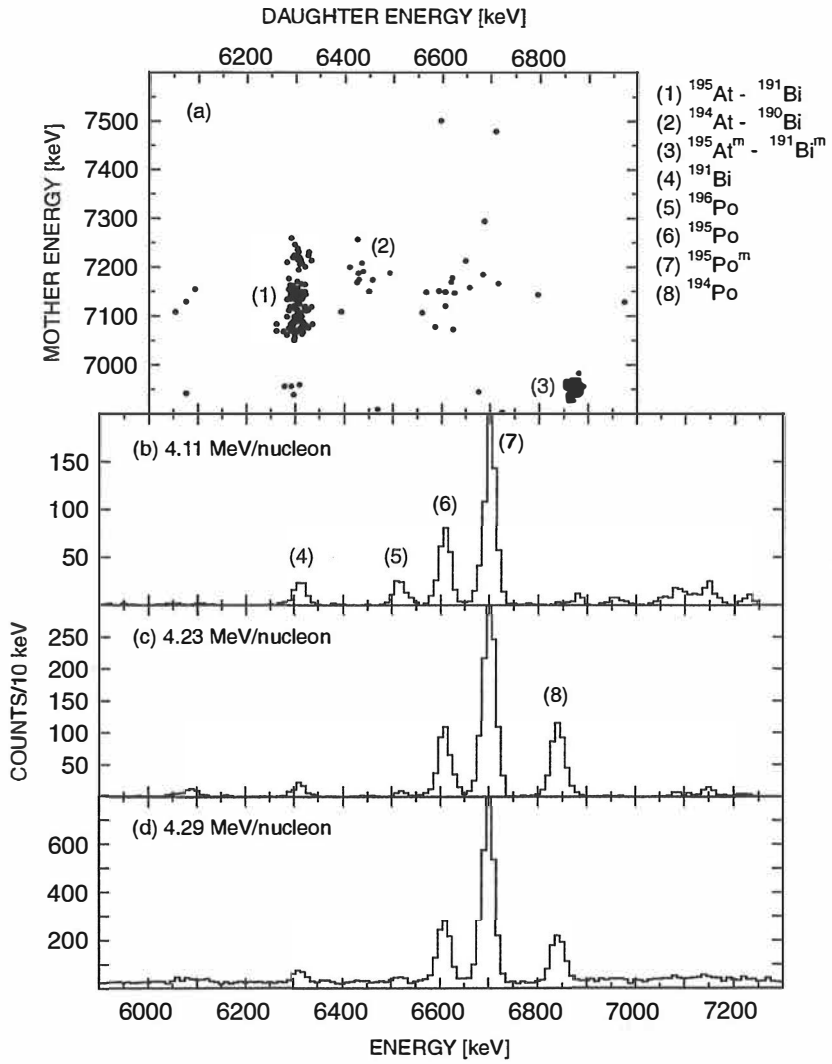

Figure 4.2 (a) Mother and daughter alpha particle energies for all correlated chains of the type evaporation residue – mother alpha particle – daughter alpha particle observed in the bombardment $^{56}Fe + ^{141}Pr$ with energies 4.11, 4.23 and 4.29 MeV/nucleon (group I). The alpha particle energy window was 6900 keV – 7700 keV and 6000 keV – 7000 keV for mother and daughter alpha particles, respectively. Maximum search times were 4.0 s for evaporation residue – mother alpha particle pairs and 70 s for mother – daughter alpha particle pairs if the alpha particle was observed in a beam pause. If the alpha particle was observed in a beam pulse, time windows were 2.4 s and 40 s.
(b,c,d) Singles alpha particle energy spectra with bombarding energies 4.11 (b), 4.23 (c) and 4.29 MeV/nucleon (d). Beam pause spectra are shown at energies 4.11 and 4.23 MeV/nucleon.

about 0.006 in the energy region of 6900 keV – 7000 keV (mother) and 6850 keV – 6900 keV (daughter).

The decay pattern where the daughter alpha particle decay was assigned to the ground state alpha particle decay of ^{191}Bi (E_α = (6310 ± 3) keV and $T_{1/2}$ = (12 ± 1) s [Ryt91] and labelled by (1) in figure 4.2a) was observed to be surprisingly complicated compared with what was expected on the basis of ^{197}At (two known alpha transitions: E_α = (6958 ± 5) keV, $T_{1/2}$ = (350 ± 40) ms for ground state and E_α = (6707 ± 5) keV, $T_{1/2}$ = (3.7 ± 0.25) s for isomeric state [Ryt91, Chu91]). The number of accidental triple chains in the energy region of 7000 keV – 7300 keV (mother) and 6250 keV – 6350 keV (daughter) was estimated to be 0.037 while the number of observed correlated triple chains in the same energy region was 130.

Figure 4.3a shows the alpha particle energy spectrum taken as a projection onto the vertical (mother) axis from the correlated triple chains observed in the mother alpha particle energy range of 7000 keV – 7300 keV and daughter alpha particle energy range of 6250 keV – 6350 keV. Three gaussian peaks were fitted for obtaining the alpha particle energy for the mother nucleus. The maximum likelihood method could not be used for energy determination because mother events cannot be distinguished clearly enough. As a result of the fit three mother alpha particle energies were obtained: (7081 ± 4) keV (39), (7117 ± 5) keV (22) and (7149 ± 4) keV (43). The number in parentheses after the energy gives the number of counts in the peak. The alpha particle energy of the peak with the highest energy was determined using the maximum likelihood method and the value of (7221 ± 4) keV was obtained from 25 counts.

The life time distribution of evaporation residues taken from correlated triple chains from energy region 7000 keV – 7300 keV (mother) and 6250 keV – 6350 keV (daughter) and labelled by (1) in figure 4.2a is shown in figure 4.3b. According to the life time distribution all four mother alpha transitions given above would seem to belong to one state only or to several states with roughly the same half-life. The fitted curve has not been used for the alpha particle half-life determination. Instead, the half-life has been determined by the maximum likelihood method to be (142^{+14}_{-12}) ms. For the daughter nucleus ^{191}Bi, an alpha particle energy of (6305 ± 4) keV and a half-life of $(11.3^{+1.2}_{-0.9})$ s were determined from 130 correlated triple chains.

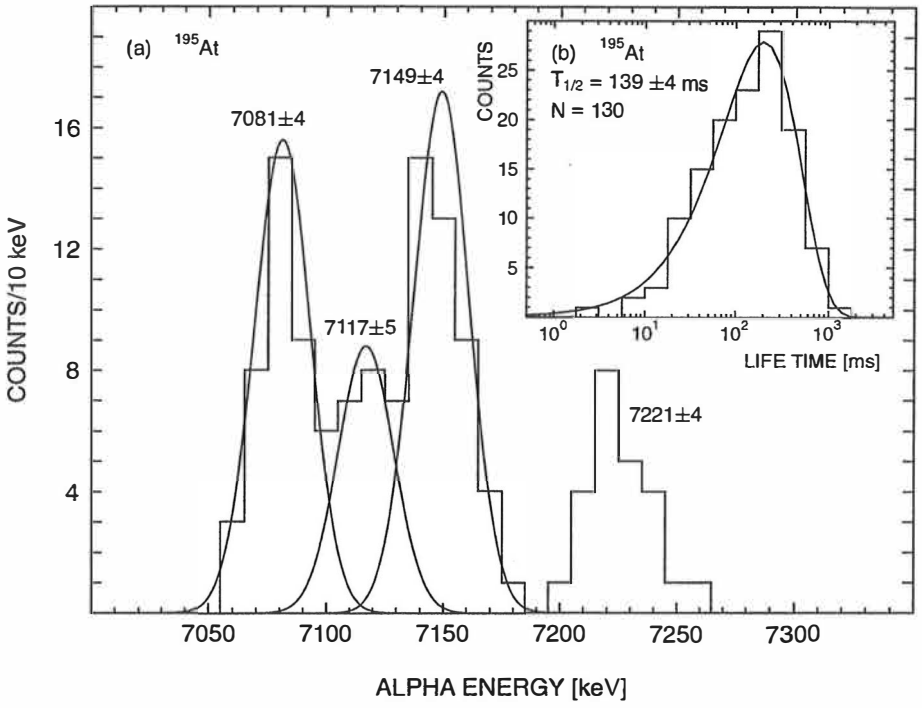

Figure 4.3 (a) Alpha particle energy spectrum of ^{195}At extracted from correlated triple chains with energy range 7000 keV – 7300 keV (mother) and 6250 keV – 6350 keV (daughter). Three mother alpha particle energies obtained by a fit of gaussian peaks are also shown. The alpha particle energy of the peak with the largest energy (~ 7220 keV) was determined using the maximum likelihood method.
(b) Life time distribution of ^{195}At, extracted from mother alpha particle life times of correlated triple chains. The fit is not used for half-life determination, but is shown rather as a quide to the eye.

All these four mother alpha particle transitions ((7081 ± 4) keV, (7117 ± 5) keV, (7149 ± 4) keV and (7221 ± 4) keV) with a common half-life (142^{+14}_{-12}) ms were assigned to the new isotope ^{195}At. In chapter 5 an interpretation in terms of fine structure in alpha particle decay of ^{195}At versus partial summing of conversion electron energies with the alpha particle energy will be discussed.

Group II

Figure 4.4 shows correlated triple chains (a) and singles alpha particle energy spectra (b-d) at bombarding energies 4.39, 4.43 and 4.57 MeV/nucleon (group

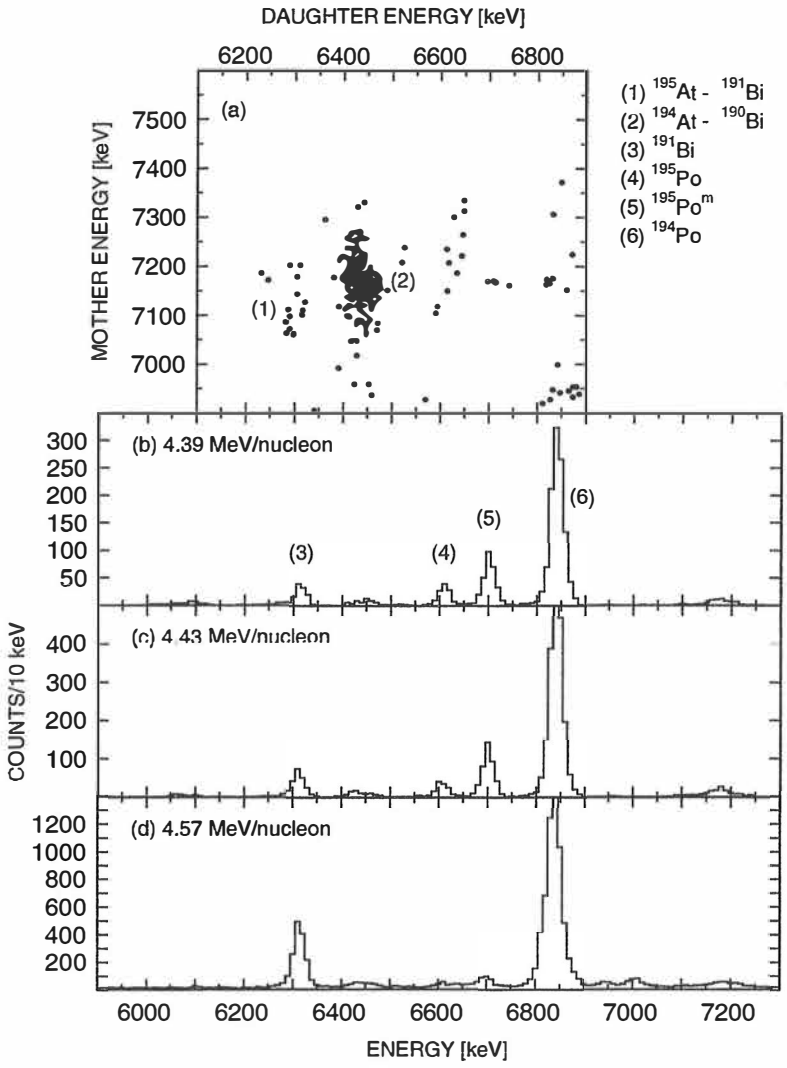

Figure 4.4 (a) Mother and daughter alpha particle energies for all correlated chains of the type evaporation residue – mother alpha particle – daughter alpha particle observed in the bombardment ^{56}Fe + ^{141}Pr with energies 4.39, 4.43 and 4.57 MeV/nucleon (group II). The alpha particle energy window was 6900 keV – 7700 keV and 6100 keV – 6900 keV for mother and daughter alpha particles, respectively. Maximum search times were 2.0 s for evaporation residue – mother alpha particle pairs and 30 s for mother – daughter alpha particle pairs when the alpha particle was observed in the beam pause. For alpha particles observed in the beam pulse, time windows were 1.6 s and 20 s, respectively.
(b,c,d) Singles alpha particle energy spectra at bombarding energies 4.39 (b), 4.43 (c) and 4.57 MeV/nucleon (d). Beam pause spectra are shown at energies 4.39 and 4.43 MeV/nucleon. (Measurements were carried out also without beam pulsing at these two energies, but the spectra are not shown.)

II). In fact, there are triple chains from five different measurements in figure 4.4a because all three bombarding energies were made use of without beam macro pulsing and moreover bombarding energies 4.39 and 4.43 MeV/nucleon were used also with beam macro pulsing. The pulsing ratio was 10 ms beam on and 10 ms beam off. The singles alpha particle energy spectra are beam off spectra at 4.39 and 4.43 MeV/nucleon. Maximum search times of 2.0 s in beam pause and 1.6 s in beam pulse were used to look for evaporation residue – mother alpha particle pairs and 30 s (off) and 20 s (on) were used for mother alpha particle – daughter alpha particle pairs.

An accumulation of correlated triple chains can be seen at daughter alpha particle energy around 6450 keV. This energy can be assigned to ^{190}Bi, where two alpha decaying states with the assumed low and high spin, respectively, have been observed ((3^+): $E_\alpha = (6430 \pm 5)$ keV and $T_{1/2} = (6.3 \pm 0.1)$ s; (10^-): $E_\alpha = (6455 \pm 5)$ keV and $T_{1/2} = (6.2 \pm 0.1)$ s [Sin90]). The corresponding broad mother alpha particle energy interval can then be assigned to the new isotope ^{194}At.

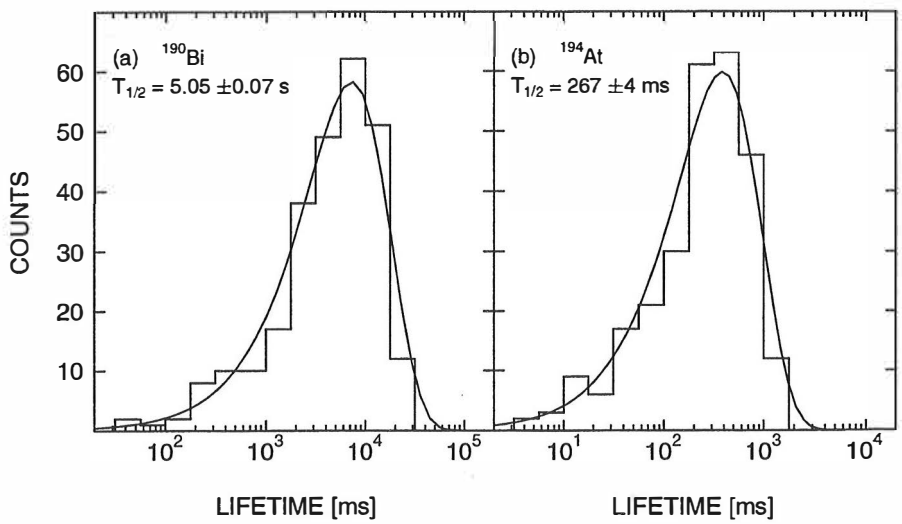

Figure 4.5 Life time distribution of ^{190}Bi and ^{194}At, extracted from daughter and mother alpha particle life times of correlated triple chains assigned to ^{194}At – ^{190}Bi pairs in the energy region 7000 keV - 7300 keV (mother) and 6350 keV – 6500 keV (daughter). The half-lives are obtained from the fit and curves are just to guide the eye.

The life time distributions of correlated triple chains of the mother and daughter activities from alpha particle energy region 7000 keV – 7300 keV (mother) and 6350 keV – 6500 keV (daughter) are shown in figure 4.5. According to these life time distributions the half-lives of the assumed low and high spin states in ^{190}Bi are very close to each other and cannot be distinguished with the statistics available. The half-lives of ^{190}Bi and ^{194}At were determined by the maximum likelihood method to be $(5.8^{+0.4}_{-0.3})$ s and (276^{+19}_{-16}) ms, respectively.

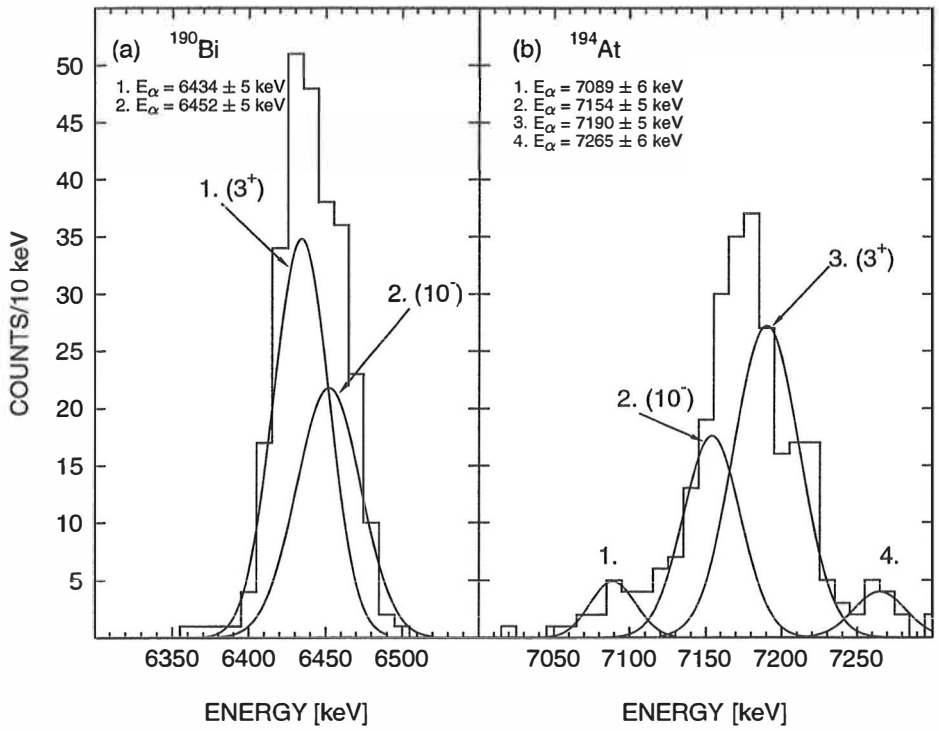

Figure 4.6 Alpha particle energy spectra of ^{190}Bi and ^{194}At extracted from correlated triple chains with energy range 7000 keV – 7300 keV (mother) and 6350 keV – 6500 keV (daughter). All alpha particle energies assigned to ^{194}At were obtained by a fit of four gaussian peaks. Transitions from the assumed low and high spin states are shown.

The determination of mother and daughter alpha particle energies is not a straightforward task in the present situation, because of the overlapping of alpha particle energy peaks. The number of correlated triple chains in the energy region 7000

keV – 7300 keV (m) and 6350 keV – 6500 keV (d) is too low for making a three dimensional alpha particle energy spectrum. Hence, projections from correlated triple chains of mother (daughter) alpha particle energies onto the vertical (horizontal) axis were used for energy determination. These spectra are shown in figure 4.6. Alpha particle energies of ^{190}Bi and ^{194}At were obtained by fitting two and four gaussian curves into the spectra of figure 4.6a-4.6b, respectively. Alpha particle energies of the assumed low and high spin states in ^{190}Bi were determined to be (6434 ± 5) keV (157) and (6452 ± 5) keV (115), respectively. The alpha particle energies of ^{194}At followed by an alpha particle decay assigned to the assumed low spin state in ^{190}Bi were determined to be (7190 ± 5) keV (147) and (7265 ± 6) keV (18). Counts in the peak are shown in parentheses after the energy value. The alpha particle energies of ^{194}At observed to populate the assumed high spin state in ^{190}Bi were determined to be (7089 ± 6) keV (18) and (7154 ± 5) keV (84). The total number of observed correlated triple chains in the energy region 7000 keV – 7300 keV (mother) and 6350 keV – 6500 keV (daughter) was 267 and the estimated number of randomly produced triple chains in the same energy window was 0.026.

In figure 4.4 correlated triple chains can be seen also at daughter alpha particle energies about 6300 keV and these triple chains can be assigned to ^{195}At – ^{191}Bi pairs. However, the alpha particle energy and half-life were not determined because of the too short maximum search time for ^{190}Bi. The number of these triple chains is, on the other hand, so low that they would not improve the statistics of ^{195}At.

Group III

Correlated chains of the type evaporation residue – mother alpha particle – daughter alpha particle belonging to the group III are shown in figure 4.7a. The corresponding singles alpha particle energy spectra are also shown. Beam pause spectra are shown in figures 4.7d-e. The alpha particle energy window was 7050 keV – 7800 keV and 6300 keV – 7400 keV for mother and daughter alpha particles, respectively. Maximum times for searching for mother alpha particles were 1.4 s and 1.0 s in beam pause and pulse, respectively, and for daughter alpha particles 8.0 s (beam off) and 5.0 s (beam on) were used. Correlated triple chains with mother and daughter alpha particles both observed during the beam pulse were also accepted due to the small number of randomly produced triple chains.

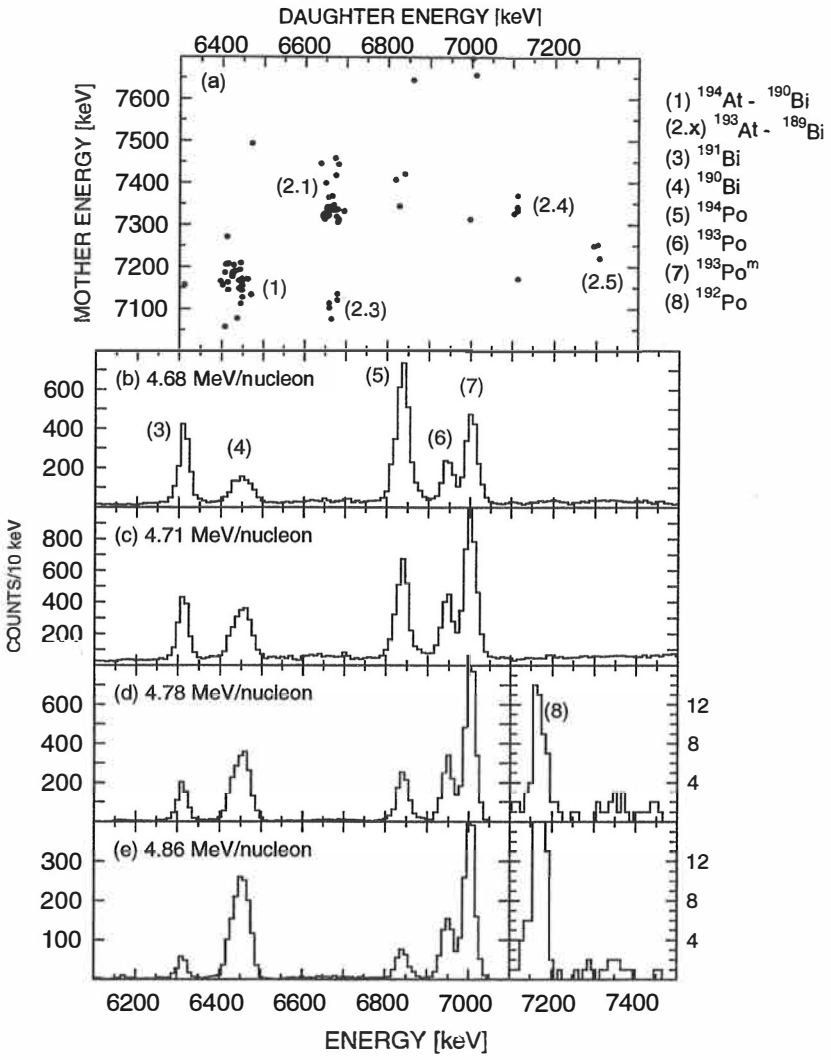

Figure 4.7 (a) Mother and daughter alpha particle energies for all correlated chains of the type evaporation residue – mother alpha particle – daughter alpha particle observed in the bombardment ^{56}Fe + ^{141}Pr with energies 4.68, 4.71, 4.79 and 4.86 MeV/nucleon (group III). The alpha particle energy window was 7050 keV – 7800 keV and 6300 keV – 7400 keV for mother and daughter alpha particles, respectively. Maximum search times were 1.4 s for evaporation residue – mother alpha particle pairs and 8.0 s for mother – daughter alpha particle pairs if the alpha particle was observed in a beam pause. If the alpha particle was observed in a beam pulse, time windows were 1.0 s and 5.0 s, respectively.
(b,c,d,e) Singles alpha particle energy spectra at bombarding energies 4.68 (b), 4.71 (c), 4.79 (d) and 4.86 MeV/nucleon (e). Beam pause spectra are shown at energies 4.79 and 4.86 MeV/nucleon.

Several different cases where the daughter alpha particle decay can be assigned to ^{189}Bi are seen in figure 4.7a. (The known decay properties of ^{189}Bi are as follows: ^{189}Bi: E_α = (6671 ± 5) keV, E_α = (7116 ± 15) keV and $T_{1/2}$ = (680 ± 30) ms [Fir90, Ryt91]; ^{189}Bi^m: E_α = (7300 ± 50) keV and $T_{1/2}$ = (5±2) ms [Fir90, And93]). These are labelled by (2.X) in figure 4.7a.

Daughter alpha particle energies of (6663 ± 4) keV and (6664 ± 6) keV were determined for groups of correlated triple chains labelled by (2.1) in figure 4.7a. The corresponding half-lives were determined to be $(1.0^{+0.3}_{-0.2})$ s and $(0.6^{+0.5}_{-0.2})$ s. These energy and half-life values were assigned to the ground state alpha particle decay of ^{189}Bi. Alpha particle energies of (7333 ± 5) keV and (7434 ± 7) keV with half-lives of (34^{+10}_{-6}) ms and (27^{+22}_{-8}) ms, respectively, were determined for mother activities which were assigned to the new isotope ^{193}At. The number of randomly produced triple chains was calculated to be 0.012 in the energy window covering both mother alpha particle energy regions. The number of observed correlated triple chains in the same energy window was 25 (20+5).

The ground state of ^{189}Bi is populated (according to the data shown in figure 4.7a) also by an alpha particle decay with the mother alpha particle energy and half-life of (7109 ± 6) keV and (28^{+22}_{-9}) ms. This decay with five observed triple chains and labelled by (2.3) was also assigned to the new isotope ^{193}At. An alpha particle energy of (6669 ± 6) keV and a half-life of $(1.2^{+1.5}_{-0.4})$ s were determined for the daughter nucleus. It was estimated that the number of randomly produced triple chains was 0.003.

An alpha particle energy of (7116 ± 15) keV with a branching ratio of 5% [Fir90] with respect to the (6671 ± 5) keV alpha transition has also been determined for the ground state of ^{189}Bi. We observed five correlated triple chains with the daughter alpha particle energy of (7111 ± 6) keV and the half-life of $(0.6^{+0.4}_{-0.2})$ s. An alpha particle energy of and a half-life of (7343 ± 7) keV and (33^{+27}_{-10}) ms, respectively, were determined for the corresponding mother nucleus, which was identified as the new isotope ^{193}At. The number of randomly produced triple chains in the energy region relevant for the present alpha transition was calculated to be 0.003. These correlated triple chains are labelled by (2.4) in figure 4.7a.

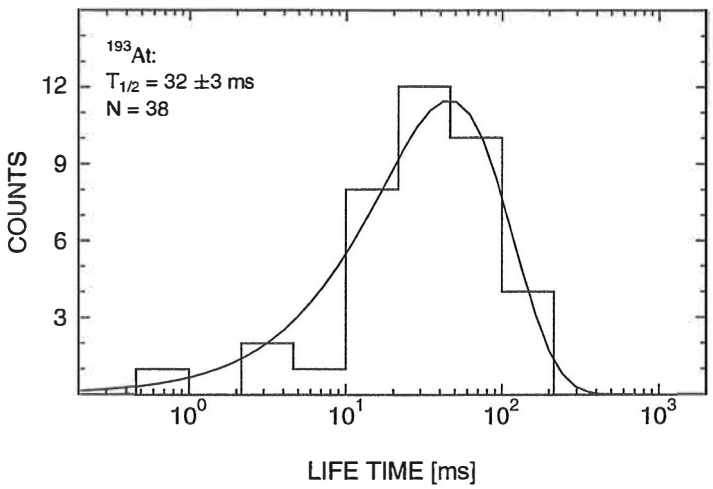

Figure 4.8 Life time distribution of ^{193}At, extracted from all events assigned to the new isotope ^{193}At. The fit is not used for half-life determination, but it is just to guide the eye. This distribution also includes life times of the three events labelled by (2.5) in figure 4.7a.

The daughter alpha particle energy and half-life of (7301 ± 8) keV and (2^{+3}_{-1}) ms, respectively, were determined from three correlated triple chains and assigned to an isomeric state of ^{189}Bi. An alpha particle energy of (7241 ± 8) keV and the half-life of (17^{+29}_{-6}) ms were obtained for the mother nucleus and it was also assigned to the new isotope ^{193}At. The number of randomly produced triple chains in the present case was estimated to be 0.003. This is labelled by (2.5) in figure 4.7a.

Figure 4.8 shows the life time distribution of all events assigned to the new isotope ^{193}At. The alpha particle half-life is not exctracted from the fit that is shown, it is rather to guide the eye. According to the distribution in figure 4.8, half-lives of all cases assigned to ^{193}At (including those labelled by (2.5) in figure 4.7a) are so close to each other that the data are compatible with decay of only one state.

Correlated triple chains labelled by (1) in figure 4.7a) can be assigned to ^{194}At – ^{190}Bi pairs. Alpha particle energies and half-lives were not determined because of the too short maximum search times.

The measured alpha particle decay properties of ^{193,194,195}At and ^{189,190,191}Bi nuclei are summarized in table 4.2 and compared with previously measured results (daughter). Measured values of production cross sections are given in table 4.3,

where E and E* refer to the bombarding and excitation energies, respectively, at which the highest value was obtained. Cross sections are also given (for comparison) for polonium isotopes ^{193,194,195}Po and they were calculated from intensities of alpha particle singles peaks in the spectra. The number of triple chains was used in cross section determination of astatine isotopes. A transmission of 20% and a detection efficiency of 70% of evaporation residues were assumed. Table 4.2 also includes the estimated half-lives of astatine isotopes calculated by using the method proposed by Rasmussen [Ras59].

Table 4.2 Alpha particle energies E_α and half-lives $T_{1/2}$ of activities measured in the present work. A half-life estimation of a mother activity $T^*_{1/2}$ is calculated using the method of Rasmussen [Ras59]. For daughter activities, a comparison with previous data is shown.

Mother nuclide	E_α [keV]	$T_{1/2}$ [ms]	Daughter nuclide	E_α [keV]	$T_{1/2}$ [s]	N	N_{acc}	E_α [keV]	$T_{1/2}$ [s]	Ref.	$T^*_{1/2}$ [ms]
^{193}At	7333±5	34^{+10}_{-6}	^{189}Bi	6663±4	$1.0^{+0.3}_{-0.2}$	20	0.012†	6671±5	0.68±0.3	[1, 2]	17
	7434±7	27^{+22}_{-8}		6664±6	$0.6^{+0.5}_{-0.2}$	5					
	7109±6	28^{+22}_{-9}		6669±6	$1.2^{+1.5}_{-0.4}$	5	0.003				
	7343±7	33^{+27}_{-10}		7111±6	$0.6^{+0.4}_{-0.2}$	5	0.003	7116±15	0.68±0.3	[1, 2]	
	7241±8	17^{+29}_{-6}		7301±8	2^{+3}_{-1}‡	3	0.003	7300±50	4±2‡	[1, 3]	36
^{194}At	7265±6	276^{+19}_{-16}	^{190}Bi	6434±5	$5.8^{+0.4}_{-0.3}$	267	0.026	6430±5	6.3±0.1	[4]	29
	7190±5										
	7154±5			6452±5				6455±5	6.2±0.1	[4]	
	7089±6										114
^{195}At	7081±4	142^{+14}_{-12}	^{191}Bi	6305±4	$11.3^{+1.2}_{-0.9}$	130	0.037	6310±3	12±1	[2]	118
	7117±5										
	7149±4										
	7221±4										39
	6953±4	390^{+100}_{-60}		6871±4	91^{+20}_{-14}‡	30	0.006	6874±5	150±15‡	[2]	330

References: 1 - [Fir90], 2 - [Ryt91], 3 - [And93], 4 - [Sin90].

N = number of observed triple chains.

N_{acc} = number of estimated accidental triple chains.

† Includes also random correlations from 7434 keV (m) and 6664 keV (d) energy region.

‡ Half-life in milliseconds.

$T^*_{1/2}$ = half-life of the mother activity calculated using the method of Rasmussen [Ras59] and assuming no hindrance.

Table 4.3 Maximum cross section values for astatine and polonium nuclei observed in the present work. The cross sections for astatine nuclides are determined from the number of correlated triple chains and for polonium nuclides from the area of the alpha peak. A transmission of 20% and a detection efficiency of 70% for evaporation residues were assumed in the cross section determinations.

Nuclide	E [MeV/u]	E* [MeV]	σ [μb]
^{193}At	4.79	51	0.05
^{194}At	4.43	37	3.1
^{195}At	4.11	24	1.3
^{195}At^{m}	4.11	24	0.5
^{193}Po	4.71	48	3.6
^{193}Po^{m}	4.71	48	9.3
^{194}Po	4.43	37	58
^{195}Po	4.29	31	10
^{195}Po^{m}	4.29	31	28

Gamma decay studies

Figure 4.9a shows the gamma ray spectrum observed using the LeGe detector in coincidense with any event registered in the PIPS detector. It is, in this sense, called the singles gamma ray spectrum. Peaks with higher intensity were identified and assigned to X-rays of lead and bismuth [Led78], which is also indicated in the figure. The peak marked by (*), at about 76 keV, could not be identified with any known X-ray or gamma ray energy. The energy of the peak marked by (**) was determined to be (103.8 $\pm$ 0.3) keV. The peak was not identified.

The singles gamma ray spectrum of figure 4.9a was further purified by requiring that the gamma ray has to be in coincidence with any alpha particle (energy between 3000 keV and 12000 keV). This gamma ray energy spectrum is shown in figure 4.9b, where one peak is observed to emerge. Figure 4.9c shows an alpha-gamma coincidence spectrum with alpha particle energy between 6900 keV and 7900 keV (corresponding to the mother alpha particle energy window used in the correlation search). It can be seen by comparing figures 4.9b-c that the peak at about 76 keV remains but the number of background events decreases significantly.

The spectrum in figure 4.9c was further cleaned using the condition that there should be an evaporation residue in correlation (time and position) with an alpha particle observed in coincidence with a gamma ray. As a result of this operation

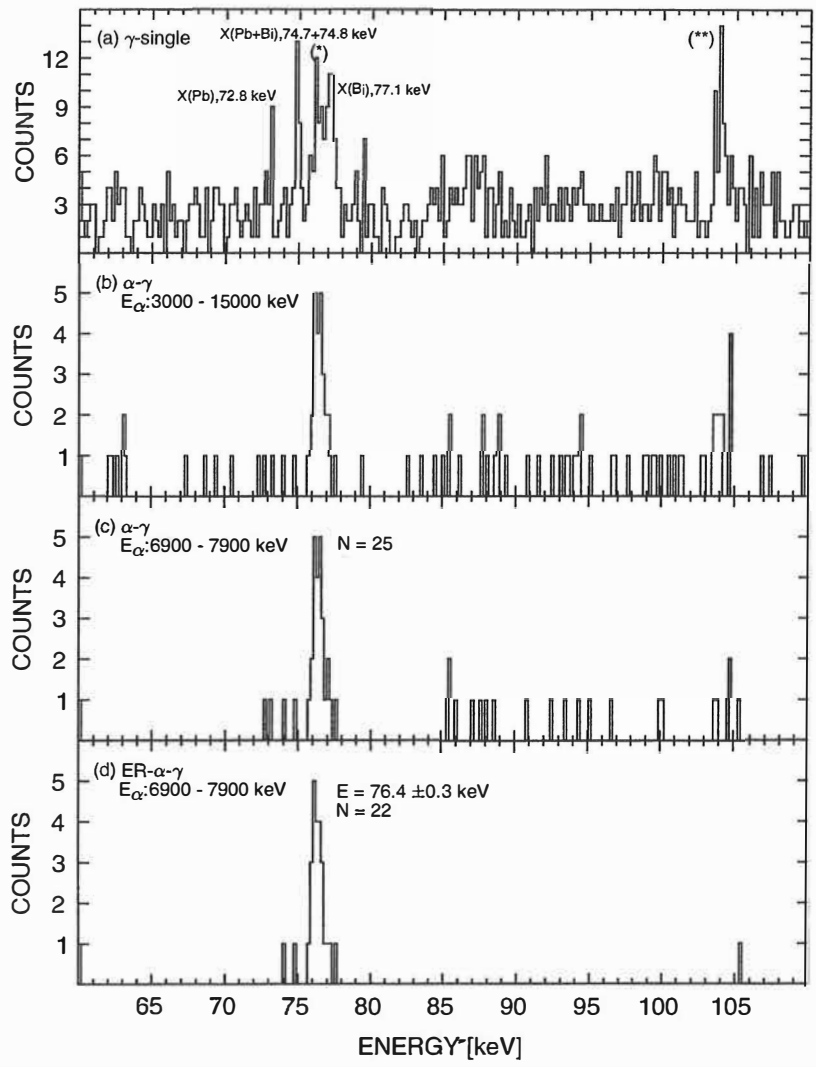

Figure 4.9 Gamma ray spectra from all irradiations observed in the present work using the LeGe detector. The sybmols * and ** are explained in the text.
(a) Gamma singles (i.e. gamma ray in coincidence with any event observed in the focal plane PIPS detector). X-rays were identified using the Table of Isotopes [Led78]
(b) and (c) Gamma singles gated with alpha particles. Alpha particle energy intervals were 3000 keV – 12000 keV (b) and 6900 keV – 7900 keV corresponding to the mother alpha particle energy interval (c).
(d) An evaporation residue was required to be in correlation with an alpha particle (6900 keV – 7900 keV) observed simultaneously with a gamma ray.

the peak appearing in figures 4.9b-c stays but the background disappears as can be seen in figure 4.9d. The energy of the peak was determined to be (76.4 ± 0.3) keV. No X-ray with an energy around 76.4 keV can be found in the lead region. There are 22 counts in the peak of figure 4.9d.

Alpha particle energies associated with the gamma peak of energy of 76.4 keV do not occur in one peak but are distributed rather uniformly within the energy region between 7100 keV and 7230 keV. There are two factors that support the assigment of this peak to ^{190}Bi. Most of the 22 counts were observed at bombarding energies with the most abundant production of ^{194}At. Secondly, there were six cases (out of 22), where a daughter alpha particle was found for mother alpha particles used in the gamma gate. Four of these daughter alpha particles were assigned to ^{190}Bi.

The calibration of the LeGe-detector was performed with a combined ^{133}Ba and ^{152}Eu source. The reference energies were taken from the paper of W.H. Trzaska [Trz90]. X-ray energies of lead and bismuth were taken from the Table of Isotopes [Led78].

4.2 The reaction ^{35}Cl + ^{169}Tm

Neutron-deficient radon isotopes were produced in the reaction ^{169}Tm(^{35}Cl, xn)$^{204-x}$Rn using bombarding energies of 5.6, 5.7, 5.9, 6.0 and 6.1 MeV/nucleon. The original beam energy from the cyclotron was 6.2 MeV/nucleon. The bombarding energies were adjusted by havar (thickness of 1.8 mg/cm^2) and nickel (1.4, 0.9 and 0.45 mg/cm^2) degrader foils. The highest bombarding energy was obtained without any degrader foils, only the beam window (0.45 mg/cm^2) reduced the energy. The beam current of ^{35}Cl^{8+} was measured from a Faraday cup in front of the target and it was typically 300 – 400 nA. A pulsed beam with a ratio of 10 ms beam on and 30 ms beam off was used. The pressure of the helium filling gas was 1.0 mbar. Excitation energies of ^{204}Rn compound nuclei were calculated to be between 80 and 94 MeV. Irradiation times were 1.2, 6.3, 9.0, 6.7 and 11 hours for the five bombarding energies, respectively. The energy region of evaporation residues was determined to be between 15 – 30 MeV in the low amplification branch.

The thickness of the ^{169}Tm target was 0.67 mg/cm^2. The reason for the use of the relatively thick ^{169}Tm target was a better yield of evaporation residues compared with yields from thinner ^{169}Tm targets [Lei95a].

Table 4.4 The alpha particle energy calibration data. These activities were produced in the reaction ^{35}Cl + ^{169}Tm. The position calibration between evaporation residues and mother alpha particles was based on the short lived activity ^{197}At.

Nuclide	E_α [keV]	$T_{1/2}$	Ref.
^{198}Po	6182.0±2.2	1.76±0.03 min	[Ryt91, Chu90]
^{197}Po	6383.4±2.4	26±2 s	[Ryt91, Chu91]
^{198}At^m	6850±4	1.5±0.3 s	[Ryt91, Chu90]
^{197}At	6958±5	350±40 ms	[Ryt91, Chu91]

The alpha particle energy and the position calibrations were based on the decay of known activities produced in the reaction ^{35}Cl + ^{169}Tm. The data used for calibration are shown in table 4.4. The position calibration was obtained using the short lived activity ^{197}At. The size of the position window between evaporation residue and mother alpha particles (low and high amplifications) was determined from the widths of the two distributions shown in figure 4.10. The size of ±11 units was chosen for the present experiment. The maximum position difference between mother and daughter alpha particles to be correlated was chosen to be ±15 units.

The half-lives of ^{199}Rn and ^{199}Rn^m are too long for being determined accurately in the present experiment (^{199}Rn: E_α = (6989±10) keV, $T_{1/2}$ = (620±30) ms and ^{199}Rn^m: E_α = (7060±15) keV, $T_{1/2}$ = (320±20) ms [Sch88, Bro95]). Consequently, the lower limit of the mother alpha particle energy window was set at 7100 keV. The upper limit of 7800 keV was used. The energy window of daughter alpha particle energies (6800 keV – 7300 keV) was chosen such that it was possible to observe the alpha particle decays from $^{192-194}$Po.

In the correlation search of ^{197}Rn and ^{198}Rn the maximum search times for mother and daughter alpha particles were determined on the basis of the estimated number of random correlations. In order to keep the number of randomly produced chains of the type evaporation residue – mother alpha particle – daughter alpha particle

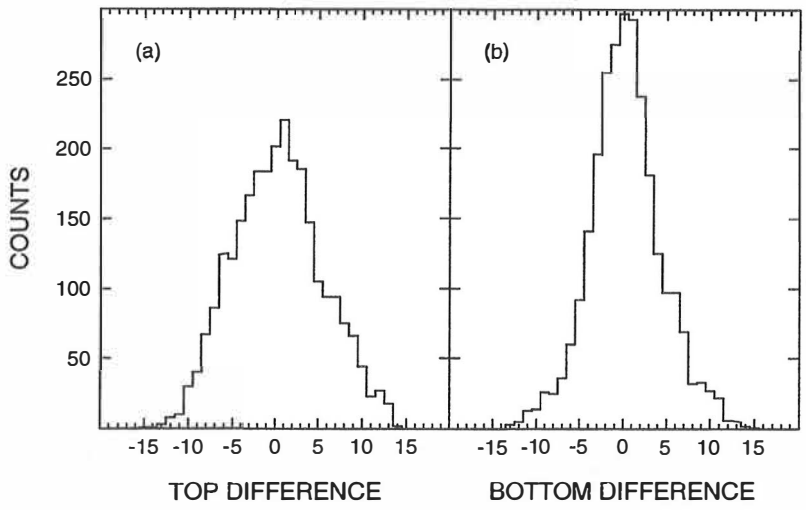

Figure 4.10 Differences of TOP (a) and BOTTOM (b) position between evaporation residue and mother alpha particle (low and high amplification) after the position calibration for the ^{197}At alpha peak produced at 6.0 MeV/nucleon bombarding energy. The size of the position window was chosen to be +11 units for the correlation search of evaporation residues and mother alpha particles from the widths of these two peaks. The position of evaporation residues in vertical direction varied between about 100 and 600 units.

sufficiently low and on the other hand to determine the half-life of ^{198}Rn in a reliable way, maximum search times of 500 ms and 2400 ms were used in the correlation search for mother and daughter alpha particles, respectively. The use of such relatively long maximum search times was possible because only alpha particle decays occurring during the beam pause were considered. The effect of the in-pulse alpha particles on the measured half-lives was investigated and found to be negligible.

Using the above given energy and time windows for mother and daughter alpha particles, altogether 66 correlated chains of the type evaporation residue – mother alpha particle – daughter alpha particle were observed in the present experiment. These correlated triple chains are plotted in the lower left corner of figure 4.11a, where three distinct groups of correlated mother – daughter alpha particle pairs can be seen. There can also be seen four triple chains that cannot be connected to any of the three groups and it was assumed that such decay chains were produced by random corrclations.

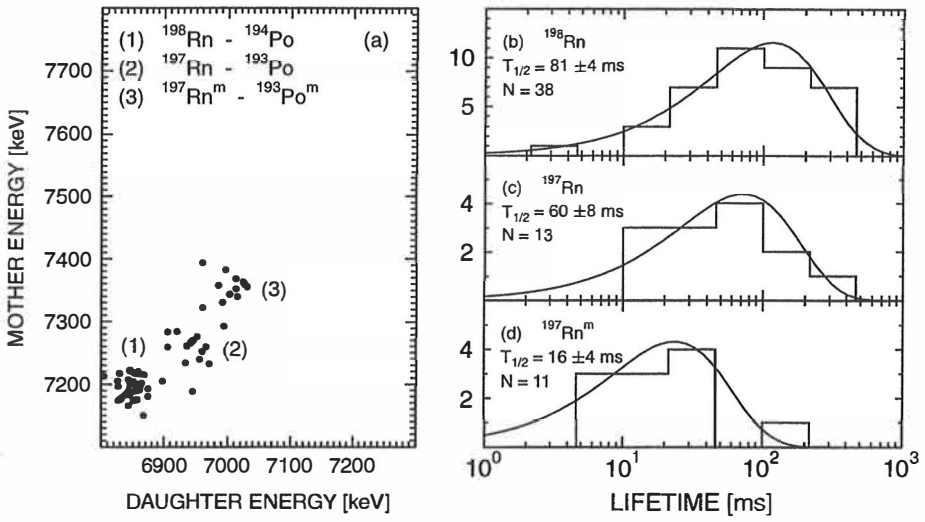

Figure 4.11 (a) Mother and daughter alpha particle energies for all correlated chains of the type evaporation residue – mother alpha particle – daughter alpha particle observed in the present experiment with bombarding energies between 5.6 and 6.1 MeV/nucleon. The alpha particle energy window was 7100 keV – 7800 keV for mother alpha particles and 6800 keV – 7300 keV for daughter alpha particles. Maximum search times were 500 ms and 2400 ms for evaporation residue – mother alpha particle pairs and mother alpha – daughter alpha particle pairs, respectively.
(b, c, d). Life time distributions of ^{198}Rn (b), ^{197}Rn (c) and ^{197}Rn^{m} (d) constructed from correlated triple chains found at all bombarding energies. The fit is not used for half-life determination, it is rather to guide the eye.

There is only one published reference concerning ^{198}Rn [Cal84], where the alpha particle energy and half-life of (7196±10) keV and (50±9) ms, respectively, were reported. An unpublished result for ^{198}Rn (E_α = (7200±20) keV and $T_{1/2}$ = (79±15) ms) is reported in [Lei83]. In the present work, the results of Calaprice et al. and Leino were confirmed. Our results for the alpha particle energy and half-life of ^{198}Rn were (7196±6) keV and (84^{+16}_{-12}) ms, respectively. They were calculated from 38 correlated triple chains that can be seen at the lower left corner in figure 4.11a. An alpha particle energy of (6849±4) keV and a half-life of (420^{+80}_{-60}) ms were measured for the daughter nucleus ^{194}Po. The corresponding values from earlier measurements are (6846±4) keV and (440±60) ms, respectively [Sin89]. Measured alpha decay energies and half-lives of ^{198}Rn and ^{194}Po are in good agreement with earlier work. The number of accidental correlations in the energy region

corresponding to the alpha decay of ^{198}Rn was estimated to be 0.1†.

In the work of Wauters et al. [Wau93], two alpha particle decaying states were observed in ^{193}Po. The alpha particle energy and half-life of the state of ^{193}Po with lower alpha particle energy were measured to be (6940±20) keV and (360±50) ms, respectively. The corresponding values for the state with higher alpha particle energy were measured by Wauters at al. to be (7000±20) keV and (260±20) ms, respectively. This state with higher alpha particle energy was assigned to the isomeric state in ^{193}Po.

In the present experiment, 13 chains of the type evaporation residue – mother alpha particle – daughter alpha particle, where the daughter decays were assigned to the state of ^{193}Po with lower alpha particle energy, were observed, see figure 4.11a. The alpha particle energy and half-life of the daughter nucleus ^{193}Po were measured to be (6942±6) keV and (290^{+110}_{-60}) ms, respectively. The corresponding values for the mother decay were (7260±7) keV and (65^{+25}_{-14}) ms. This activity was assigned to the alpha decay of the new isotope ^{197}Rn.

Eleven more correlated triple chains were observed with the daughter alpha particle energy and half-life of (7011±6) keV and (370^{+160}_{-90}) ms, respectively. This decay was assigned to the assumed isomeric state in ^{193}Po. An alpha particle energy of (7356±7) keV and a half-life of (19^{+8}_{-4}) ms were measured for the mother activity which was assigned to an assumed isomeric state in ^{197}Rn.

The estimated number of triple chains produced by accidental correlations was obtained to be 0.04† and 0.02† in the energy regions relevant for ^{197}Rn and ^{197}Rn^{m} alpha decays, respectively.

Life time distributions of ^{197}Rn and ^{197}Rn^{m} are shown in figure 4.11c-d. The solid line is a fit to the data points, but the result of the fit has not been used for half-life determination. The fit is rather a guide for the eye.

†In ref. [Enq96a] the calculation of the number of estimated accidental triple chains was based on a concervative number of single detector units in the PIPS detector. The estimate of 10 detector units in one PAD-strip was used while a more realistic value is between 20 and 25. In the present work the value of 20 was used in the calculation of error probabilities.

Table 4.5 The evaporation residue production cross sections for ^{197}Rn, ^{197}Rn^{m} and ^{198}Rn measured in the present work. In the table, E and E* refer to the bombarding and excitation energies, respectively, at which the highest value was obtained.

Nuclide	E [MeV/u]	E* [MeV]	σ [nb]
^{198}Rn	5.6	80	74
^{197}Rn	5.9	88	12
^{197}Rn^{m}	6.0	91	12

Production cross sections of ^{197}Rn, ^{197}Rn^{m} and ^{198}Rn are presented in table 4.5. They were calculated from the observed number of correlated triple chains assuming 20% transmission of evaporation residues for all bombarding energies. It was also assumed that 70% of the transmitted evaporation residues were implanted into the focal plane detector. Corrections to the number of correlated triple chains were made due to escape alpha particles and beam pulsing. E and E* refer to the bombarding and excitation energies, respectively, at which the highest value was obtained.

Alpha decay properties of neutron-deficient radon isotopes ^{197}Rn, ^{197}Rn^{m} and ^{198}Rn obtained from the reaction ^{35}Cl + ^{169}Tm are summarized in table 4.6. The half-lives have also been calculated (assuming no hindrance) using the procedure proposed by Rasmussen [Ras59]. Systematics of alpha particle energies and reduced alpha widths of neutron-deficient radon isotopes are discussed in chapter 5.

4.3 The reaction ^{35}Cl + ^{170}Yb

Alpha decay properties of neutron-deficient francium isotopes were studied using the reaction ^{170}Yb(^{35}Cl, xn)$^{205-x}$Fr. The beam current of ^{35}Cl^{8+} projectiles was typically 300 – 400 nA in front of the target as measured regularly from a Faraday cup. The thickness of the ^{170}Yb target (72 % enrichment) was 0.35 mg/cm^2. The initial beam energies from the cyclotron were 5.8 and 6.2 MeV/nucleon and nickel degrader foils with thicknesses of 2.7 and 1.8 mg/cm^2 were used to adjust bombarding energies to 4.9, 5.1 and 5.3 MeV/nucleon. Corresponding excitation energies of the ^{205}Fr compound nucleus were estimated to be 54, 60 and 65 MeV,

Table 4.6 Alpha particle energies E_α and half-lives $T_{1/2}$ of mother and daughter activities measured in the present work and compared with earlier measurements. The half-life estimation is calculated using the method of Rasmussen [Ras59].

Nuclide	E_α [keV]	$T_{1/2}$ [ms]	N_{obs}	N_{acc}	E_α [keV]	$T_{1/2}$ [ms]	Ref.	$T_{1/2,calc.}$ [ms]
$^{197}Rn^m$	7356±7	19^{+8}_{-4}	11	0.02	7370±20	18^{+9}_{-5}	[Mor95]	33
$^{193}Po^m$	7011±6	370^{+160}_{-90}			7000±20	260±20	[Wau93]	
^{197}Rn	7260±7	65^{+25}_{-14}	13	0.04	7261±20	51^{+35}_{-15}	[Mor95]	68
^{193}Po	6942±6	290^{+110}_{-60}			6940±20	360±50	[Wau93]	
^{198}Rn	7196±6	84^{+16}_{-12}	38	0.1	7196±10	50±9	[Cal84]	109
^{194}Po	6849±4	420^{+80}_{-60}			6846±4	440±60	[Sin89]	

N_{obs} = Number of observed triple chains.

N_{acc} = Number of estimated accidental triple chains.

respectively. Irradiation times were 2.2, 3.2 and 16 hours for these three bombarding energies. A beam window of 0.45 mg/cm^2 nickel was used to separate the high vacuum of the cyclotron and the helium filling gas (pressure 1.0 mbar) of the separator.

The excitation energy of the compound nucleus ^{205}Fr is probably too high for 2n and 3n exit channels in the present work. Isotopes ^{202}Fr and ^{203}Fr observed in this work are probably formed from impurities (^{171}Yb 18%, ^{172}Yb 5%, others less than 3%) in the target material.

The alpha particle energy calibration data can be seen in the table 4.4 (chapter 4.2). The calibration was based on the reaction ^{35}Cl + ^{169}Tm because suitable alpha peaks for energy calibration were not produced in the reaction ^{35}Cl + ^{170}Yb. The position calibration between evaporation residues and alpha particles was obtained from the alpha peak of ^{197}At produced in the bombardment of the ^{169}Tm target.

Correlated chains of type evaporation residue – mother alpha particle – daughter alpha particle produced at bombarding energies 4.9 and 5.1 MeV/nucleon are shown in figure 4.12. The alpha particle energy windows used at both bombarding energies were 7070 keV – 8070 keV and 6580 keV – 7070 keV for mother and daughter alpha particles, respectively. At the lower bombarding energy maximum

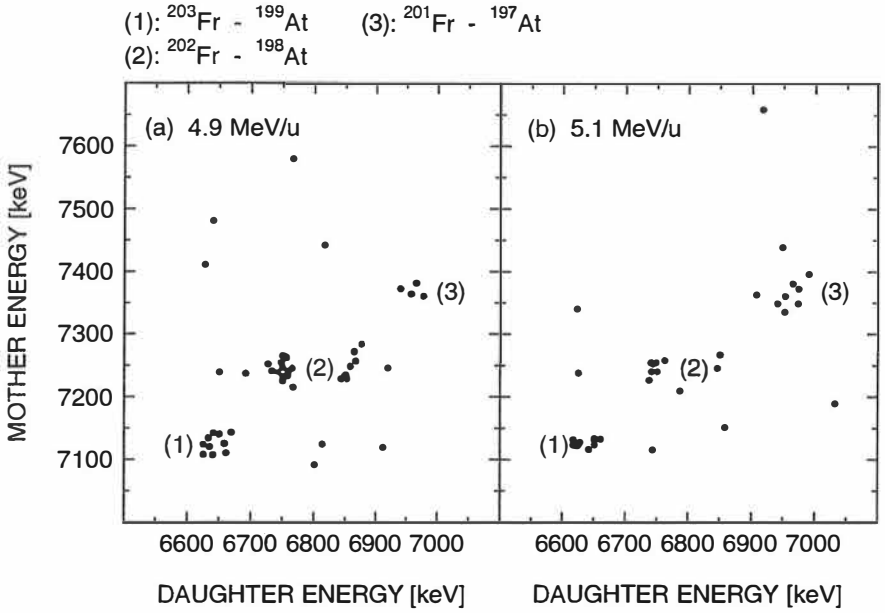

Figure 4.12 Mother and daughter alpha particle energies for all correlated chains of the type evaporation residue – mother alpha particle – daughter alpha particle observed in the reaction $^{35}Cl + ^{170}Yb$ with bombarding energies of 4.9 and 5.1 MeV/nucleon.
At 4.9 MeV/nucleon (a) the maximum search times were 1400 ms and 12 s for the evaporation residue – mother alpha particle pair and mother alpha – daughter alpha particle pair, respectively.
At 5.1 MeV/nucleon (b), the corresponding search times were 1200 ms and 8 s.
Energy windows of 7070 keV – 8070 keV for mother alpha particles and 6580 keV – 7070 keV for daughter alpha particles were used at both bombarding energies.

search times used to search for mother alpha and daughter alpha particles were 1400 ms and 12 s, respectively. The corresponding values at the higher bombarding energy were 1200 ms and 8 s.

The search times of 1400 ms and 12 s were too short for reliable determination of half-lives for ^{203}Fr (E_α = (7133±5) keV, $T_{1/2}$ = (550±20) ms [Ryt91, Ewa80]) and ^{199}At (E_α = (6642.7±2.2) keV, $T_{1/2}$ = (7.0±0.5) s [Ryt91]). In the same way, the search times of 1200 ms and 8 s were too short for determining half-lives for transitions connecting the assumed low-spin (3^+) isomers in ^{202}Fr and ^{198}At.

Alpha particle energies of ^{203}Fr and ^{199}At were determined from 19 correlated triple chains observed at 4.9 and 5.1 MeV/nucleon bombarding energies. Values of (7126±6) keV and (6641±5) keV were obtained, respectively. The lower limit estimates of 250 ms and 3.4 s were determined for half-lives of ^{203}Fr and ^{199}At from 10 triple chains observed at 4.9 MeV/nucleon bombarding energy.

Two distinct groups of mother – daughter particle pairs can be seen in figure 4.12 (labelled by (2)) and figure 4.13 (labelled by (4)). These groups were assigned to the alpha particle decays connecting the assumed low-spin (3^+) and high-spin (10^-) isomers in ^{202}Fr and ^{198}At [Huy92]. Alpha particle energies of (7243±6) keV and (6753±4) keV were determined from 29 correlated triple chains observed at all the three bombarding energies for the assumed low-spin states in ^{202}Fr and ^{198}At, respectively. It was possible to determine the half-lives only from 13 triple chains observed at the lowest bombarding energy. The results were (230^{+80}_{-40}) ms and $(4.6^{+1.8}_{-1.0})$ s for ^{202}Fr and ^{198}At, respectively. Measured alpha particle energies and half-lives are in good agreement with published values (^{202}Fr: E_α = (7237±8) keV and $T_{1/2}$ = (340±40) ms; ^{198}At (E_α = (6755±4) keV and $T_{1/2}$ = (4.2±0.3) s [Huy92, Sch87]).

Alpha particle energies of the assumed high-spin isomers in ^{202}Fr and ^{198}At were determined from 15 correlated triple chains observed at 4.9, 5.1 and 5.3 MeV/nucleon bombarding energies. Half-lives were determined from 10 triple chains only, because maximum search times used were too short for allowing the half-life determination of high-spin states in ^{202}Fr and ^{198}At at the highest bombarding energy. Th alpha particle energy and half-life of the assumed high-spin isomer in ^{202}Fr were measured to be (7242±6) keV and (230^{+140}_{-50}) ms, respectively. An alpha particle energy of (6855±4) keV and a half-life of $(1.3^{+0.8}_{-0.3})$ s were measured for the high-spin isomer in ^{198}At. The agreement with earlier measurements is good (^{202}Fr: E_α = (7237±8) keV and $T_{1/2}$ = (340±40) ms; ^{198}At (E_α = (6856±4) keV and $T_{1/2}$ = (1.0±0.2) s [Huy92, Sch87]).

The numbers of chains of type evaporation residue – mother alpha particle – daughter alpha particle produced randomly was estimated to be 0.4 and 0.1 for transitions connecting the assumed low-spin and high-spin isomer in ^{202}Fr and ^{198}At, respectively. The numbers of observed correlated triple chains were correspondingly 29 and 15.

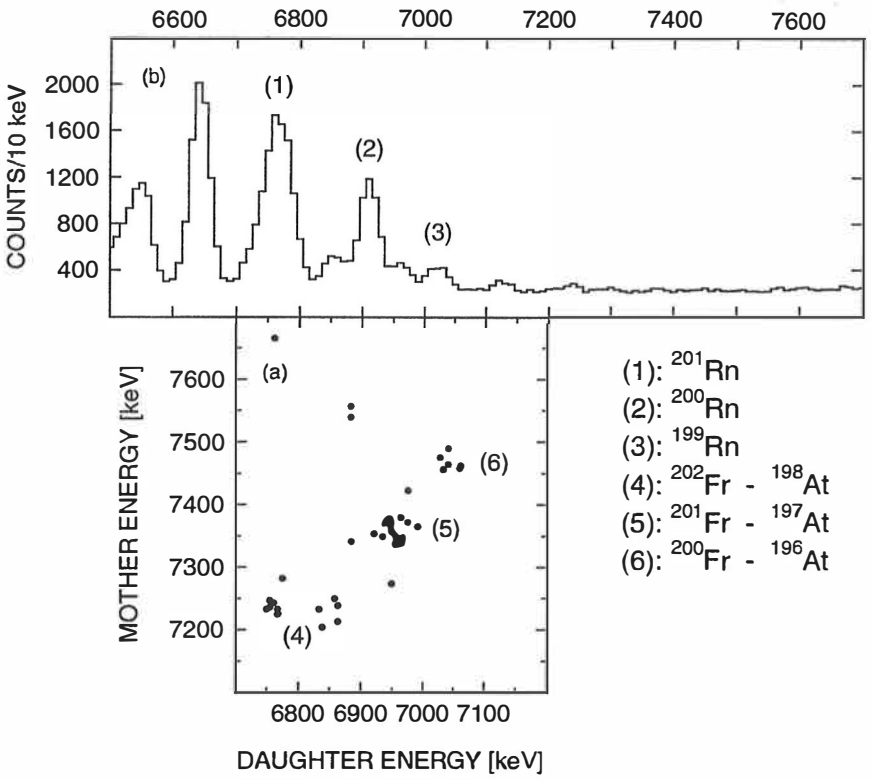

Figure 4.13 (a) Mother and daughter alpha particle energies for all correlated triple chains observed in the reaction $^{35}Cl + {}^{170}Yb$ at the bombarding energy of 5.3 MeV/nucleon. Maximum search times were 400 ms and 3.5 s for evaporation residue – mother alpha particle pair and mother alpha – daughter alpha particle pair, respectively. The alpha particle energy range was 7150 keV – 8150 keV for mother alpha particles and 6750 keV – 7150 keV for daughter alpha particles.
(b) Singles alpha particle energy spectrum.

In the correlation search for ^{200}Fr and ^{201}Fr maximum search times used were 400 ms and 3.5 s for mother and daughter alpha particles, respectively. The corrections to measured half-lives of ^{201}Fr and ^{197}At were calculated on the basis of 400 ms and 3.5 s maximum search times. At 4.9 and 5.1 MeV/nucleon bombarding energies longer search times were used, but the effect of the difference of search times longer than 400 ms and 3.5 s to the correction was negligible. All triple chains observed at the bombarding energy of 5.3 MeV/nucleon are shown in figure 4.13a. Altogether 29 correlated chains of type evaporation residue – mother alpha particle

– daughter alpha particle observed at the three different bombarding energies were assigned to the alpha particle transitions of ^{201}Fr and ^{197}At. The alpha particle energy and half-life of ^{201}Fr were measured to be (7361±7) keV and (69^{+16}_{-11}) ms, respectively. An alpha particle energy of (6956±5) keV and a half-life of (370^{+90}_{-60}) ms were obtained for ^{197}At. Our results are in satisfactory agreement with earlier work concerning ^{201}Fr and ^{197}At (^{201}Fr: E_α = (7388±15) keV and $T_{1/2}$ = (48±15) ms [Ewa80]; ^{197}At: E_α = (6958±5) keV and $T_{1/2}$ = (350±40) ms [Ryt91, Chu91]).

Six correlated triple chains were observed with a daughter alpha particle energy of (7044±7) keV and a half-life of (390^{+270}_{-120}) ms at the 5.3 MeV/nucleon bombarding energy (see figure 4.13a)). This decay was assigned to ^{196}At with reported alpha particle energy and half-life of (7055±7) keV and (300±100) ms [Tre67], respectively. The mother activity was measured to have an alpha particle energy of (7468±9) keV and a half-life of (19^{+13}_{-6}) ms and it was assigned to the new isotope ^{200}Fr.

The number of randomly produced triple chains in the case of ^{200}Fr and ^{201}Fr was estimated to be 0.02 and 0.03 respectively.

A summary of measured decay properties of the francium and astatine isotopes at bombarding energies of 4.9, 5.1 and 5.3 MeV/nucleon is given in table 4.7. In the last column of the table, the estimated half-life is calculated according to the method proposed by Rasmussen [Ras59]. In the calculation, s-wave transitions were assumed ($\Delta\ell = 0$).

The isotope ^{200}Fr was previously unknown, but it was also independently identified by Morita et al. [Mor95] using a gas-filled recoil separator at RIKEN. Their half-life for ^{200}Fr was, however, extraordinarily long (see chapter 5 for a more detailed discussion).

The production cross section for ^{200}Fr at a bombarding energy of 5.3 MeV/nucleon was estimated to be 6 nb. It was assumed that the transmission of evaporation residues was 20% and that 70% of transmitted evaporation residues were implanted in the focal plane detector. Production cross sections for ^{200,201,202}Fr are presented in table 4.8, where E and E* refer to the bombarding and excitation energies, respectively, at which the highest value was obtained.

Table 4.7 Alpha particle energies E_α and half-lives $T_{1/2}$ of activities measured in the present work and compared with previous data. Half-life estimations are calculated using the method of Rasmussen [Ras59].

Nuclide	E_α [keV]	$T_{1/2}$ [ms]	N_{obs}	N_{acc}	E_α [keV]	$T_{1/2}$ [ms]	Ref.	$T_{1/2,calc.}$ [ms]
^{200}Fr	7468±9	19^{+13}_{-6}	6	0.02	7500±30	570^{+270}_{-140}	[Mor95]	27
^{196}At	7044±7	300^{+270}_{-120}			7055±7	300±100	[Tre67]	
^{201}Fr	7361±7	69^{+16}_{-11}	29	0.03	7388±15	48±15	[Ewa80]	69
^{197}At	6956±5	370^{+90}_{-60}			6958±5	350±40	[Ryt91,Chu91]	
^{202}Fr	7243±6	230^{+80}_{-40}	29	0.4	7237±8	340±40	[Huy92,Sch87]	167
^{198}At	6753±4	4600^{+1800}_{-1000}			6755±4	4200±300	[Huy92]	
^{202}Fr	7242±6	230^{+140}_{-50}	15	0.1	7237±8	340±40	[Huy92,Sch87]	
^{198}At	6855±4	1300^{+800}_{-300}			6856±4	1000±200	[Huy92]	
^{203}Fr	7126±6	250^{+120}_{-60}	19		7133±5	550±20	[Ryt91,Ewa80]	400
^{199}At	6641±5	3400^{+1600}_{-800}			6642.7±2.2	7000±500	[Ryt91]	

N_{obs} = Number of observed triple chains.

N_{acc} = Number of estimated accidental triple chains.

Table 4.8 The evaporation residue production cross section for ^{200}Fr, ^{201}Fr and the assumed low-spin and high-spin isomers in ^{202}Fr. E and E* refer to the bombarding and excitation energies, respectively, at which the highest value was obtained.

Nuclide	E [MeV/u]	E* [MeV]	σ [nb]
^{202}Fr (3^+)	4.9	54	120
^{202}Fr (10^-)	4.9	54	70
^{201}Fr	5.1	60	580
^{200}Fr	5.3	65	6

5 Discussion

Astatine, radon and francium isotopes studied in this work are discussed in this chapter. Section 5.1 deals with astatine isotopes and sections 5.2 and 5.3 radon and francium isotopes, respectively. In section 5.4 alpha particle decay systematics are discussed. Transfer reactions are discussed briefly in section 5.5.

5.1 Astatine isotopes

The astatine isotope ^{196}At (E_α = (7055 ± 7) keV and $T_{1/2}$ = (300 ± 100) ms [Tre67]) was not observed in the present work, because of too high excitation energy at the Coulomb barrier ($E^* \sim 28$ MeV). This isotope was identified using He-jet technique at the HILAC in Berkeley nearly 30 years ago and has not later been investigated. Treytl and Valli [Tre67] assigned only one alpha particle transition to ^{196}At and concluded that a possible isomeric transition was beyond their time threshold. The alpha decay daughter nuclides of astatine isotopes ^{194,195}At were observed also by Treytl and Valli, but the mother half-lives were too short to be detected with their method.

In the works of Yashita [Yas83] and Leino [Lei83] (both works are unpublished) astatine isotopes ^{194,195}At were produced. The values of the alpha particle energy and half-life obtained by Yashita were (7200 ± 30) keV and (180 ± 80) ms, respectively, for ^{194}At and (7120 ± 20) keV and (200 ± 100) ms for ^{195}At. Leino essentially agreed with the values of Yashita, but found an additional alpha particle transition in ^{195}At with an alpha particle energy of (7190 ± 30) keV and a half-life of (140 ± 50) ms. A preliminary report on ^{195}At has been given also by Nomura [Nom95] with an alpha particle energy of about 7130 keV and a half-life of (24^{+34}_{-10}) ms. The gas-filled recoil separator at RIKEN and the method of time and position correlated decay chains have been used.

^{195}At and ^{193}At isotopes

An alpha particle transition with the energy of (6953 ± 4) keV and the half-life of (390^{+100}_{-60}) ms was seen very clearly in this work and assigned to isotope ^{195}At (see in figure 4.2a triple chains labelled by (3)) but was not observed in the works of Yashita and Leino. The alpha particle energy and half-life of the daughter level are (6874 ± 5) keV and (150 ± 15) ms, respectively [Ryt91]. In the present work, essentially the same decay energy but a somewhat shorter half-life of (91^{+20}_{-14}) ms (from 30 counts) were obtained. The spin and parity of this level in ^{191}Bi are given as $(\frac{1}{2}^+)$ [Bro89, Bro95]. Considering this a favoured alpha particle decay (the hindrance factor calculated from table 4.2 is 1.2), the spin and parity of the corresponding level in ^{195}At can be expected to be the same $(\frac{1}{2}^+)$. In isotope ^{197}At this level was interpreted as a shell model intruder state with the excitation energy of (52 ± 10) keV [Coe86]. Coenen et al. concluded (based on the energy systematics) that this low excitation energy suggests that for isotope ^{195}At the $(\frac{1}{2}^+)$ intruder state becomes the ground state.

According to figures 4.3a and 4.3b in chapter 4, four alpha particle transitions with a common half-life were determined to belong to the isotope ^{195}At in addition to the transition connecting $(\frac{1}{2}^+)$ intruder states. Based on the information of the two states known in ^{191}Bi (ground state: $(\frac{9}{2}^-)$, E_α = (6310 ± 3) keV, $T_{1/2}$ = (12 ± 1) s and isomeric state: $(\frac{1}{2}^+)$, E_α = (6874 ± 5) keV, $T_{1/2}$ = (150 ± 15) ms [Ryt91]) it is difficult to interpret the observed transitions.

A possible explanation of the broad mother alpha particle energy range in ^{195}At is the partial summing of conversion electron energies with the alpha particle energy. In the present case, the excited level de-exciting by emitting conversion electrons (and gamma quanta) should exist in ^{191}Bi.

If it is assumed that the peak at the energy of (7149 ± 4) keV in figure 4.3a is due to the summing of conversion electrons which fully deposit their energy, then the kinetic energy of these electrons would be about 70 keV (= 7149 keV – 7081 keV). The binding energy of the K-electron in bismuth is 90.5 keV [Led78] giving the excitation energy of 160 keV for the level in bismuth. The binding energies of L_1, L_2, L_3 and M electrons are 16.4, 15.7, 13.4 and about 3 keV [Led78], respectively. If the binding energy of the L-electrons (15 keV) is subtracted from the level energy

(160 keV) the energy of the alpha particle (after the summing of the L-electrons) would be 7226 keV (= 7081 keV + 160 keV - 15 keV), which indeed can be seen in figure 4.3a. The bump at the right hand side of the 7221 keV peak is probably due to the summing of M-electrons.

The spectrum in the region between the (7081 ± 4) keV and (7149 ± 4) keV peaks has probably been formed by electrons which escaped from the focal plane detector so that only a part of the kinetic energy of the electron contributes to the observed total energy. It was estimated that the energy deposited by the K conversion electron is at minimum about 15 keV which means that in the (7081 ± 4) keV peak there is also a contribution from conversion electrons (assuming a large total conversion coefficient; see below).

The spin and parity of the excited level with 160 keV level energy can be estimated through conversion coefficients from the areas of peaks in figure 4.3a. The sum of the counts in the two peaks with higher energies (7149 keV, 7221 keV) is 67 and it can be assumed that these peaks are seen as a result of summing of K-electrons and L- and M-electrons, respectively. The range of 100 keV electrons in silicon is about 60 μm and the same percentage of escaping electrons as escaping alpha particles can thus be assumed (the implantation depth of evaporation residues is estimated to be about 15 μm). The number of electrons which deposited their full energy being 67, the number of escaped electrons should be 55. This is almost equal to the sum of the counts in the peaks with lower energies (7081 keV, 7117 keV) meaning that partial summing of conversion electron energies occurs and a relatively large total conversion coefficient can be expected. The number of counts in the two lowest energy peaks is 61.

In the determination of the conversion coefficient the error comes mainly from the small number of alpha particle events with no summing of conversion electron energies. In the present work, the conversion coefficient was estimated by calculating the ratio of K conversion coefficient (α_K) to L and M conversion coefficient (α_{L+M}) and comparing with the (α_K/α_{L+M}) ratios of different multipoles obtained from the table of Rösel et al. [Rös78].

From the table of Rösel et al., following results for electric and magnetic multipoles

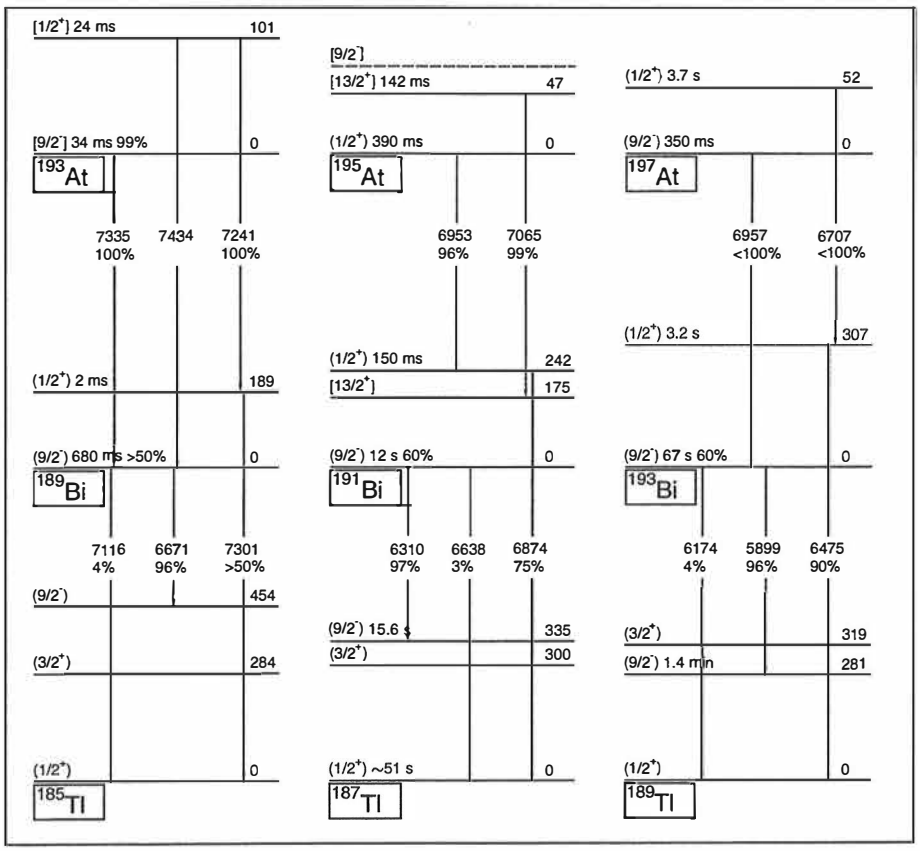

Figure 5.1 Alpha particle energy systematics and low energy decay schemes of odd-mass neutron-deficient astatine and bismuth isotopes. Alpha particle energies of the isotopes ^{193,195}At have been taken from the present work, other values have been taken from literature or derived from systematics. All energies are in keV. Beta particle half-lives calculated by Takahashi et al. [Tak73] have been used in determination of alpha particle branching ratios, $\lambda_\alpha/\lambda_\beta$. See the text for more details.

were obtained ($\bar{\alpha} = \alpha_K/(\alpha_L + \alpha_M)$):

$\bar{\alpha}(E1) = 5.7$	$\bar{\alpha}(M1) = 5.9$	$\alpha_{TOT}(E1) = 0.13$	$\alpha_{TOT}(M1) = 2.7$
$\bar{\alpha}(E2) = 0.91$	$\bar{\alpha}(M2) = 3.2$	$\alpha_{TOT}(E2) = 0.99$	$\alpha_{TOT}(M2) = 15$
$\bar{\alpha}(E3) = 0.14$	$\bar{\alpha}(M3) = 0.94$	$\alpha_{TOT}(E3) = 13$	$\alpha_{TOT}(M3) = 74$
$\bar{\alpha}(E4) = 0.034$	$\bar{\alpha}(M4) = 0.32$	$\alpha_{TOT}(E4) = 150$	$\alpha_{TOT}(M4) = 510$

From figure 4.3a the value of 1.5 (= 38/25) for the ratio $\alpha_K/(\alpha_L + \alpha_M)$ can be obtained. The background subtraction of 5 counts (43 - 5 = 38) in 7149 keV peak

has been made. According to the above calculations, the multipolarity of this transition would be E2, M2 or M3. The high total conversion coefficient excludes the E2 transition ($\alpha_{TOT}(E2) = 0.99$). If the transition to the ($\frac{9}{2}^-$) ground state in ^{191}Bi is assumed, the spin and parity of the initial state would be ($\frac{5}{2}^+$ or $\frac{13}{2}^+$) or ($\frac{3}{2}^-$ or $\frac{15}{2}^-$) if the multipolarity of the transition is M2 or M3, respectively. Considering the shell model proton levels between closed shells 82 and 126, candidates of $\frac{3}{2}^-$, $\frac{13}{2}^+$, and $\frac{5}{2}^+$ for the spin and parity can be found. Because the state in ^{195}At is isomeric, a relatively high spin value can be assumed. This then excludes the spin and parity candidates of $\frac{3}{2}^-$ and $\frac{5}{2}^+$, because multipolarities for transitions between these levels and the assumed $\frac{1}{2}^+$ ground state are E1 and E2, respectively. The only candidate left for the spin and parity of the 160 keV level in ^{191}Bi is $\frac{13}{2}^+$. In ^{195}At, decay from the $\frac{13}{2}^+$ excited state to the ground state corresponds to the multipolarity of E6, which is highly hindered for gamma transition. The spin and parity can be assumed to be the same in ^{191}Bi and ^{195}At because the hindrance factor for 7065 keV alpha particle transition is near unity (142 ms/133 ms) and the number of observed decays (triple chains) is large (130).

The actual alpha particle energy of the isomeric state in ^{195}At should be reduced by an amount of about 15 keV (this was the estimated energy release of electrons at minimum) from 7081 keV because of the small number of events without a contribution from summing of conversion electron energies. The alpha particle energy of (7065 ± 10) keV can be estimated for the isomeric state in ^{195}At. The half-life of this state is (142^{+14}_{-12}) ms. The excitation energy of the final state in ^{191}Bi would also change by an amount of 15 keV to 175 keV (= 160 keV + 15 keV).

Although there remains some uncertainty as to the accurate alpha particle energy and the spin and parity assigments of the excited states in ^{191}Bi and ^{195}At, the same half-life of (142^{+14}_{-12}) ms of all the four peaks (see figure 4.3a-b) and good matching of energy differences of these peaks with electron binding energy differences in bismuth strongly suggest that the apparent broad mother alpha particle energy distribution is due to summing of conversion electron energies with the single alpha particle energy and fine structure in the decay of ^{195}At can be excluded. The question still remains where the $\frac{9}{2}^-$ state in ^{195}At is. It is not excluded that part of the structure seen in figure 4.3a is due to alpha decay between $\frac{9}{2}^-$ states. On the other hand, the systematics concerning the positions of $\frac{1}{2}^+$ and $\frac{9}{2}^-$ states

in heavier neutron-deficient astatine isotopes is still quite incomplete and it is difficult to draw definite conclusions.

A complicated decay structure was observed also in the case of ^{193}At (see figure 4.7a). There have been some discrepancies in the level energy assignment of the isomeric state in ^{189}Bi [Coe85, And93, Bat95]. Recent investigations [And93, Bat95] report the alpha particle energy of ^{189}Bi^{m} to be (7300 ± 40) keV and (7340 ± 30) keV, respectively, with corresponding half-lives of (4 ± 2) ms and (7 ± 2) ms. In the present work, the alpha particle energy and half-life of (7301 ± 8) keV and (2^{+3}_{-1}) ms, respectively, was determined for ^{189}Bi^{m} (from three chains) confirming the results in [And93, Bat95]. An alpha particle energy of (7241 ± 8) keV and a half-life of (17^{+29}_{-6}) ms were determined for the mother activity, which can be assigned to an isomeric state in ^{193}At. The spin and parity of this isomeric state, assuming an unhindered transition between initial and final states, can be expected to be ($\frac{1}{2}^{+}$) according to the same values of the corresponding level in ^{189}Bi.

This decay of ^{193}At can be explained in terms of fine structure and isomerism. Placement of different alpha particle transitions observed in ^{193}At is shown in figure 5.1. The excitation energy of the ($\frac{1}{2}^{+}$) intruder state in ^{193}At was determined to be about 100 keV. The excitation energy of the ($\frac{1}{2}^{+}$) state in ^{189}Bi was also determined from the results of the present work to be about 190 keV. This result would indicate that there is a parabolic behaviour of the ($\frac{1}{2}^{+}$) intruder state excitation energies as a function of neutron number with the minimum in ^{195}At.

The alpha line with an energy of (7434 ± 7) keV was assigned to the transition from the ($\frac{1}{2}^{+}$) intruder state in ^{193}At. This transition can be thought to be a crossing decay between ($\frac{1}{2}^{+}$) and ($\frac{9}{2}^{-}$) states, five such chains were observed. A drawback of this crossing decay interpretation is that more alpha particle transitions (5 events) were observed to connect ($\frac{1}{2}^{+}$) and ($\frac{9}{2}^{-}$) states than ($\frac{1}{2}^{+}$) and ($\frac{1}{2}^{+}$) states (3 events). A possible explanation is the high alpha particle energy (7434 ± 7) keV of the transition connecting levels with different spin and parity. This energy difference between 7434 and 7241 keV compensates for the effect of the raise of potential barrier due to the increase of angular momentum ($\ell = 5$). A calculation with the method suggested by Rasmussen [Ras59] gives an intensity ratio of approximately 3:1 in favour of the 7241 keV transition, so a discrepancy

Table 5.1 Alpha particle energies and half-lives determined in the present work for the astatine isotopes ^{193,195}At. These values differ slightly from those given in table 4.2. Assumed spin and parity of initial and final states are also given. In the case of the (7065 ± 10) keV transition in ^{195}At spin and parity is assumed to be one of the three candidates and the same configuration is assumed for initial and final states due to the unhindered transition.

Nuclide	E_α [keV]	$T_{1/2}$ [ms]	J_i^π	J_f^π
^{193}At	7335±5	34^{+9}_{-6}	$\frac{9}{2}^-$	$\frac{9}{2}^-$
	7241±8	24^{+13}_{-6}	$\frac{1}{2}^+$	$\frac{1}{2}^+$
	7434±7		$\frac{1}{2}^+$	$\frac{9}{2}^-$
	7109±6	28^{+22}_{-9}		
^{195}At	6953±4	390^{+100}_{-60}	$\frac{1}{2}^+$	$\frac{1}{2}^+$
	7065±10	142^{+14}_{-12}	$\frac{13}{2}^-$	$\frac{13}{2}^-$

still remain. This discrepancy can be only partly explain by the higher alpha particle energy of the hindered ($\frac{1}{2}^+ - \frac{9}{2}^-$) transition. However, definite conclusions cannot be made due to insufficient statistics. The half-life of the ($\frac{1}{2}^+$) intruder state in ^{193}At was determined to be (24^{+13}_{-6}) ms from eight events.

The production rate of the ($\frac{1}{2}^+$) intruder state in ^{197}At was reported to be less than 1% of that of the ($\frac{9}{2}^-$) ground state in heavy-ion-induced reactions [Coe86]. In the present work, the relative production rates of the ($\frac{1}{2}^+$) intruder state and the ($\frac{9}{2}^-$) ground state in ^{193}At were determined to be 24% and 76%, respectively. In ^{195}At, the relative production rates of 19% and 81% for ($\frac{1}{2}^+$) ground state and ($\frac{13}{2}^+$) excited state, respectively, were determined.

Figure 5.1 shows the low energy decay scheme of odd-mass astatine and bismuth nuclei. Values for the isotopes ^{193,195}At come from the present work. The (7109 ± 6) keV alpha particle transition from ^{193}At could not be placed in the decay scheme seen in figure 5.1. The excitation energy of the ($\frac{1}{2}^+$) state in ^{189}Bi has been determined to be (189 ± 10) keV from this work and the alpha particle energy of (7301 ± 8) keV of that state comes also from the present work. The alpha particle energy of the ^{189}Bi ground state transition, (6671 ± 5) keV, has been taken from [Ryt91]. The excitation energy of the ($\frac{1}{2}^+$) intruder state in ^{193}At was calculated to be (101 ± 12) keV and of the ($\frac{13}{2}^+$) state in ^{195}At (47 ± 13) keV. Table 5.1 summarizes the results obtained for the isotopes ^{193,195}At. Values

in table 5.1 can be slightly different from values in table 4.2.

^{194}At isotope

The assumed low (3^+) and high (10^-) spin states in ^{190}Bi were both observed to be populated in the present work by two alpha particle transitions from ^{194}At. Measured alpha particle energies and half-lives of ^{190}Bi are in good agreement with earlier data (see, for example table 4.2). The areas of the observed alpha particle peaks in ^{190}Bi were obtained to be 157 and 115 counts for the assumed low and high spin states, respectively. Four alpha particle energies of (7089 ± 6) keV, (7154 ± 5) keV, (7190 ± 5) keV and (7265 ± 6) keV with a common half-life were determined for ^{194}At. The number of observed counts were 18, 84, 147 and 18, respectively, as determined from the areas of the peaks.

The two highest alpha particle energies of ^{194}At were observed to populate the low spin state in ^{190}Bi and the two lowest alpha particle energies were observed to populate the high spin state. It can be assumed, that an alpha particle transition with an energy of (7190 ± 5) keV connects the low spin (3^+) states in ^{194}At and ^{190}Bi. Similarly, the high spin (10^-) states can be assumed to be connected by an alpha particle transition with an energy of (7154 ± 5) keV. According to the alpha particle decay systematics of even-mass astatine and bismuth isotopes (see figure 5.2), fine structure can be expected to occur and the two alpha particle energies observed in the present work with lower intensities (7089 ± 6 keV and 7265 ± 6 keV) can be explained in terms of fine structure in alpha particle decay of ^{194}At.

A gamma ray of energy of (76.4 ± 0.3) keV was observed in the present work in coincidence with time and position correlated evaporation residue – mother alpha particle pairs (see figure 4.9). As mentioned in chapter 4, there is some evedence that this is a gamma transition in ^{190}Bi. First, no X-ray with an energy of 76.4 keV was found from literature [Led78]. Secondly, based on the correlated evaporation residue – mother alpha – daughter alpha particle pairs, the gamma line can tentatively be connected to isotope ^{190}Bi. Moreover, most of the alpha particle gated gamma transitions were observed at intermediate bombarding energies, i.e. at energies where the production of ^{194}At was the most abundant. It is not possible, with the information available, to fix this gamma ray transition to any certain level.

Half-lives of the assumed low and high spin states in ^{194}At are so similar that with

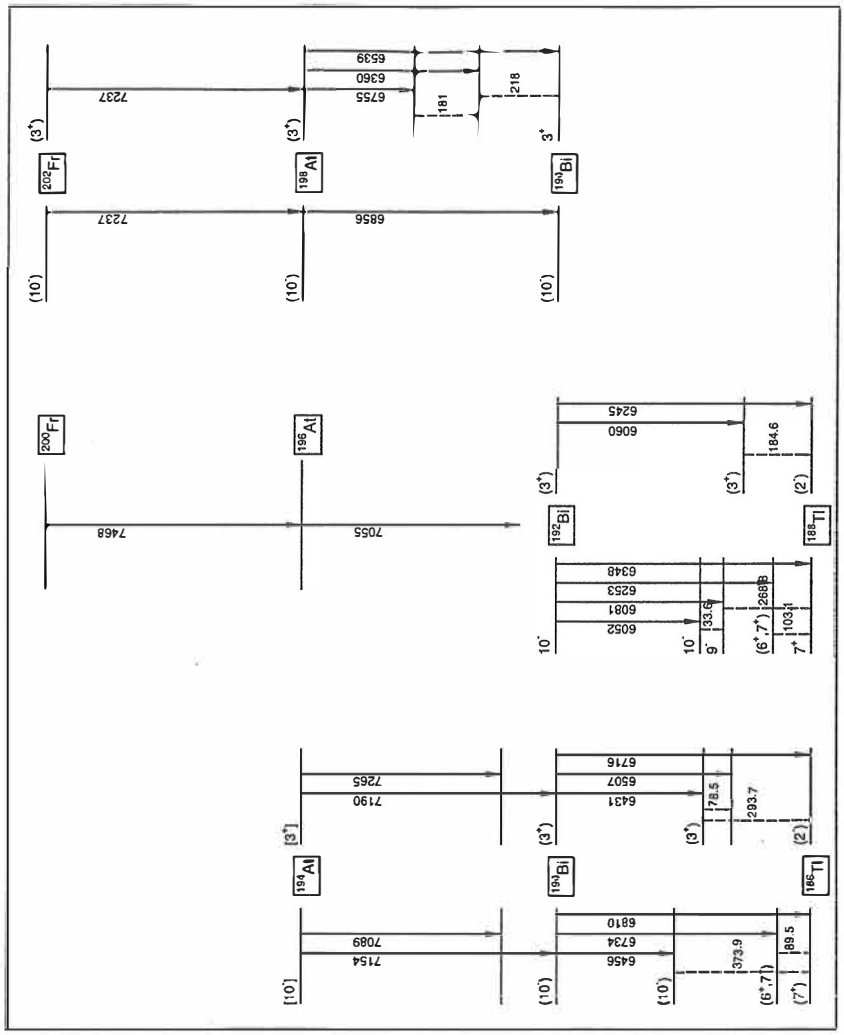

Figure 5.2 The alpha particle decay scheme of neutron-deficient even-mass bismuth, astatine and francium isotopes showing the fine structure in the alpha particle decay. Alpha transitions are marked by a solid line and gamma transitions by a dashed line.
Figure adopted from [Tre67, Dup91, Huy92] and present work.

current statistics it is not possible to separate the states (see figure 4.5). The same situation occurs also in ^{190}Bi.

5.2 Radon isotopes

The radon isotope ^{197}Rn and its isomeric state were independently produced and identified also at RIKEN by Morita et al. [Mor95]. A gas-filled recoil separator (GARIS) with a positive sensitive silicon detector (PSD: 64 mm × 64 mm) at the focal plane and a large-area microchannel plate (MCP) for time-of-flight measurements were used. The analysis was based on the position and time correlated alpha particle decay chains. The alpha particle energy and half-life of ^{197}Rn and ^{197}Rn^{m} were measured to be (7261 ± 20) keV and (51^{+35}_{-15}) ms and (7370 ± 20) keV and (18^{+9}_{-5}) ms, respectively. Numbers of observed counts are not reported, neither for ^{197}Rn nor ^{197}Rn^{m} by Morita et al. In the same paper, identification of the new isotope ^{196}Rn is considered to be highly probable based on one observed triple chain. The alpha particle energy of ^{196}Rn, E_α = (7428 ± 35) keV, measured by Morita et al. is included in figure 5.4 for alpha particle energy systematics.

In the present work, the alpha particle energy and half-life of ^{197}Rn were determined to be (7260 ± 7) keV and (65^{+25}_{-14}) ms, respectively. For the isomeric state, an alpha particle energy of (7356 ± 7) keV and a half-life of (19^{+8}_{-4}) ms were obtained. The numbers of observed triple chains were 13 and 11.

Our E_α and $T_{1/2}$ assigments of ^{197}Rn and ^{197}Rn^{m} are in very good agreement with the results of Morita et al. [Mor95]. Alpha particle energies of ^{197}Rn and ^{197}Rn^{m} also fit very well to the decay energy systematics, as can be seen in figure 5.4. In fact, due to better statistics, our results can be considered to be more accurate than those of Morita et al.

The existence of isomerism in ^{197}Rn is obvious from the fact that it has two alpha particle decaying states with different alpha particle energies and half-lives. Experimental observation of alpha particle emitting isomeric states in the neighbouring nuclei ^{199,201,203}Rn and in the daughter nucleus ^{193}Po also supports the existence of isomerism in ^{197}Rn (see, for example, figure 5.4). Probable values of spin and parity of the ground state and isomeric state in ^{197}Rn are $(\frac{3}{2}^{-})$ and $(\frac{13}{2}^{+})$, respectively, in analogy with the neighbouring odd-mass radon and polonium isotopes.

The alpha particle energy and half-life of radon isotope ^{198}Rn is not reported in [Mor95] although decay chain(s) assigned to ^{198}Rn – ^{194}Po were observed. Our

data on ^{198}Rn (E_α = (7196 ± 6) keV and $T_{1/2}$ = (84^{+16}_{-12}) ms) confirm the results obtained by Calaprice et al. [Cal84] (E_α = (7196 ± 10) keV and $T_{1/2}$ = (50 ± 9) ms). Similar results for isotopes ^{198}Rn (E_α = (7200 ± 12) keV and $T_{1/2}$ = (79 ± 15) ms) and ^{197}Rn (only tentative) were obtained also by Leino [Lei83].

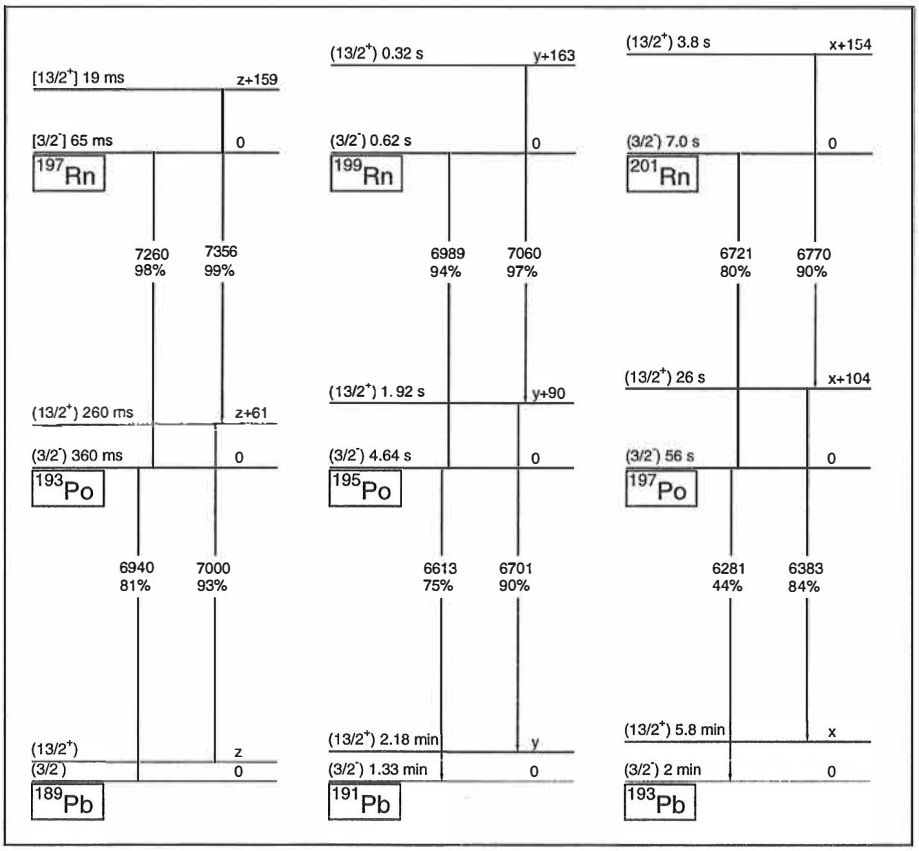

Figure 5.3 Alpha particle energy systematics and low energy decay scheme of odd-mass neutron deficient radon and polonium isotopes. Alpha particle energies of the isotope ^{197}Rn have been taken from the present work, other values have been taken from literature or derived from systematics. All energies are in keV. Beta particle half-lives calculated by Takahashi et al. [Tak73] have been used in determination of alpha particle branching ratios, $\lambda_\alpha/\lambda_\beta$. See the text for more details.

Alpha particle decay schemes of neutron-deficient radon and polonium isotopes are shown in figure 5.3. Alpha particle energies and half-lives of the isotope ^{197}Rn are from the present work. For other isotopes, they have been taken from literature. Alpha particle branching ratios, $\lambda_\alpha/\lambda_\beta$, have been estimated from beta particle half-lives calculated by Takahashi et al. [Tak73]. Spin and parity values have been deduced from the systematics of heavier radon and polonium isotopes.

Absolute positions of the assumed ($\frac{13}{2}^+$) isomeric states in radon and polonium isotopes cannot be given because the excitation energy of the corresponding state in lead isotopes is unknown. Relative excitation energies with respect to the ground state of lead isotopes, however, have been determined from alpha particle energies, and are shown in figure 5.3. The extrapolated excitation energy (from ($\frac{13}{2}^+$) levels in ^{199}Pb(424 keV), ^{197}Pb(319 keV) and ^{195}Pb(202 keV)) of ^{193}Pb is 100 keV [Shi90] and this value has been used in figure 5.3 (x = 100 keV). According to this systematics it seems that spin and parity of the ground state of ^{191}Pb would be ($\frac{13}{2}^+$). However, in figure 5.3 the decreases of 25 keV and 50 keV are assumed in level energies of ^{191}Pb and ^{189}Pb, respectively, from that (100 keV) in ^{193}Pb (y = 75 keV, z = 50 keV).

Theoretical calculations, performed for example by Möller et al. [Möl95], predict that the neutron-deficient radon isotopes with mass number below 202 have rather deformed oblate shapes (down to mass 194). The absolute values of the calculated ground state quadrupole deformation parameters (ϵ) range from 0.192 (^{201}Rn) to 0.233 (^{194}Rn) [Möl95].

The alpha particle decay of ^{204}Ra has been studied recently by Leino et al. [Lei96] and no indication of fine structure in the alpha particle energy of ^{204}Ra was seen. Because of the limited statistical uncertainty (30 alpha particle decay chains of ^{204}Ra – ^{200}Rn were observed) and due to lack of information on the nature of the excited states of ^{200}Rn, definite conclusions concerning the deformation were not possible. In the case of ^{200}Rn, roughly 20% population of the 2_1^+ state would be expected (with the level energy of 140 keV [Ram89, Gro62]) in the alpha particle decay of ^{204}Ra [Lei96] on the basis of the ground state quadrupole deformation parameter 0.200 of ^{200}Rn as calculated by Möller at al. [Möl95]. Laser spectroscopy studies in the neutron-deficient radon region [Geo95] also support the conclusion that pronounced deformation does not exist in radon isotopes with neutron number

114 or 115. In the present work, no influence of the predicted deformation on the alpha particle energies or half-lives of ^{197}Rn, ^{197}Rn^{m} and ^{198}Rn was seen.

5.3 Francium isotopes

Huyse et al. [Huy92] observed in ^{202}Fr only one alpha particle transition with the energy of (7237 ± 8) keV and the half-life of (340 ± 40) ms [Sch87]. However, they concluded, based on the two observed alpha particle decaying isomers in ^{198}At (E_α = (6755 ± 4) keV and $T_{1/2}$ = (4.2 ± 0.3) s for the assumed low spin (3^+) state, and E_α = (6856 ± 4)keV and $T_{1/2}$ = (1.0 ± 0.2) s for the assumed high spin (10^-) state [Huy92]), that this one observed alpha particle transition in ^{202}Fr is, in fact, a doublet and that there are at least two alpha particle decaying isomeric states in ^{202}Fr.

In the present work, our studies confirmed the existence of isomerism in ^{202}Fr. In figures 4.12 and 4.13 two clearly distinct groups of mother and daughter alpha particle energies assigned to the decay chains of ^{202}Fr – ^{198}At were observed. Measured half-lives of the two isomers in ^{202}Fr were obtained to be (230^{+80}_{-30}) ms and (230^{+140}_{-50}) ms for the assumed low and high spin states, respectively. The production rate (or the number of correlated triple chains) of the assumed low spin state (3^+) in ^{202}Fr was twice that of the high spin state (10^-).

Isomerism in ^{202}Fr is also supported by the systematics: three isomeric states with significant alpha particle decay branches have been observed in francium isotopes ^{204,206}Fr [Huy92]. This was the first time when using the alpha decay spectroscopy it was observed that states in ^{202}Fr and ^{198}At are connected in pairs.

Contrary to the behaviour of ^{202,204,206}Fr, no evidence of isomerism was found in ^{200}Fr. We measured the alpha particle energy of (7468 ± 9) keV and the half-life of (19^{+13}_{-6}) ms for ^{200}Fr from the six correlated triple chains. However, this small number of observed triple chains could be the reason for not observing a possible isomeric alpha particle transition. Only one alpha particle transition was also observed in ^{196}At by Treytl and Valli [Tre67].

Our half-life assigment on ^{200}Fr is in good agreement with the systematics of half-

lives of the heavier neutron-deficient francium isotopes. Also the calculated half-life, using the method proposed by Rasmussen [Ras59], 27 ms is in good agreement with our measured value. The half-life of ^{200}Fr, reported by Morita et al. [Mor95], (570^{+270}_{-140}) ms (with the alpha particle energy of (7500 ± 30) keV) differs from our value by a factor of 30. Applying the method of Rasmussen and assuming the hindrance from the change in orbital angular momentum, the half-life of 570 ms corresponds to a difference of 5 units between initial and final angular momenta.

In the paper of Morita et al. [Mor95], it is not stated clearly which maximum search times were used for ^{200}Fr. For radon isotopes (^{196}Rn, ^{197}Rn and ^{197}Rn^{m}) search times of 200 ms and 1 s for evaporation residue – mother alpha particle and mother alpha – daughter alpha particle pairs, respectively, were used. However, the half-life of 570 ms cannot be obtained by a maximum search time of 200 ms. In the present work, the longest individual life-time observed for ^{200}Fr with 400 ms search time was 66 ms. By increasing the search time to 3 s, we found one additional triple chain (the mother life time was 630 ms) with alpha particle energies compatible with the assigment to ^{200}Fr. The random probability for this chain was 0.08. Our short half-life does not, however, exclude the possible existence of an isomer with much longer half-life in an odd-odd nuclide.

The alpha particle energy assigments on ^{200}Fr of the present work and Morita et al. [Mor95] are in agreement with each other and with the theoretical predictions of 7390 keV from Liran and Zeldes [Lir76] and 7460 keV from P. Möller et al. [Möl95].

The alpha particle energy and half-life data for ^{201}Fr (E_α = (7388 ± 15) keV and $T_{1/2}$ = (48 ± 15) ms [Ewa80]) given by Ewan et al. were confirmed in the present work. There was a small difference between our alpha particle energies and those of Ewan et al. The alpha particle energy obtained in the present work was (7361 ± 7) keV. The difference between our alpha particle energy for ^{201}Fr and that from the work of Ewan et al. is reduced somewhat if the alpha particle energy calibration data from [Ewa80] are adjusted according to the compilation of Rytz [Ryt91]. Furthermore, the difference in E_α values between Ewan et al. [Ewa80] and Huyse et al. [Huy92] point to a possible systematic error in the energy calibration of Ewan et al. The half-life of ^{201}Fr obtained in this work was (69^{+16}_{-11}) ms, from 29 correlated triple chains. It is in good agreement with the value of Ewan et al.

In the present work, the maximum search times for mother and daughter alpha particles were too short for a reliable determination of half-lives of ^{203}Fr and ^{199}At. The determined alpha particle energies of these two activities are in good agreement with the previously published data.

The isotope ^{197}At, daughter of ^{201}Fr, has two alpha particle decaying states [Coe86]. The alpha particle energy and half-life of the $(\frac{9}{2}^-)$ ground state have been determined to be (6958 ± 5) keV and (350 ± 40) ms [Ryt91, Chu91], respectively. For the $(\frac{1}{2}^+)$ isomeric intruder state, an alpha particle energy of (6707 ± 5) keV and a half-life of (3.7 ± 2.5) s [Chu91] have been reported.

We observed 29 correlated chains of the type evaporation residue – mother alpha – daughter alpha particle which were assigned to ^{201}Fr – ^{197}At pairs. This alpha particle transition is unhindered and connecting ground states with spin and parity of $(\frac{9}{2}^-)$ of these two nuclei.

Existence of isomerism in ^{197}At gives a reason to expect an isomeric state also in ^{201}Fr. However, correlated triple chains were not found at the daughter energy region of about 6700 keV, and no isomeric state was found in the present work. The $(\frac{1}{2}^+)$ intruder state can, however, exist in ^{201}Fr, because in ^{197}At the production rate of the $(\frac{1}{2}^+)$ isomeric state relative to the $(\frac{9}{2}^-)$ ground state was reported to be less than 1% by Coenen et al. [Coe86] in the heavy ion reaction they used (^{20}Ne + ^{nat}Re). This would explain why alpha particle transitions connecting $(\frac{1}{2}^+)$ intruder states cannot be seen in the present work. This value (1%) is in agreement with the production ratio of the $(\frac{1}{2}^+)$ isomer and $(\frac{9}{2}^-)$ ground state in the bismuth nuclei [Coe85].

One alpha particle transition was also observed in ^{203}Fr in the present work. The situation is probably the same in ^{203}Fr as in ^{201}Fr. The production rate of the $(\frac{1}{2}^+)$ intruder state is too low to be observable in the heavy ion reactions with low statistics.

In figure 4.13a two triple chains can be seen at mother and daughter alpha particle energies of about 7550 keV and 6880 keV and half-lives of about 100 ms and 1.5 s, respectively. We can presently not assign this activity. Both chains have probabilities on the order of 10^{-2} of being accidental.

5.4 Alpha particle decay systematics

Alpha particle energy systematics

Figure 5.4 shows the alpha particle energy systematics as a function of neutron number for neutron-deficient isotopes of elements of polonium, radon and radium. Alpha particle energies of ^{197}Rn and ^{197}Rn^{m} (marked by an arrow in the figure) are from the present work and, for ^{196}Rn the value obtained by Morita et al. [Mor95] is used. Alpha particle energies of radium isotopes ^{203,204}Ra (including the isomer) were taken from refs. [Lei96, Led95]. Other values were taken from the compilation of Rytz [Ryt91], when possible, or from Nuclear Data Sheets. New alpha particle energies of ^{196}Rn, ^{197}Rn and ^{197}Rn^{m} can be seen to fit very well into the systematics.

Systematic occurrence of isomeric states (open symbols in figure 5.4) can be observed with neutron number less than 118. According to this systematics, the observed alpha particle energy for ^{191}Po would belong to the isomeric state (but this is not the subject of the present work). Another striking feature of these curves is the step-like behaviour with neutron number above 118.

One anomalous feature can, however, be seen in figure 5.4. It is the observed [Heß87] alpha particle decaying isomeric state in ^{207}Ra with an alpha particle branching ratio of about 25%. In fact, it may be expected that isomerism occurs also in lighter even-Z elements at N = 119, but their alpha particle branching ratios may be too low to be detectable.

Alpha particle energy systematics of neutron-deficient astatine isotopes are shown in figure 5.5 and compared with predictions of the semiempirical model of Liran and Zeldes [Lir76]. Only isotopes with even neutron number are included. Alpha particle energies of astatine isotopes are grouped according to the spin (and parity) of the level. Spin and parity of the ground states in neutron-deficient astatine isotopes is $(\frac{9}{2}^{-})$ except in ^{195}At where the ground state is $(\frac{1}{2}^{+})$ intruder, based on the present work. In isotopes ^{193}At and ^{197}At alpha particle energies of transitions between the $(\frac{1}{2}^{+})$ intruder excited states are shown in figure 5.5.

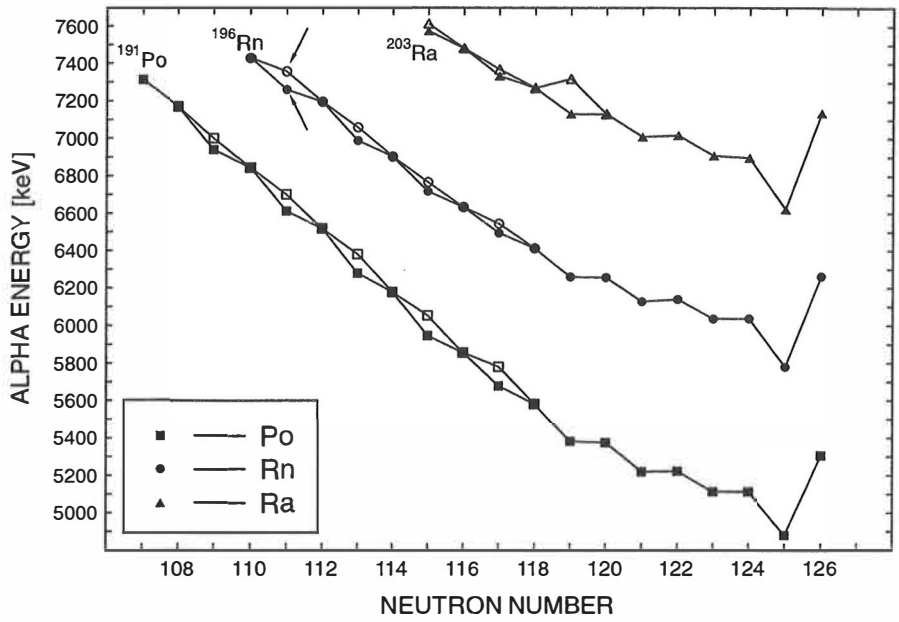

Figure 5.4 Alpha particle energy systematics as a function of neutron number for neutron-deficient isotopes of even-Z elements polonium, radon and radium. The data for radon isotope ^{197}Rn are from the present work, polonium and radium are shown for completeness. Full symbols represent alpha particle transitions from the ground state and open symbols from the isomeric state.

The agreement of alpha particle energies predicted by Liran and Zeldes with experimental alpha particle energies from $(\frac{9}{2}^-)$ states in astatine is moderate, near the closed neutron shell 126 the deviation is largest and decreases smoothly with decreasing number of neutrons. The three alpha particle energies measured for $(\frac{1}{2}^+)$ intruder states lie along a straight line.

A clear change in the systematics of experimental alpha particle energies for $(\frac{9}{2}^-)$ states can be seen at neutron number 110 (at ^{195}At). According to the result of the present work, the ground state spin and parity would change into $(\frac{1}{2}^+)$ from $(\frac{9}{2}^-)$ in the isotope ^{195}At and would again change back to $(\frac{9}{2}^-)$ in isotope ^{193}At. This change of the ground state spin and parity may affect the change in alpha particle energy (systematics). There is also a clear change in the systematics of alpha particle energies predicted by Liran and Zeldes at neutron number 110.

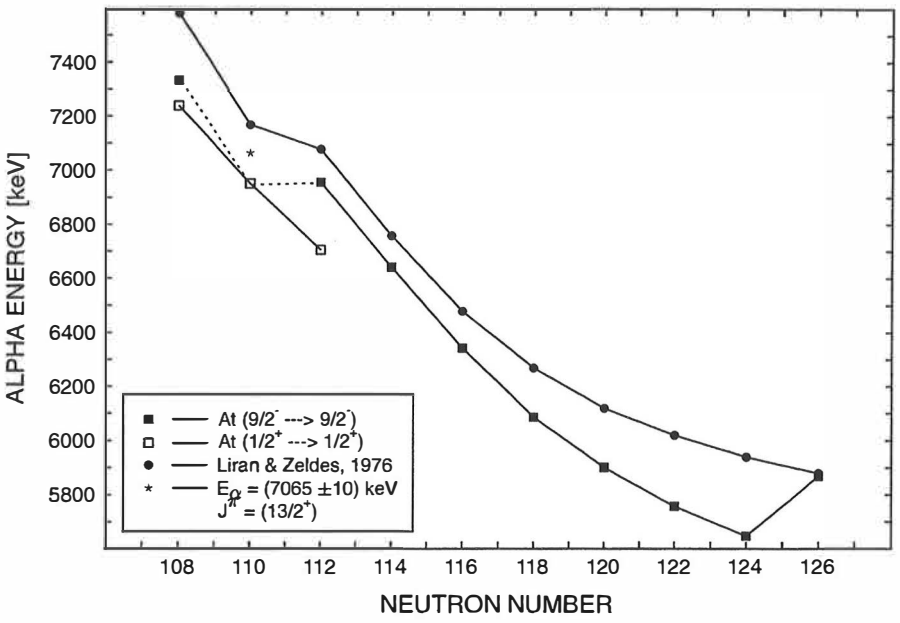

Figure 5.5 Alpha particle energy systematics as a function of neutron number for neutron-deficient astatine isotopes with even neutron number. Alpha particle energies for transitions between states with spin and parity of $(\frac{9}{2}^-)$ are marked by a black square, and for states with $(\frac{1}{2}^+)$ by an open square. An asterix (*) marks the alpha particle energy assigned to the level of ^{195}At with estimated spin and parity of $(\frac{13}{2}^+)$. Predicted alpha particle energies are from the semiempirical massformula of Liran And Zeldes [Lir76] which are marked by a full circle.

The systematics of the reduced alpha particle widths

Figure 5.6 shows the systematics of the reduced alpha particle widths (δ^2) of polonium, astatine and radon isotopes with an even neutron number. They are calculated using the method proposed by Rasmussen [Ras59] and scaled with respect to ^{212}Po such that $\delta^2(^{212}\text{Po}) = 1$ keV. Alpha particle energies, branching ratios and half-lives have been taken from the compilations of Rytz [Ryt91], when possible, or from Nuclear Data Sheets.

The reduced alpha particle widths of these three elements behave very similarly. The minimum occurs at the magic neutron number 126 with a very sharp rise in reduced width toward higher neutron number. Toward smaller neutron numbers reduced widths are increasing more slowly.

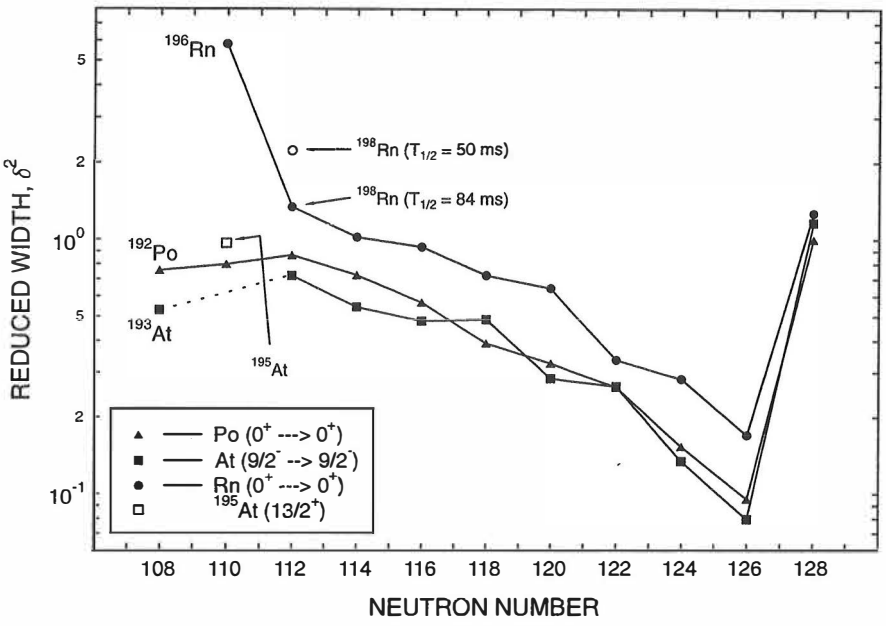

Figure 5.6 The reduced alpha particle widths of even-N polonium, astatine and radon isotopes. Alpha particle decay of these isotopes can be considered as an unhindered or favoured decay. The method proposed by Rasmussen [Ras59] was used for calculation. See the text for discussion of isotopes which do not follow the systematic trends.

The open square (^{195}At, state with spin and parity of $(\frac{13}{2}^+)$ does not seem to fit to the systematics of full squares (At, $(\frac{9}{2}^-)$ ground state to ground state transitions) suggesting that the structure (i.e. the spin and parity) of this level is different from $(\frac{9}{2}^-)$. $\Delta\ell = 0$ is assumed in the calculation of the reduced alpha particle width of the state marked by an open square in figure 5.6.

The half-life determined in the present work was used in the calculation of the reduced alpha particle width for ^{198}Rn. This value gives a better fit to the systematics than the reduced width calculated with the reported half-life of 50 ms [Cal84] (the open circle in figure 5.6). A deviation from systematics of astatine isotopes can be seen at N = 118 (^{203}At). Alpha particle energy, branching ratio and half-life of 6087 keV, 31% and 7.4 min [Ryt91], respectively were used for calculating the reduced alpha particle width of ^{203}At. If the alpha particle branching ratio is reduced from 31% to 20%, then ^{203}At also would follow the systematics. The reported alpha particle branching ratio of ^{207}At (8.7% [Ryt91]) may also be

slightly too large. The reduced alpha particle width of ^{196}Rn has been calculated from the half-life of 3.5 ms based on observation of one ovent only [Mor95]. According to the systematics (assuming 100% branching) the half-life of ^{196}Rn would be about 15 ms.

The decreasing trend in the reduced alpha particle widths of astatine and polonium isotopes when moving toward the more neutron-deficient nuclei can be seen. The mid-shell between two closed neutron shells is reached at N = 104 (between 82 and 126) and there could occur a local minimum of the reduced alpha particle widths.

5.5 Transfer reactions

Low energy alpha particles were observed in the present work in the reaction ^{56}Fe + ^{141}Pr at the two lowest bombarding energies of 4.11 and 4.23 MeV/nucleon. Alpha particle energy spectra from these two bombarding energies are shown in figure 5.7, where beam pause alpha particles are shown only. The interpretation of these low energy (4000 keV – 5000 keV) alpha particle peaks is that they belong to transfer reaction products. The identification of these peaks is given in table 5.2. The "cluster of nucleons" that has effectively been transferred from beam particle to target particle is of the form xp1n or xp2n. Transfer channels with more neutrons transferred cannot be observed in the present work because transfer products would no longer be alpha active. The reported half-life of all the identified transfer products is too long for correlation search and their half-lives cannot be determined in the present work.

In the super heavy element experiments at GSI, Darmstadt transfer reaction products of elements above lead with neutron numbers 126 and 127 have been observed. Lead or bismuth targets have been used in these experiments [Lei96b].

Table 5.2 Alpha particle energies, half-lives and branching ratios of the transfer reaction products from the reaction of ^{56}Fe + ^{141}Pr at the bombarding energies of 4.11 and 4.23 MeV/nucleon.

Peak	Nuclide	E_α [keV]	E_α [keV]	$T_{1/2}$	P_α	Ref.
1	^{149}Tb	3974±5	3966.6±1.9	4.1 h	16%	[Ryt91]
2	^{151}Dy	4071±5	4069.4±2.4	17 min	5.6%	[Ryt91]
3	^{150}Dy	4238±4	4235.1±1.7	7.2 min	38%	[Ryt91]
4	^{151}Ho	4523±5	4522.1±2.2	36 s	18%	[Ryt91]
5	$^{151}Ho^m$	4613±5	4610.6±2.2	47 s	13%	[Ryt91]
6	^{152}Er	4803±5	4804.3±1.6	10 s	90%	[Ryt91]

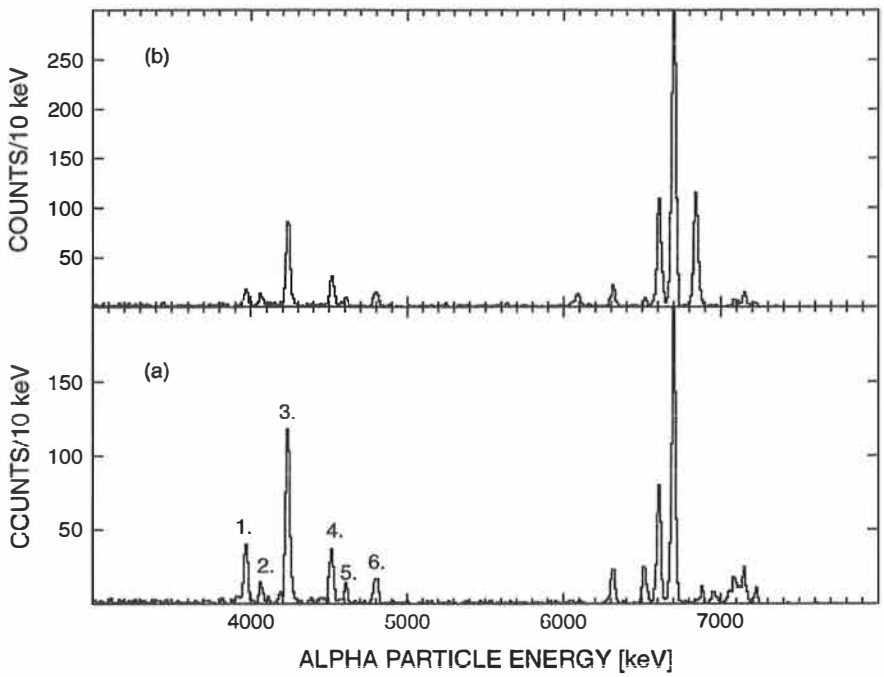

Figure 5.7 Alpha particle energy spectra from the reaction ^{56}Fe + ^{141}Pr at the bombarding energies of 4.11 (a) and 4.23 (b) MeV/nucleon. The low energy alpha particle peaks (4000 keV – 5000 keV) were identified as belonging to transfer products. Table 5.2 shows the identification of these peaks.

References

[And93] A.N. Andreyev, D.D. Bogdanov, V.I. Chepigin, V.A. Gorshkov, K.V. Mikhailov, A.P. Kabachenko, G.S. Popeko, S. Saro, G.M. Ter-Akopian, A.V. Yeremin and Sh.S. Zeinalov, Nucl. Instr. Meth. **A330** (1993) 125.

[Arm61] P. Armbruster, Nukleonik **3** (1961) 188.

[Arm71] P. Armbruster, J. Eidens, J.W. Griiter, H. Lawin, E. Roeckl and K. Sistemich, Nucl. Instr. Meth. **91** (1971) 499.

[Bas80] Rainer Bass, Nuclear Reactions with Heavy Ions, Springer-Verlag, Berlin (1980).

[Bat95] J.C. Batchelder, K.S. Toth, D.M. Moltz, T.J. Ognibene, M.W. Rowe, C.R. Bingham, E.F. Zganjar and B.E. Zimmerman, Phys. Rev. **C52** (1995) 1807.

[Bet72] H.D. Betz, Rev. Mod. Phys. **44** (1972) 465.

[Bie80] J.P. Biersack and L.G. Haggmark, Nucl. Instr. Meth. **174** (1980) 257.

[Bra80] R.A. Braga, W.R. Western, J.L. Wood, R.W. Fink, R. Stone, C.R. Bingham and L.L. Riedinger, Nucl. Phys. **A349** (1980) 61.

[Bro89] E. Browne, Nuclear Data Sheets **56** (1989) 709.

[Bro95] E. Browne and S.Y. Chu, Nuclear Data Sheets **74** (1995) 611.

[Cal84] F. Calaprice, G.T. Ewan, R.-D. von Dincklage, B. Jonson, O.C. Jonsson and H.L. Ravn, Phys. Rev. **C30** (1984) 1671.

[Chu89] Z. Chunmei, Nuclear Data Sheets **57** (1989) 1.

[Chu90] Z. Chunmei, Nuclear Data Sheets **60** (1990) 527.

[Chu91] Z. Chunmei, Nuclear Data Sheets **62** (1991) 433.

[Coh58] B.L. Cohen and C.B Fulmer, Nucl. Phys. **6** (1958) 547.

[Coe85] E. Coenen, K. Deneffe, M. Huyse, P. Van Duppen and J.L. Wood, Phys. Rev. Lett. **54** (1985) 1783.

[Coe86] E. Coenen, K. Deneffe, M. Huyse, P. Van Duppen and J.L. Wood, Z. Phys. **A324** (1986) 485.

[Dio89] J.S. Dionisio, Ch. Vieu, J.M. Lagrange, M. Pautrat, J. Vanhorenbeek and A. Passoja, Nucl. Instr. Meth. **A282** (1989) 10.

[Dup91] P. Van Duppen, P. Decrock, P. Dendooven, M. Huyse, G. Reusen and J. Wauters, Nucl. Phys. **A529** (1991) 268.

[Eas75] D.A. Eastham, Nucl. Instr. Meth. **125** (1975) 277.

[Enq96a] T. Enqvist, P. Armbruster, K. Eskola, M. Leino, V. Ninov, W.H. Trzaska and J. Uusitalo, Zeitschrift für Physik **A354** (1996) 9.

[Enq96b] T. Enqvist, K. Eskola, A. Jokinen, M. Leino, W.H. Trzaska, J. Uusitalo, V. Ninov and P. Armbruster, Zeitschrift für Physik **A354** (1996) 1.

[Ewa80] G.T. Ewan, E. Hagberg, B. Jonson, S. Mattson and P. Tidemand-Petersson, Z. Phys. **A296** (1980) 223.

[Fir90] R.B. Firestone, Nuclear Data Sheets **59** (1990) 243.

[Geo95] U. Georg, M. Keim, A. Klein, R. Neugart, M. Neuroth, P. Lievens, R.E. Silverans, L. Vermeeren and the ISOLDE Collaboration, Proc. Int. Conf. on Exotic Nuclei and Atomic Masses ENAM95, Arles, France, 1995, Edition Frontiéres, Gif sur Yvette (in press).

[Ghi88] A. Ghiorso, S. Yashita, M. Leino, L. Frank, J. Kalnins, P. Armbruster, J.-P. Dufour and P.K. Lemmertz, Nucl. Instr. Meth. **A269** (1988) 192.

[Gro62] L. Grodzins, Phys. Lett. **2** (1962) 88.

[Hal79] J. Halperin, Nuclear Data Sheets **28** (1979) 485.

[Hei95] P. Heikkinen and E. Liukkonen, 14th International Conference on Cyclotrons and Their Applications, Cape Town, October 8-13, 1995.

[Hey83] K. Heyde, P. Van Isacker, M. Waroquier, J.L. Wood and R.A. Meyer, Phys. Rev. Rep. **102** (1983) 291.

[Heß87] F.P. Heßberger, S. Hofmann, G. Münzenberg, A.B. Quint, K. Sümmeren and P. Armbruster, Europhys. Lett. **3** (8) (1987) 895.

[Huy92] M. Huyse, P. Decrock, P. Dendooven, G. Reusen, P. Van Duppen and J. Wauters, Phys. Rev. **C46** (1992) 1209.

[Kar69] V.A. Karnaukhov, L. Rubinskya, G. Terakop'yan, V. Titov and V.A. Chugreev, JINR P13-4454, Dubna (1969); I. Bacho, D.D. Bogdanov, Sh. Dorotsi, V.A. Karnaukhov, L.A. Petrov and G.M. Terakop'yan, JINR P13-4453, Dubna (1969).

[Koi94] H. Koivisto, J. Ärje and M. Nurmia, Nucl. Instr. Meth. **B94** (1994) 291.

[Laz93] JINR report E7-93-274, Dubna 1993, vol. 2B497.

[Led78] C. Michael Lederer and Virginia S. Shirley, Table of Isotopes, John Wiley & Sons, Inc., 1978.

[Led95] M.J. Leddy, S.J. Freeman, J.L. Durell, A.G. Smith, S.J. Warburton, D.J. Blumenthal, C.N. Davids, C.J. Lister and H.T. Penttilä, Phys. Rev. **C51** (1995) R1047.

[Lei81] M.E. Leino, S. Yashita and A. Ghiorso, Phys. Rev. **C24** (1981) 2370.

[Lei83] M. Leino, thesis, University of Helsinki Report Series in Physics, HU-P-D37 (1983), unpublished.

[Lei94] M. Leino, J. Uusitalo, T. Enqvist, K. Eskola, A. Jokinen, K. Loberg, W.H. Trzaska and J. Äystö, Z. Phys. **A348** (1994) 151.

[Lei95a] M. Leino, J. Äystö, T. Enqvist, P. Heikkinen, A. Jokinen, M. Nurmia, A. Ostrowski, W.H. Trzaska, J. Uusitalo, K. Eskola, P. Armbruster and V. Ninov, Nucl. Instr. Meth. **B99** (1995) 653.

[Lei95b] M. Leino, J. Äystö, T. Enqvist, A. Jokinen, M. Nurmia, A. Ostrowski, W.H. Trzaska, J. Uusitalo, K. Eskola, P. Armbruster and V. Ninov, Acta Physica Polonica **B26** (1995) 309 - 322.

[Lei95c] M. Leino, T. Enqvist, W.H. Trzaska, J. Uusitalo, K. Eskola, P. Armbruster and V. Ninov, Proc. Int. Conf. on Exotic Nuclei and Atomic Masses ENAM95, Arles, France, 1995, Edition Frontiéres, Gif sur Yvette (in press).

[Lei96] M. Leino, J. Uusitalo, R. Allatt, P. Armbruster, T. Enqvist, K. Eskola, S. Hofmann, S. Hurskanen, A. Jokinen, V. Ninov, R. Page and W.H. Trzaska, Z. Phys **A** (in press).

[Lei96b] M. Leino, private communication.

[Lir76] S. Liran and N. Zeldes, Atom. Data Nucl. Data Tables **17** (1976) 431.

[May79] T. Mayer-Kuckuk, Kernphysik, Teubner Verlag, Stuttgart, 1979.

[Mor95] K. Morita, Y.H. Pu, J. Feng, M.G. Hies, K.O. Lee, A. Yoshida, S.C. Jeong, S. Kubono, T. Nomura, Y. Tagaya, M. Wada, M. Kurakawa, T. Motobayashi, H. Ogawa, T. Uchobori, K. Sueki, T. Ishizuka, K. Uchiyama, Y. Fujita, H. Miyatake, T. Shimoda, T. Shinozuka, H. Kudo, Y. Nagai and S.A. Shin, Z. Phys. **A352** (1995) 7.

[Miy87] H. Miyatake, T. Nomura, H. Kawakami, J. Tanaka, M. Oyaizu, K. Morita, T. Shinozuka, H. Kudo, K. Sueki and Y. Iwata, Nucl. Instr. and Meth. **B26** (1987) 309.

[Möl95] P. Möller, J.R. Nix, W.D. Myers and W.J. Swiatecki, Atom. Data Nucl. Data Tables 59 (1995) 185.

[Nin95] V. Ninov, P. Armbruster, F.P. Heßberger, S. Hofmann, G. Münzenberg, Y. Fujita, M. Leino, and A. Lüttgen, Nucl. Instr. Meth. **A357** (1995) 486.

[Nom95] T. Nomura, Proc. Int. Conf. on Exotic Nuclei and Atomic Masses ENAM95, Arles, France, 1995, Edition Frontiéres, Gif sur Yvette (in press).

[Nor70] L.C. Northcliffe and R.F. Schilling, Nuclear Data Tables **A7** (1970) 233.

[Pau89] M. Paul, B.G. Glagola, W. Henning, J.G. Keller, W. Kutschera, Z. Liu, K.E. Rehm, B. Schneck and R.H. Siemssen, Nucl. Instr. Meth. **A277** (1989) 418.

[Oga91] Yu.Ts. Oganessian, Yu.V. Lobanov, A.G. Popeko, F.Sh. Abdullin, Yu.P. Kharitonov, A.A. Ledovskoy and Yu.S. Tsyganov, JINR LNR Scientific Report 1989–1990 (1991) 160.

[Oga95] Yu.Ts. Oganessian, private communication.

[Ram89] S. Raman, C.W. Nestor jr., S. Kahane, K.H. Bhatt, At. Data Nucl. Data Tables **42** (1989) 1.

[Ras59] J.O. Rasmussen, Phys. Rev. **113** (1959) 1593.

[Ryt91] A. Rytz, Atom. Data Nucl. Data Tables **47** (1991) 205.

[Rös78] F. Rösel, H.M. Fries, K. Alder and H.C Pauli, Atom. Data Nucl. Data Tables **21** (1978) 291.

[Sch79] K.-H. Schmidt, W. Faust, G. Münzenberg, H.-G. Clerc, W. Lang, K. Pielenz, D. Vermeulen, H. Wohlfarth, H. Ewald and K. Güttner, Nucl. Phys. **A318** (1979) 253.

[Sch84] K.-H. Schmidt, C.-C. Sahm, K. Pielenz, H.-G. Clerc, Z. Phys. **A316** (1984) 19.

[Sch84a] J. Schneider, GSI report 84-3 (1984), unpublished.

[Sch87] M.R. Schmorak, Nuclear Data Sheets **50** (1987) 669.

[Sch88] M.R. Schmorak, Nuclear Data Sheets **53** (1988) 331.

[Sea90] G.T. Seaborg and W.D. Loveland, the Elements beyond Uranium, John Wiley & Sons, Inc., 1990.

[Seg65] Emilio Segrè, Nuclei and Particles, An Introduction to Nuclear and Subnuclear Physics, W.A. Benjamin, Inc., New York, Amsterdam (1965).

[Shi90] V.S. Shirley, Nuclear Data Sheets **61** (1990) 519.

[Sin89] B. Singh, Nuclear Data Sheets **56** (1989) 75.

[Sin90] B. Singh, Nuclear Data Sheets **61** (1990) 243.

[Taa61] R. Taagepera and M. Nurmia, Scientiarnum Fennicae **78** (1961).

[Tak73] K. Takahashi, M. Yamada and T. Kondoh, Atom. Data Nucl. Data Tables **12** (1973) 101.

[Tre67] W. Treytl and K. Valli, Nucl. Phys. **A97** (1967) 405.

[Trz90] W.H. Trzaska, Nuclear Instruments and Methods in Physics Research **A297** (1990) 223.

[Uus96] J. Uusitalo, thesis (1996), unpublished

[Ver84] D. Vermeulen, thesis, GSI Report 84-2 (1984), unpublished.

[Wau93] J. Wauters, P. Dendooven, M. Huyse, G. Reusen and P. Van Duppen, Phys. Rev. **C47** (1993) 1447.

[Yas83] S. Yashita, thesis (1983), unpublished.